SELECTIVE PREVENTION OF MDGA-NEUROLIGIN-2 INTERACTIONS INCREASES INHIBITORY SYNAPTIC TRANSMISSION, FEAR MEMORY, AND ANXIETY

Jie Jiang

A DISSERTATION SUBMITTED TO

THE FACULTY OF GRADUATE STUDIES

IN PARTIAL FULFILLMENT OF THE REQUIREMENTS

FOR THE DEGREE OF

DOCTOR OF PHILOSOPHY

GRADUATE PROGRAM IN BIOLOGY

YORK UNIVERSITY

TORONTO, ONTARIO

JUNE 2025

Abstract

Within the CNS, synapse organizer proteins serve as potent modulators of synapse development and function. Among the known synapse organizers, neuroligins (NLs) have well-established roles in promoting synapse development. In contrast, MAM domain containing glycosylphosphatidylinositol anchor (MDGA) proteins repress synapse formation. Human gene linkage analysis has implicated NLs and MDGAs in brain dysfunction. For example, mutations in NL2 or MDGAs contribute to major neurodevelopmental disorders, including autism. However, how NL2/MDGA interactions specifically regulate synapse properties and behavioral outputs remains unclear. NL2 is an inhibitory synapse-specific synapse organizer, whereas MDGAs suppress synapses through blocking the interaction of NL2 and presynaptic NRXNs. To examine the roles of NL2-MDGA interactions in regulating excitatory (glutamatergic) and inhibitory (GABAergic) balance (E/I balance) in synaptic connectivity, we designed a novel and specific NL2ΔSite II transgenic mouse model with the NL2 site II mutated which selectively disrupts NL2/MDGA binding, without affecting other protein interactions. Using a combination of immunohistochemistry, diverse behavior paradigms, and electrophysiology techniques, we sought to determine how synapse development, neural transmission and behaviors are altered in male NL2ΔSite II transgenic mice. We found that NL2ΔSite II mice showed increased anxiety, elevated fear memory and impaired social memory. These mice also exhibited increased expression of inhibitory synapse proteins and upregulated GABAergic transmission whereas excitatory synapse proteins and synaptic transmission appeared normal. Overall, our results suggest that NL2ΔSite II specifically modulates inhibitory synapses and leads to behavioral abnormalities, which could have clinical implications for treatment of neurodevelopmental disorders including autism, schizophrenia and bipolar disorders.

A second major project focused on addressing the critical question of how loss of both MDGAs (*Mdga*1/2 double knockout; DKO) in adult mice affects synapse development *in vivo.* Preliminary results revealed that MDGA1/2 DKO in hippocampal CA1 pyramidal neurons elevates intrinsic excitability of CA1 pyramidal neurons, increases excitatory synaptic transmission but decreases inhibitory synaptic transmission. These findings suggest dual loss of MDGAs elevates the excitation/inhibition ratio if favor of glutamatergic transmission which may have implications for understanding increased susceptibility to neurodevelopmental disorders following MDGA loss of function.

Acknowledgements

First of all, I would like to thank my advisors, Drs. Steven Connor and Yicheng Xie. I really appreciate that they spared no effort establishing a collaboration provided me with a rare opportunity to start my doctoral journey. During the first two years in China, Dr. Xie provided an exciting experimental atmosphere and ongoing academic guidance. Whenever I encountered academic difficulties, he always provided support and critically thought with me, but not for me. Although there is 12-hour time difference between China and Toronto, Dr. Connor still offered me the opportunity to participate in lab meetings and gave me a warm welcome when I came to Toronto. Also, Dr. Connor provided training into cutting-edge electrophysiological experiment techniques and helped revise manuscripts very patiently. Both labs established a friendly atmosphere that was mutually beneficial. It is an honor to be their student and I really enjoyed their rigorous approach and enthusiasm for science which set excellent examples for me.

Secondly, I would like to thank my committee members, Drs. Logan Donaldson and Chun Peng. They have witnessed my academic growth and provided essential support in terms of contribution of time, knowledge and sharp questions which helped improve my project and allowed me to move forward in my development as an independent scientist.

I would like to also thank all the members in the Xie lab and the Connor labs. I would like to thank Drs. Zahra Ghasemi and Xuehui Wang for guiding me into the patch clamp realm. Thanks also to Kyle Patel, Katherine Andrec and Samuel Holm`s help in providing training and guidance in extracellular field potential recordings. Finally, special thanks to Donghui Lin, Xinyan Dong,

Yuhua Liu, Cihang Zhu and Ningxiao Xia for their support and help in my scientific research and life.

I would like to thank my parents and other family members for always unconditionally supporting my choices and decisions, both financially and spiritually. Their love for me has become my driving force and a powerful source of inspiration as I pursue my career.

I would like to also acknowledge the key role the animals used in these experiments played in helping me make key discoveries that hopefully lay the foundation or medical breakthroughs that benefit Humanity going forward.

Statement of contributions

Donghui Lin performed western blot experiments depicted in Figure 19A and Figure 20A and Sanger sequencing in Figure 14E.

Dr. Yicheng Xie designed and bought the NL2 $^{flox/flox,\ Mut/Mut}$ and CMV-Cre mice from Biocytogen company. Donghui Lin, Jie Jiang and Anqi Yang bred the mice.

Lifen Gong performed bioinformatics experiments depicted in Figure 15, Figure 16, Figure 22, and Figure 23.

All other experiments including electrophysiology (mIPSC, mEPSC, PPR, cell excitability), immunostaining (Density of inhibitory synapse and excitatory synapse), behaviors (Open field, elevated plus maze, rotarod test, novel object recognition, Y maze, social memory, fear conditioning), genotyping, viral injection were performed by me. I was responsible for writing this dissertation, the first author manuscripts, and generating all figures.

Table of Contents

List of tables

List of figures

List of Abbreviations

AAV	Adeno-associated viruses
ACSF	Artificial cerebrospinal fluid
ADHD	Attention deficit hyperactivity disorder
AMPAR	α-amino-3-hydroxy-5-methyl-4-isox-azolepropionic acid receptor
ANOVA	Analysis of variance
AP	Anteroposterior
AP(s)	Action potential(s)
APP	Amyloid precursor protein
APV	DL-2-amino-5-phosphonovaleric acid
ASD	Autism spectrum disorder
ATP	Adenosine triphosphate
BCA	Bicinchoninic Acid Assay
BL	Black
BLA	Basolateral amygdala
BP	Biological process
BP(s)	Basal progenitors
BSA	Bovine Serum Albumin
BTBR	Black and Tan BRachyury
CA	Cornus ammonis
CC	Cellular component
CMV	Cytomegalovirus
CNQX	Cyanquixaline
CNS	Central nervous system
CNTNAP2	Contactin Associated Protein 2
CO2	Carbon dioxide
CRE	Cyclization Recombination Enzyme
DAPI	4',6-diamidino-2-phenylindole
DEG	Differentially expression gene
DG	Dentate gyrus
dKO	Double knockout
DNA	Deoxyribonucleic acid
DV	Dorsoventral
EC	Extracellular calcium
EC	Entorhinal cortex
ECM	Extracellular matrix
EGTA	Ethylene Glycol Tetraacetic Acid
EP	Eppendorf
EPM	Elevated plus maze

fMRI	Functional magnetic resonance imaging
FS	Follistatin
FXS	Fragile X Syndrome
GABA	γ-aminobutyric acid
GABAARs	Gamma-aminobutyric acid type A receptors
GAD	Glutamate decarboxylase
GEO	Gene Expression Omnibus
GO	Gene ontology
GPI	Glycosylphosphatidylinositol
GSE	Gene Expression Omnibus Series
GTP	Guanosine triphosphate
HEPES	2-[4-(2-hydroxyethyl)piperazin-1-yl]ethanesulfonic acid
hGH	Human growth hormone gene
HPA	Hypothalamic-pituitary-adrenal
ID	Identity document
ID	Intellectual disability
KA	Kainic acid
KD	Knockdown
KI	Knock-in
KO	Knockout
LEC	Lateral entorhinal cortex
LFP	Local field potential
LNS	Laminin, NRX, sex-hormone-binding globulin
LS	Lateral septum
LTP	Long-Term Potentiation
MAM	Memprin, A5 protein, receptor protein tyrosine phosphatase mu
MDGAs	MAM domain-containing GPI anchor proteins
MEC	Medial entorhinal cortex
MECP2	Methyl-CpG Binding Protein 2
mEPSC	Miniature excitatory postsynaptic currents
mIPSC	Miniature inhibitory postsynaptic currents
ML	Mediolateral
mPFC	Medial prefrontal cortex
mPSC	Miniature postsynaptic currents
mRNA	Messenger ribonucleic acid
NA	Numerical aperture
NCBI	National Center for Biotechnology Information
NDD	Neurodevelopmental disorder
NL	Neuroligin
NMDAR	N-Methyl-D-Aspartate Receptor
NOR	Novel object recognition

NRXN	Neurexin
OCT	Optimal cutting temperature compound
OE	Overexpression
PAGE	Polyacrylamide gel electrophoresis
PBS	Phosphate buffered saline
PCA	Principle component analysis
PCR	Polymerase chain reaction
PDZ	PSD-95/disc-large/zona-occludens-1
PFA	Paraformaldehyde
PLC	Phospholipase C
PMSF	Phenylmethylsulfonyl fluoride
PN	Pyramidal neuron
PPD	Paired Pulse Depression
PPF	Paired Pulse Facilitation
PPR	Paired-pulse ratio
PSD	Postsynaptic density protein
PTX	Picrotoxin
PV+	Parvalbumin expressing
PVDF	Polyvinylidene difluoride
Rin	Input resistance
RMP	Resting membrane potential
RNAseq	RNA sequencing
RTT	Rett syndrome
SC	Schaffer Collateral
SCZ	Schizophrenia
SDS	Sodium dodecyl sulfate
SEM	Standard error of mean
SHANK3	SH3 And Multiple Ankyrin Repeat Domains 3
sIPSC	Spontaneous inhibitory postsynaptic currents
SLM	Stratum lacunosum-moleculare
SNP	Single nucleotide polymorphism
SNX27	Sorting nexin 27
SO	Stratum oriens
SOM+	Somatostatin-expressing
SP	Stratum pyramidale
SPARC	Secreted protein acidic and rich in cysteine
SPARCL	SPARC-like 1, secreted protein acidic and rich in cysteine-like 1
SPF	Specific pathogen free
SPR	Surface plasmon resonance
sPSC	Spontaneous postsynaptic currents
SR	Stratum radiatum

SS	Splicing sites
SSA	Splicing site A
SSB	Splicing site B
SST+	Somatostatin+
SUB	Subiculum
Syn GO	Synaptic Gene Ontology
TAE	Tris Acetate-EDTA buffer
TBS	Tris buffered saline
TBST	Tris buffered saline with Tween-20
TLE	Temporal lobe epilepsy
TRIS	Tris(hydroxymethyl)aminomethane
TSC	Tuberous sclerosis complex
TTX	Tetrodotoxin
UTR	Untranslated Regions
vg/mL	Viral Genome copy per milliliter
VGAT	Vesicular GABA transporter
VGLUT	Vesicular glutamate transporter
vHPC	Ventral hippocampus
VIAAT	Vesicular inhibitory amino acid transporter
VIP	Vasoactive intestinal polypeptide
WPRE	Woodchuck Hepatitis Virus (WHV) Posttranscriptional Regulatory Element
WT	Wildtype

Chapter 1: General introduction

1.1 Neurodevelopment disorders

NDDs are cognitive and behavioral disorders including intellectual disability (ID), autism spectrum disorder (ASD), attention-deficit/hyperactivity disorder (ADHD), schizophrenia (SCZ) and bipolar disorder the onset of which can occur early in key developmental stages. These disorders often lead to significant difficulties in cognitive, motor, language/communication, emotional or social functions (Mental disorders (who.int)). The global prevalence of NDDs fluctuates between 4.7-88.5% (Francés et al., 2022), which varies as a function of the particular disorder. It is estimated that 10-17% of all children in Canada live with NDDs (Improving the quality of life for children with neurodevelopmental disabilities — Health Insight), with males being at a ~4 times higher risk of presenting with NDDs relative to females (May et al., 2019).

Within the family of NDDs, ASD presents unique challenges. Globally, 1 in 100 children are diagnosed with ASD by the age of 8 (Salari et al., 2022). The documented behavioural phenotypes of ASD include communication and social aversion, excessive repetitive and stereotyped behaviors (Lord et al., 2020) and deficits in sensory (Klintwall et al., 2011), motor (Harris, 2017), and cognitive development (Brunsdon et al., 2015). ASD symptoms are clinically detectable at ~6 months of age, thus early diagnosis and treatment of NDDs is crucial for improving the life quality of patients and their guardians as soon as possible (Elder et al., 2017).

The causes of NDDs are not entirely clear, yet studies have indicated that both biological and environmental risk factors are involved (Bale et al., 2010). Many genes involved in NDDs are related to synaptic development and function which modulate excitatory/inhibitory (E/I) balance

within brain circuits (Darnell, 2020). Accordingly, understanding the impacts of loss of E/I balance as the brain develops is essential for understanding the onset and progression of NDDs.

Given the ontological diversity of NDDs, treatments remain limited and there are currently no cures for this family of disorders. Furthermore, treatment strategies show limited efficacy. Established treatments including behavioral therapy, transcranial magnetic stimulation and medication, have shown modest positive effects for improving symptoms (Y.-H. Kim, 2021; Masuda et al., 2019). Additionally, current pharmacotherapies including stimulants and antidepressants mainly enhance cognition (Y.-H. Kim, 2021).

These findings all point to a critical need to advance our ability to effectively treat NDDs. Exploring the mechanisms underlying NDDs provides a means to increase our ability to understand and selectively target core pathologies that set the conditions for NDDs. Given the development nature of NDDs, and the clear link between synapse development and disorder etiology, understanding how synapses change should yield novel insights that can be leveraged for developing more efficacious treatments.

1.1.1 Neural underpinnings of ASD

Pre-clinical models for ASD, have provided many essential insights into the mechanistic nature of NDDs. Much work has focused on mouse models of monogenic ASD syndromes including CNTNAP2, MECP2, MDGAs, NL3, NL4, NRXN1, SHANK3 and TSC1/2 and ASD-linked copy number variants including 15q11-q13 deletion and duplication, 15q13.3 microdeletion, 16p11.2 deletion and duplication (Varghese et al., 2017). Animal models based upon treatment with valproic acid, an environmental risk factor, are also widely employed in ASD research (Nicolini & Fahnestock, 2018). These animal models have identified numerous cellular

mechanisms including excitatory/inhibitory (E/I) imbalances and abnormal neurotransmitter receptor expression (Muhle et al., 2018). Different kinds of behavioral paradigms used for measuring ASD-like behaviors in these models have identified autism-like deficits, including social memory impairments and repetitive behaviours (Kazdoba et al., 2016). Therefore, despite the etiological diversity of these models, they often converge in terms of behavioral phenotypes and mechanistically at the level of synapses.

1.2 Hippocampus

1.2.1 The anatomy of hippocampal formation

The hippocampal formation is composed of 3 principal subfields: the dentate gyrus (DG), cornu ammonis 3 (CA3) and cornu ammonis 1 (CA1). The entorhinal cortex provides the primary inputs into the DG via perforant pathway projections which form synapses onto DG granule cells. These neurons, in turn, project to pyramidal neurons within the CA3 region via the mossy fiber pathway. CA3 cells project through CA2 onto CA1 pyramidal cells via the Schaffer collateral (SC) pathway to complete the trisynaptic circuit. Finally, CA1 neurons send projections to the subiculum, the primary output pathway of the hippocampus (See Figure 1).

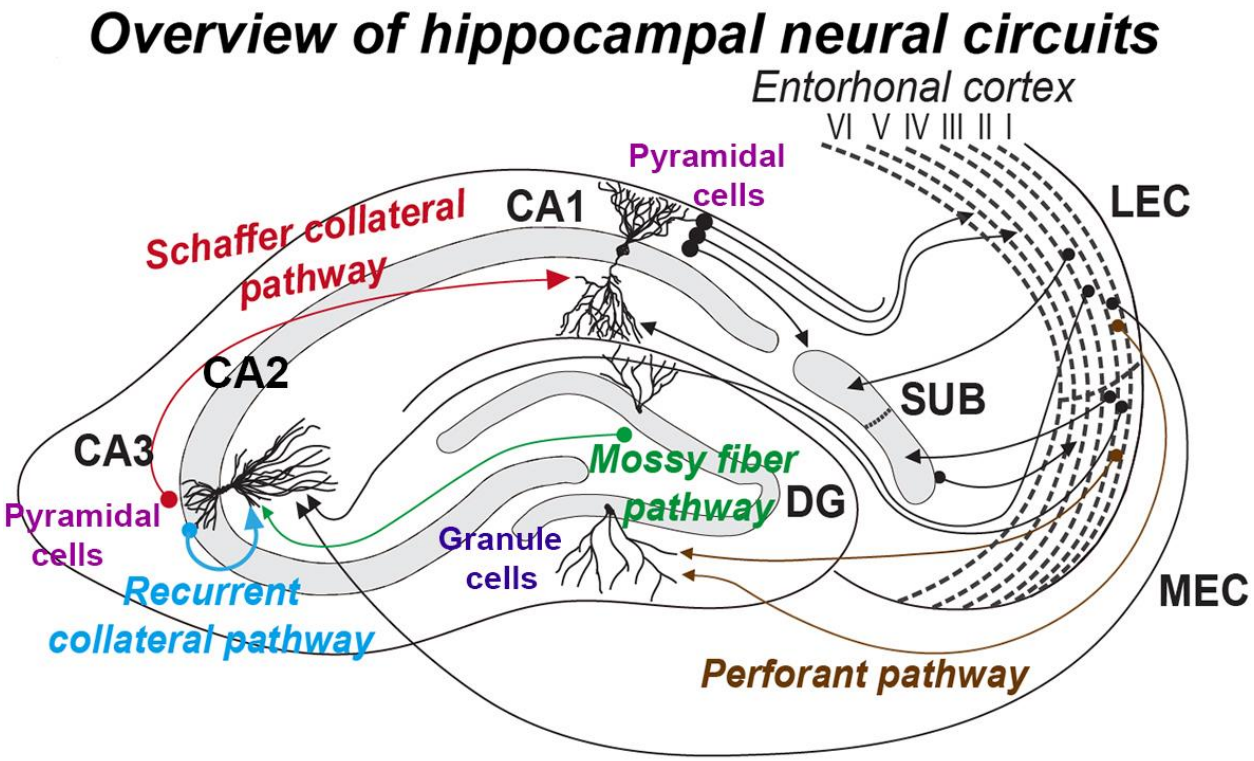

Figure 1. Overview of the basic neural circuit architectures of the hippocampus.

Illustration of the hippocampal circuitry. The canonical projections involving entorhinal cortical neurons and various hippocampal neurons are depicted by solid arrows. Image is modified from (Park et al., 2018).

According to the Allen Brain Atlas (ABA, www.brain-map.org), pyramidal neurons in hippocampal CA1 and CA3 show clear regional and laminar specificities in C57BL6 mice (Figure 2). The CA1, CA2 and CA3 are stratified, meaning they have distinct, highly organized layers. These layers are generally classified based on the cellular structures and neuronal subtypes that reside within them. Resting upon the pyramidal cell body layer is the stratum oriens (S.O.) followed by stratum pyramidal (S.P.), stratum radiatum (S.R.) and stratum lacunosum-moleculare

(S.L.M.). The cell bodies of CA1 pyramidal neurons are limited to S.P. The S.O. is composed of the basal dendrites of pyramidal neurons and different types of interneurons. The S.R. contains apical dendrites of pyramidal cells and interneurons, and the S.L.M. contains the terminal branches of the dendrites of pyramidal cells and interneurons (Ahmed & Mehta, 2009; Schultz & Engelhardt, 2014).

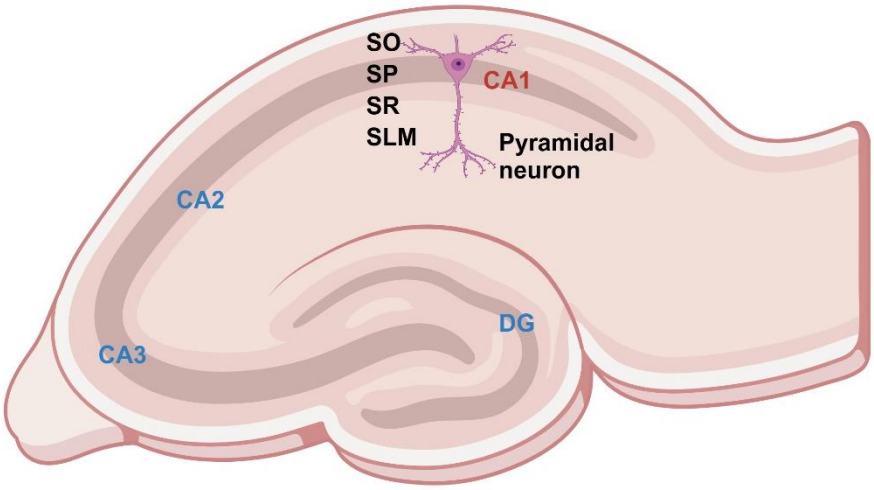

Figure 2. Hippocampus laminar structure.

The most superficial layer of the CA1 region is the stratum oriens (S.O.) which contains a diverse complement of interneurons. Below this is the stratum pyramidal (S.P.) which contains the cell bodies of pyramidal neurons. The stratum radiatum (S.R.) is below the S.P. and contains pyramidal neuron dendrites that serve as a primary site of glutamatergic synaptic inputs. The stratum lacunosum-moleculare (S.L.M.) is located below the S.R. and contains the most distal dendritic segments of the CA1 pyramidal neurons. (Image generated with BioRender.com).

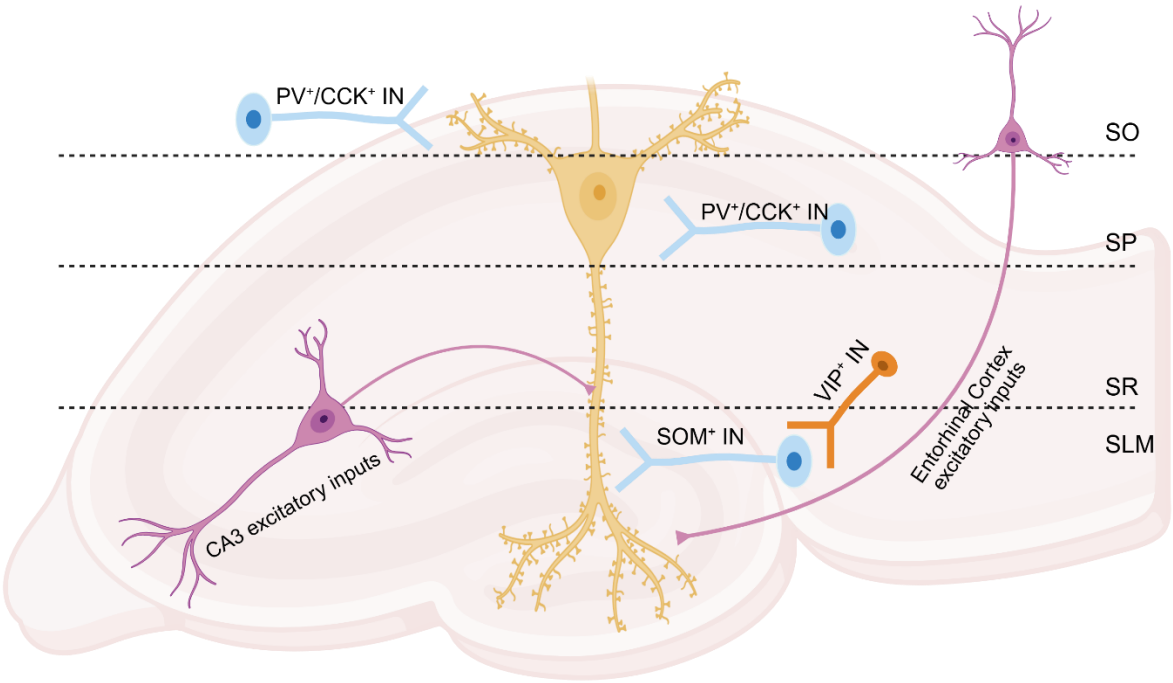

Figure 3. Excitatory and inhibitory inputs to hippocampal CA1 pyramidal neurons (PNs). Parvalbumin interneurons (PV$^+$ INs), Cholecystokinin interneurons (CCK$^+$ INs), Somatostatin interneurons (SOM$^+$ INs), vasoactive intestinal peptide interneurons (VIP$^+$ INs).

The Schaffer collaterals (SC) refer to the glutamatergic (excitatory) projections from CA3 and CA2 to CA1, terminating in the S.R. and S.O. CA3 is the largest source of excitatory synapses.

Direct excitatory input is also from the Entorhinal Cortex (EC), targeting S.L.M. The inhibitory input of Pyramidal Neurons (PNs) in the CA1 region of the hippocampus is provided by a variety of GABAergic Interneurons (INs). Parvalbumin interneurons (PV$^+$ INs) and Cholecystokinin interneurons (CCK$^+$ INs) target the cell body (Soma) and proximal dendrites of PNs (S.O. and S.P.). Somatostatin interneurons (SOM$^+$ INs) target the distal apical dendrites (S.L.M.) of PNs. vasoactive intestinal peptide interneurons (VIP$^+$ INs) mainly inhibit other INs (such as SOM+ INs) and indirectly disinhibits PNs (Figure 3).

A single CA1 pyramidal cell receives ~30,000 excitatory inputs primarily located on dendritic spines (Megías et al., 2001). There are far fewer synapses (~ 1800) from EC to CA1, all of which are in S.L.M. (Megías et al., 2001). The perforant pathway projection from the EC to the DG travels, in part, to the S.L.M forming synapses on the distal apical dendrites of the hippocampal pyramidal neurons (Schultz & Engelhardt, 2014). Contrary to CA3, CA1 pyramidal neurons do not project to other CA1 neurons, but project to the subiculum, the primary output from the hippocampus proper.

Extrinsic inputs to the hippocampus consist of various cortical regions, the amygdaloid complex, the medial septal region, the thalamus, the supramamillary region and multiple monoaminergic brainstem nuclei (Rosene & Van Hoesen, 1977; Schultz & Engelhardt, 2014).

A single pyramidal neuron receives ~1700 γ-aminobutyric acid (GABA)ergic inhibitory inputs located in the CA1 cell body and dendrites (Megías et al., 2001). The major source of inhibitory inputs onto a CA1 pyramidal neurons are from local interneurons restricted to the CA1 region. The cell bodies of these interneurons are located in S.P, S.O, or near the border between S.R. and S.L.M., and form synapses on the proximal dendrites, cell bodies or distal dendrites of the CA1 pyramidal neurons (Klausberger & Somogyi, 2008; Somogyi & Klausberger, 2005).

1.2.2 Hippocampal involvement in ASD

Previous studies have revealed that numerous brain regions are involved in ASD. For instance, amygdala, fusiform gyrus, superior temporal sulcus and cerebellum. These regions contribute to the regulation of various functions that are compromised in ASD, including

movement, language, social processing, executive functioning and repetitive behaviours (D'Mello & Stoodley, 2015; Hernandez et al., 2015).

Additionally, phenotypes of ASD patients are characterized by impaired social communication and repetitive behaviors. Apart from these core symptoms, there are also comorbidities linked to the impaired hippocampus function such as episodic memory and spatial reasoning deficits (Banker et al., 2021; Severino et al., 2024).

Hippocampal volume is atypical within some ASD patients. A wealth of studies have observed exaggerated hippocampal volume in children and adolescents with ASD, yet other studies also found that the children had decreased or no significant differences in hippocampal volume (Barnea-Goraly et al., 2014; Groen et al., 2010; Schumann et al., 2004). Collectively, these results suggest that the function and perhaps structure of hippocampus is altered in many cases of ASD, demonstrating the need to better understand the implications of autism-linked insults to this brain region.

1.2.3 Dorsal and ventral hippocampus

The hippocampus modulates not only contextual and spatial cognitive functions but also emotional behaviors, which appear to depend on different areas along the dorso-ventral axis of the hippocampus. Accordingly, there is a well-established body of evidence indicating that the dorsal and ventral hippocampus support different functions (Moser & Moser, 1998). Specifically, the ventral hippocampus is linked to emotional content, whereas the dorsal hippocampus is more related to spatial navigation/cognition and memory (Bannerman et al., 2002; Fanselow & Dong, 2010; Henke, 1990; Kheirbek et al., 2013; Kjelstrup et al., 2002; Moser et al., 1995).

1.3 Brief introduction of synapses

In the nervous system, synapses are structures of intercellular junctions allowing presynaptic neurons to transfer chemical or electrical information to the postsynaptic target cells (Südhof, 2018). Neural circuits consist of a population of excitatory and inhibitory neurons interconnected by synapses and multiple neural circuits wired together to form large scale neural networks (Ghatak et al., 2021). At chemical synapses, presynaptic terminals release neurotransmitters to receptors located on postsynaptic neurons. Pyramidal neurons primarily releasing glutamate are excitatory neurons, while interneurons primarily releasing γ-aminobutyric acid (GABA) are inhibitory neurons. Glutamate and GABA are principle excitatory and inhibitory neurotransmitters mediating excitatory and inhibitory synapse transmission, respectively (Ghatak et al., 2021). GABA, widely spreads in the CNS and is synthesized from glutamate through two enzyme isoforms of GAD, GAD65 and GAD67 (Kajita & Mushiake, 2021). Following it's synthesis, it is packaged into synaptic vesicles by the vesicular GABA transporter (VGAT) (McIntire et al., 1997) also called VIAAT (Y. Wang et al., 2009). These two isoenzymes are co-expressed in most GABAergic interneurons, where GAD67 is mainly expressed in soma and GAD65 is mainly expressed in the presynaptic terminals (Kajita & Mushiake, 2021). Thus, GAD65-expressing puncta represent GABAergic inhibitory synaptic terminals. Gephyrin is a postsynaptic marker, as it can anchor the $GABA_A$ receptors postsynaptically and self-assembles into a scaffold protein which interacts with the cytoskeleton (Tyagarajan & Fritschy, 2014). Conversely, glutamate can be transported into synaptic vesicles by VGLUTs. VGLUT1 is mainly expressed in cortex, hippocampus and cerebellum, VGLUT2 is predominantly expressed in thalamus, amygdala and hypothalamus and VGLUT3 is mainly found not only in presynaptic terminals but postsynaptically in cell bodies and dendrites (Du et al., 2020). Finally, the

postsynaptic density protein-95 (PSD-95) is a major postsynaptic scaffolding protein of glutamatergic synapses (Nowacka et al., 2020). (See Figure 4). Notably, excitatory synapses are primarily localized at dendritic spines (DeFelipe & Fariñas, 1992) while inhibitory synapses are predominantly located at dendritic shafts, axon initial segments, and the soma (Boivin & Nedivi, 2018; Kubota, 2014). Although interneurons account for approximately 10-15% of the total neurons in the hippocampus (Pelkey et al., 2017) and ~20% of all synapses in cortical microcircuits are inhibitory (Kubota, 2014), inhibition form this class of neurons and inputs is essential for modulating neural activity.

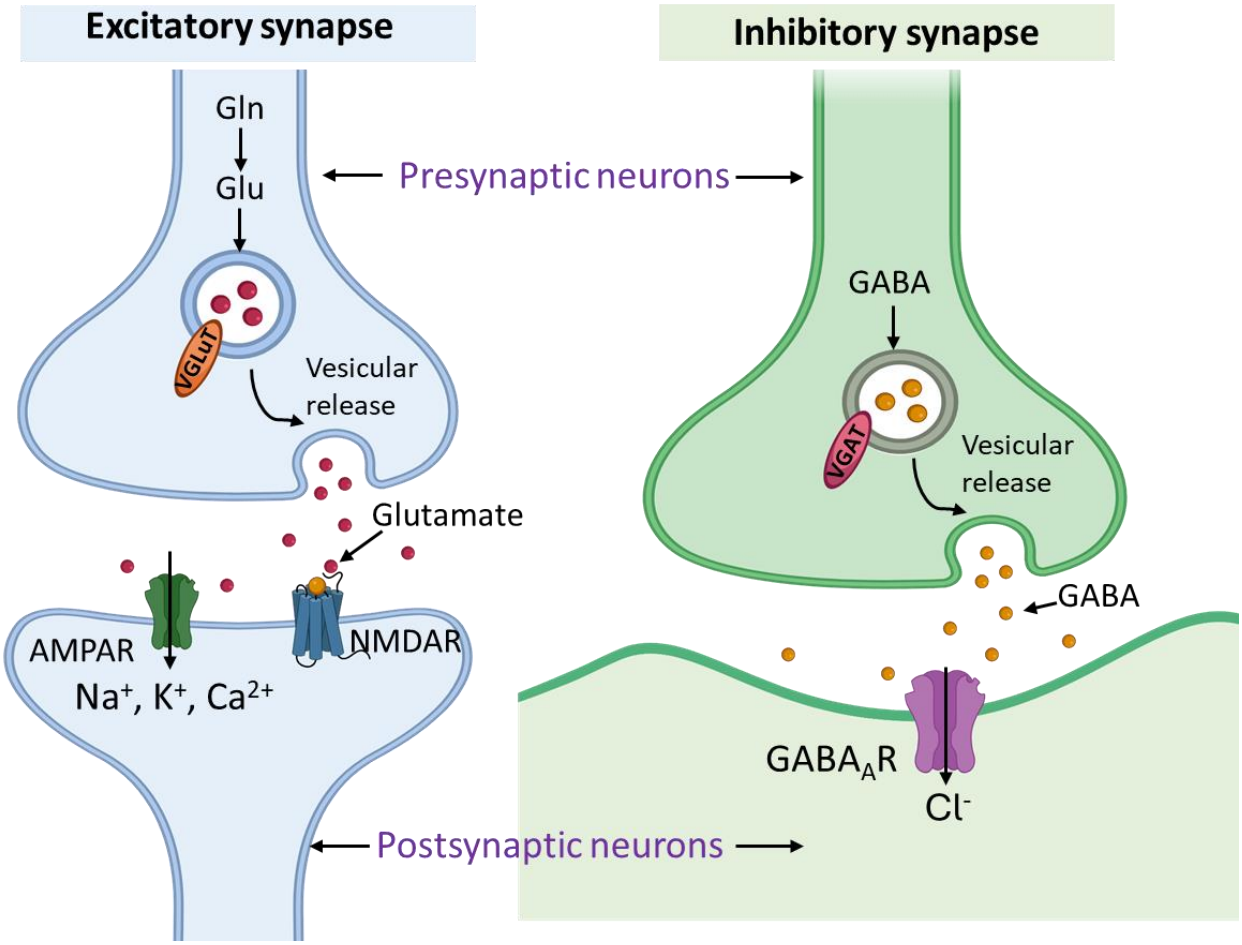

Figure 4. Chemical excitatory and inhibitory synapses.

Glutamate is transported into synaptic vesicles by VGLUT. After released from presynapse, glutamate binds to α-amino-3-hydroxy-5-methyl-4-isoxazolepropionic acid receptor (AMPAR) and N-methyl-D-aspartate receptor (NMDAR) allowing cations to go through the postsynaptic membrane. GABA is packaged into synaptic vesicles by the VGAT. After released from presynapse, GABA binds to $GABA_AR$ allowing anions to go through the postsynaptic membrane. (Image generated with BioRender.com).

1.3.1 Excitatory/Inhibitory (E/I) balance

E/I balance is defined as the dynamic balance between excitatory (glutamatergic) and inhibitory (GABAergic) inputs spanning from the single neuron to the level of large scale neural circuits (Hengen et al., 2013; Iascone et al., 2018). In terms of the effects on neuronal activity, shifts in E/I balance favoring excitation (increase in excitation or decrease in inhibition), will increase neuronal activity. Conversely, when inhibition exceeds excitation, neuronal activity will decrease (Sohal & Rubenstein, 2019). NDDs emerge, in part, due to in the perturbation of E/I balance, termed E/I imbalance in which can result in neural network dysfunction. Accordingly, E/I imbalance has been diagnosed both in ASD patients (Bruining et al., 2020) and in ASD animal models (Giovedí et al., 2014). Thus, understanding the neural mechanisms that alter E/I ratio can provide insights that can be used to rebalance neural networks.

1.4 Neurexin-Neuroligins

Among the multitude of cellular events that determine the identity (inhibitory/excitatory), physiological properties and diversity of CNS synapses, the complement of synapse organizers, specialized molecules that coordinate synapse formation, refinement and plasticity, are particularly

important for establishing and modulating cellular connectivity. Among these organizers, neuroligins (NLs) have emerged as a family of synapse promoting molecules that help drive neural circuit development. There are four neuroligin genes in rodents (NL1, NL2, NL3 and NL4), and five neuroligin genes in humans (NL1, NL2, NL3, NL4 (X-chromosome linked) and NL5 (also named NL4Y because of its location on the Y chromosome)) (Lisé & El-Husseini, 2006). NL1, NL2 and NL3 are highly expressed in the brain (Ichtchenko et al., 1996a). Analysis of translated amino acid sequencing revealed that the three neuroligins are highly homologous with 52% identical residues. In pairwise comparisons, NL 1 and 2 share 59% identity; 1 and 3 share 66% identity; and 2 and 3 share 59% identity (Ichtchenko et al., 1996a). Further domain sequencing analysis showed that the cytoplasmic sequences are the most divergent regions (31% identity) compared to the extracellular domains (55% identity) and the transmembrane regions (91% identity) (Ichtchenko et al., 1996a). Therefore, the diversified C-terminal may contribute to functional specificity among different members. The C-terminal intracellular domain of NL such as the PDZ binding motif directly binds to postsynaptic scaffold proteins such as PSD95 and gephyrin, determining its location at the synapse. On their cholinesterase scaffold, all neuroligins contain the classic SSA, whereas NL1 has an additional SSB. Thus, there are four potential NL1 variants (NL1(-), NL1A, NL1B, and NL1AB) (Ichtchenko et al., 1996a) and two different isoforms of NL2 (NL2(-) and NL2A) (Chih et al., 2006). These alternative splicing sites affect NL's binding affinity with the presynaptic ligand NRXN, thereby determining the type of synapse such as excitability and the specificity of inhibitory synapses. Moreover, modifications such as glycosylation (like N-glycosylation of NL1) regulate its stability, transport and interaction with NRXN (Zhang et al., 2018). Neurexins also contain alternative splicing sites. There are over 1000 splice variants of neurexins expressed from two alternative promoters yielding long α- and short

β- neurexins within three *NRXN* gene (Schreiner et al., 2014; Ullrich et al., 1995; Ushkaryov et al., 1992). This large molecular diversity is generated from five alternative SS1-SS5 (Missler & Südhof, 1998).

1.4.1 Structure and molecular interactions of NL2

E/I imbalances in NDDs have been linked to synapse organizers which play essential roles in regulating synapse development, differentiation and function (Südhof, 2008a, 2017). Two well-studied examples of these organizers are neurexins and neuroligins.

Neuroligins are postsynaptic type I transmembrane adhesion proteins which bind to presynaptic NRXNs, mediating formation, maturation, maintenance and function of synapses. All neuroligins share similar structures: a short cytoplasmic domain which can connect to the PDZ binding motif and gephyrin-collybistin motif, a highly conserved single transmembrane domain, and a N-terminal hydrophobic cleaved signal peptide followed by a large extracellular cholinesterase-like homology domain (Ichtchenko et al., 1996b). The N-terminal extracellular domains are responsible for dimerization and interaction with α/β-NRXN1-3 LNS6 domain (Araç et al., 2007; X. Chen et al., 2008; Fabrichny et al., 2007). Crystal structure analysis revealed that the NRXN binding site and NL dimerization interface are located on opposite sides of NLs (Koehnke et al., 2008). Also, dimerization is a prerequisite for functions of NLs, which can efficiently assemble the NRXN monomers, thereby promoting assembly of presynaptic zones (Ali et al., 2020). In addition, the C-terminal intracellular domain can recruit $GABA_A$ receptors ($GABA_AR$, mediate inhibitory synaptic transmission as a ligand-gated chloride channels) as well as scaffolding proteins such as gephyrin and collybistin and trigger downstream signaling pathways (Krueger-Burg et al., 2017) (Figure 5). Also, the intracellular domain can interact with

endosome-cargo adaptor SNX27, blocking lysosomal degradation and promoting recycling of NL2 to inhibitory synapses (Binda et al., 2019; Halff et al., 2019).

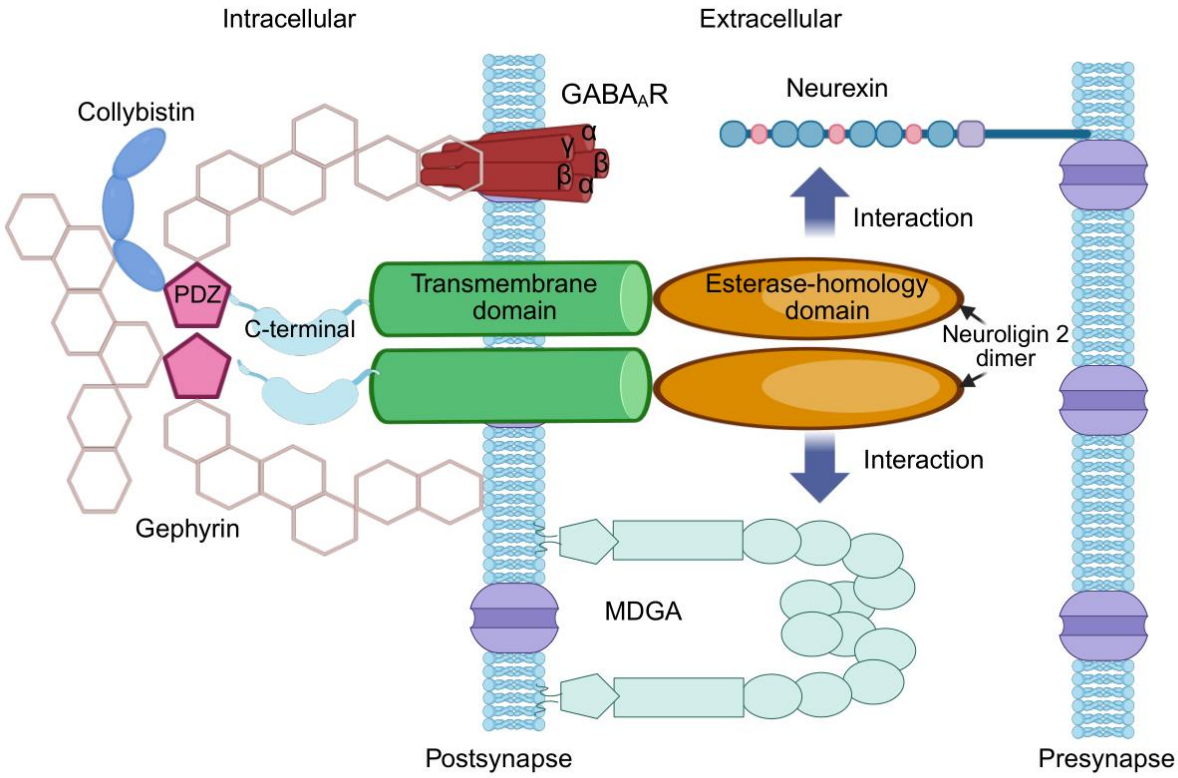

Figure 5. Structure and function of NL2 at inhibitory synapses.

NL2 dimers form transsynaptic interactions with presynaptic NRXNs and postsynaptic complex including gephyrin, collybistin and recruit $GABA_A$Rs to the synapses. (Image generated with BioRender.com).

1.4.2 Synaptic distribution of NLs

Different neuroligins localize to different synapses. NL1 is majorly expressed in excitatory neurons and interacts with PSD95, mainly distributed in dendritic spines, participating in the formation of excitatory (glutamatergic) synapses (Song et al., 1999), whereas NL2 is highly

expressed in inhibitory neurons, and tends to be located in dendritic trunks or cell bodies, located at inhibitory (GABAergic), and binds to gephyrin to regulate inhibitory synaptic function (Graf et al., 2004; Uchigashima et al., 2016; Varoqueaux et al., 2004). NL3 and NL4 are expressed in both excitatory and inhibitory neurons. The localization of NL3 and NL4 is rather diverse and may be related to different synaptic types or non-synaptic functions. NL3 localizes to both excitatory and inhibitory synapses (Budreck & Scheiffele, 2007), and NL4 is predominantly expressed at inhibitory glycine synapses (Hoon et al., 2011).

At the molecular level, there are several possible mechanisms underlying the localization of neuroligin isoforms to specific synapses. First, neuroligin splice variants selectively bind to different presynaptic neurexin isoforms to mediate selective recruitment to distinct synapses. α-NRXNs and SS4 (+)-NRXNs have higher binding affinity for NL2 relative to β-NRXNs and SS4 (-)-NRXNs (Chih et al., 2005; Graf et al., 2006; Kang et al., 2008). Secondly, neuroligin isoforms localize to glutamatergic and GABAergic synapses through interactions with synapse-specific cytoplasmic scaffolding proteins (Chih et al., 2006). For example, NL2 binds to the collybistin-gephyrin complex through its cytoplasmic motif to promote specific localization at inhibitory synapses (Poulopoulos et al., 2009) and regulate perisomatic inhibition via possible phosphorylation activity (Bemben et al., 2015). Notably, the splice form-specific extracellular binding of NRXNs is the major determining factor of the localization of NLs to specific synapses. The interaction of the intracellular domain is necessary for the recruitment of subsequent signaling components but not for the initial localization of NLs (Futai et al., 2013; Nguyen et al., 2016; Patrizi et al., 2008).

1.4.3 Function of NL2 at inhibitory synapses

NLs specify and validate synapse function, with distinct NLs acting on different types of synapses. This property has been demonstrated within hippocampal neurons, as NLs mediate the formation and function of excitatory and inhibitory synapses in this region (Chih et al., 2005). Among these, NL2 is shown to selectively localize to inhibitory synapses as OE or KO of NL2 either in cultured neurons or in vivo increases or decreases inhibitory, but not excitatory, synaptic responses, respectively (Chubykin et al., 2007; Van Zandt et al., 2019).

NL2 is highly expressed in pyramidal neurons and all three subtypes of interneurons (PV+, SST+ and VIP+) (Liang et al., 2015; Longley et al., 2022). Deletion of NL2 from mouse glutamatergic or GABAergic neurons in the cortex decreases inhibition in a cell-autonomously fashion without affecting excitation, thereby disrupting E/I balance which can be lethal. Interestingly, constitutive KO of NL2 or simultaneously KO of NL2 from both glutamatergic and GABAergic neurons is viable in mice, suggesting the imbalance between inhibitory synapses onto both excitatory and inhibitory neurons individually leads to lethality while disrupting both cell types simultaneously results in a more mild E/I imbalance, allowing the survival of the animals (Longley et al., 2022). In most brain regions, the strength (current carrying capacity) and frequency of mIPSCs or sIPSCs are significantly reduced in NL2 KO mouse neurons (reviewed in (Ali et al., 2020)). For instance, conditional KO of NL2 in adult mPFC neurons results in a progressive reduction in the number and strength of inhibitory synapses, indicating that NL2 is essential to the long-term maintenance and restructuring of inhibitory synapses in the mPFC (Liang et al., 2015). However, within the amygdala and the thalamic reticular nucleus, mIPSCs were intact with the absence of NL2 (Babaev et al., 2016; Cao et al., 2020). This suggests regional variation in the requirement for NL2 mediated maintenance of inhibitory synaptic transmission.

In NL2 KO mice, inhibitory postsynaptic complexes containing $GABA_A$Rs and gephyrin are decreased in virtually all brain regions (Ali et al., 2020). In hippocampal CA1, KO of NL2 results in a significant enhancement of intracellular gephyrin, suggesting that the normal recruitment of gephyrin to postsynaptic membrane is disrupted (Poulopoulos et al., 2009). Consistent with the decrease in postsynaptic complexes, KO of NL2 leads to reduced inhibitory synaptic transmission assessed in the form of amplitude and frequency of mIPSCs or sIPSCs throughout the brain (Ali et al., 2020). The alteration of IPSC amplitude reflects the change in the number or functions of postsynaptic $GABA_A$Rs, whereas the alteration of IPSC frequency reflects a change in presynaptic GABA release. Given that NL2 is a postsynaptic protein, one possible mechanism for reduced IPSC frequency may be that there is no longer reliable detection of reduced amplitude events. Alternatively, transsynaptic signaling regulated by NRXNs may be compromised, affecting presynaptic GABA release (Ali et al., 2020).

Notably, NL2 not only plays an important role in initial establishment and development of synapses but is also required for synapse maintenance during adulthood. This was demonstrated by the observation that virus-mediated deletion of NL2 in the mPFC or LS in adulthood decreased GABAergic synaptic transmission, consistent with results in constitutive NL2 KO mice (Liang et al., 2015; Troyano-Rodriguez et al., 2019). Furthermore, constitutive KO of NL2 only reduces gephyrin and $GABA_A$Rs puncta in the perisomatic (perisomatic synapse is formed by fast-spiking interneurons such as PV-positive basket neurons) but not dendritic (targeted by SOM-positive neurons) region of neurons in the hippocampus and BLA (Babaev et al., 2016; Jedlicka et al., 2011; Poulopoulos et al., 2009). Additionally, KO of NL2 only reduced IPSCs amplitude originating from PV-positive interneurons but not SOM-positive interneurons (Gibson et al., 2009). However, KD of NL2 in organotypic hippocampal slices decreased light-evoked IPSCs from both PV- and

SOM-positive interneurons (Horn & Nicoll, 2018). Thus, the mechanisms of synapse specificity of NL2 remains to be further defined.

1.4.4 Function of NL2 in behavioral circuits

Over the past few decades, numerous studies have shown that NLs play important roles in regulating E/I balance between neurons. Aberrant NL-NRXN interactions or signaling have been implicated in the pathogenesis of ASD and schizophrenia (Südhof, 2008b). Additionally, shifting E/I balance in either direction at NL2-mediated synapses generates anxiety-like behaviors. Specifically, constitutive KO or OE of NL2 can lead to anxiety-like phenotypes (Hines et al., 2008). It also appears that constitutive KO of NL2 impacts sensory functions including audition, olfaction and pain sensitivity (Wöhr et al., 2013). However, OE of NL2 did not detectably alter sensory function (Hines et al., 2008). Loss or gain of NL2 function has modest affects of motor behavior. In the accelerated rotarod test, KO of NL2 impaired motor learning and coordination (Wöhr et al., 2013), whereas OE of NL2 only reduced locomotor activity (Hines et al., 2008).

Regarding social behavior which includes sociability, defined as preferred exploration of a novel animal over a novel object, social learning and memory, which refers to the preference for exploring a novel animal over a familiar animal, NL2 KO mice showed similar phenotypes to WT mice (Blundell et al., 2009; Cao et al., 2020; Wöhr et al., 2013). Intriguingly, local KO or KD of NL2 in mPFC (Liang et al., 2015) or dopamine D1 receptor-expressing neurons (Heshmati et al., 2018) in adulthood leads to decreases in sociability. NL2 overexpression studies in the context of sociality has resulted in mixed results (Hines et al., 2008; Kohl et al., 2013, 2015; van der Kooij et al., 2014). For example, hippocampal OE of NL2 has no impact on sociability and social

memory (Kohl et al., 2013). However, viral OE of NL2 in adulthood impaired early-life stress induced social memory which was reversed by viral KD of NL2 in the adulthood (Kohl et al., 2015). For cognitive function, conditional deletion of NL2 from the mPFC resulted in disruption of fear memory acquisition and consolidation but not retrieval (Liang et al., 2015). Interestingly, the same manipulation caused no alteration of spatial memory assayed by Y-maze test. Finally, constitutive KO of NL2 had no effect on memory ability in novel object recognition task, suggesting that NL2 is dispensable for these forms of cognition in this region (Cao et al., 2020).

1.5 MDGAs

1.5.1 MDGAs proteins

There are two MDGA homologues which encode MDGA1 and MDGA2 proteins (R. Wang et al., 2019). More than 40% and 85% of amino acids of MDGA1 and MDGA2 are identical and conserved, respectively (R. Wang et al., 2019). Structurally, MDGA proteins possess similar domain organization. They are attached to the postsynaptic membrane via a C-terminal GPI anchor, and harbor large (~900 amino acids) extracellular domains composed of six immunoglobulin-like (Ig) domains, a fibronectin type III-like (FnIII7) domain, MAM domain and a N-terminal signal peptide (Elegheert et al., 2017; Litwack et al., 2004) (Figure 6). Each structure plays a functional role. The MAM domain was reported to interact with axon-rich regions suggesting a role in axon guidance and synapse selectivity (Fujimura et al., 2006). MDGA1 MAM domain directly interacts with presynaptic APP to disrupt the GABAergic synapse maintenance and accelerate GABAergic synapse elimination (J. Kim et al., 2022). Through the GPI anchor, MDGA1 is specifically localized to lipid rafts which is essential for membrane trafficking, transduction of intracellular

signals and endocytosis (Díaz-López et al., 2005). The GPI anchor is susceptible to cleavage by PLC (Díaz-López et al., 2005) and the extracellular domain of MDGAs can shed to extracellular space (R. Wang et al., 2019). The immunoglobulin superfamily (IgSFs) are the largest families of axon guidance molecules and plays a pivotal role in formation and maintenance of neural circuits (Burden-Gulley & Lemmon, 1995). The extracellular six Ig domains and FnIII7 domain make MDGAs similar to IgSFs.

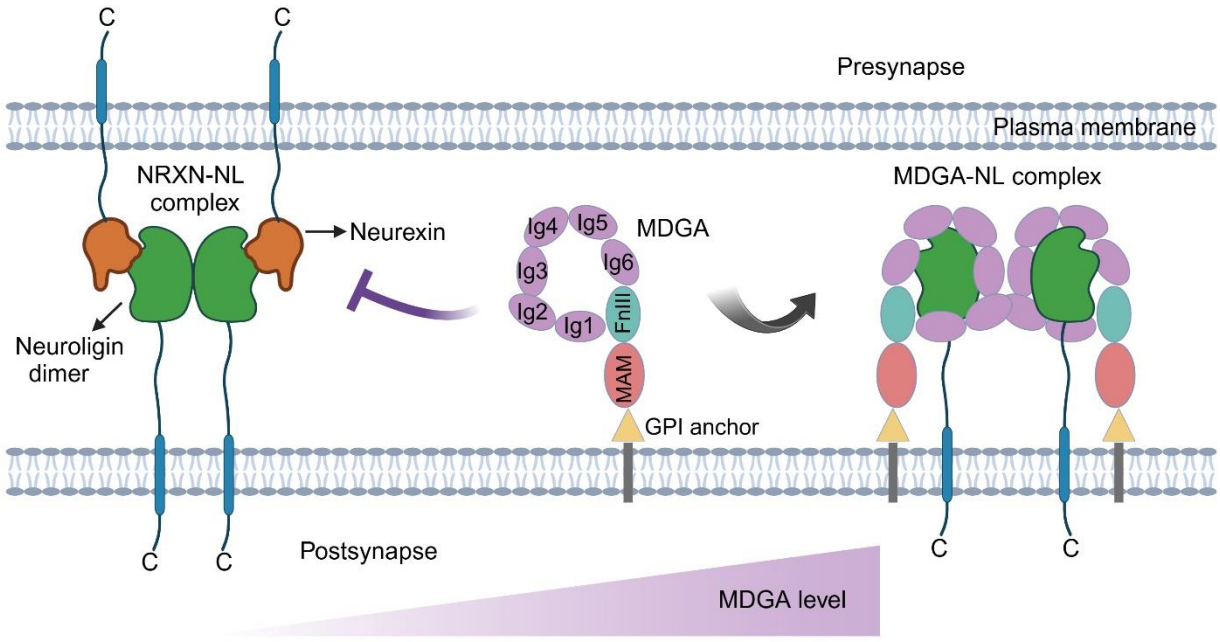

Figure 6. MDGAs and NRXN competes for binding to NLs at synapse.

When MDGA levels are low (left), NLs are able to bind with presynaptic NRXN. This NL-NRXN complex subsequently recruits the cellular machinery required for synapse validation and formation. In the presence of MDGAs (right), NLs tend to bind with MDGAs, disrupting the NL-NRXN complex. Prevention of NL-NRXN complex formation will reduce synapse formation or shift the synaptic profile in favor or NLs not bound to MDGAs. (Image generated with BioRender.com).

1.5.2 MDGAs expression and localization

The MDGAs are expressed by neurons in both central and peripheral nervous systems including basilar pons, cerebellum, hippocampus, cerebral cortex, spinal cord, amygdala and trigeminal ganglia at embryonic and postnatal stages, with continued expression in the adult brain (Connor et al., 2016a, 2017a; Litwack et al., 2004). Generally, MDGA1 expression is higher than that of MDGA2 throughout brain regions (Litwack et al., 2004). Both MDGAs are expressed in astrocytes, which are star-shaped glia cells in brain and spinal cord, playing essential roles in central nervous system (Toledo et al., 2022). Within the hippocampus, MDGA1 is expressed in pyramidal neurons but not interneurons while MDGA2 is expressed in both pyramidal neurons and interneurons, primarily localizing to the PV+ subtype of interneuron (Connor et al., 2016a, 2017a).

At the subcellular level, MDGA1 is expressed in the BPs cell membrane where it associates with the gap junction protein Connexin43 (Perez-Garcia & O'Leary, 2016). Using recombinant epitope-tagged proteins, recombinant MDGA1 was observed throughout axons and dendrites at both excitatory and inhibitory postsynaptic sites (Loh et al., 2016; Pettem et al., 2013a). However, the localization of MDGA2 is debatable. One study found that MDGA2 localization was diffuse throughout neurons (Connor et al., 2016a). Another lab discovered that MDGA2 was localized primarily at inhibitory synapses but not excitatory synapses using a more sensitive tag (Loh et al., 2016) . Recent research revealed that MDGA1 is preferentially localized at excitatory synapses, while MDGA2 is expressed at both excitatory and inhibitory synapses (Bemben et al., 2023).

1.5.2 MDGAs act as synapse suppressors

MDGAs act as negative regulators of NL-NRXN complex formation through cis-interactions (Elegheert et al., 2017; K. Lee et al., 2013; Pettem et al., 2013b). MDGA1 was reported to suppress inhibitory synapse function by blocking the NL2-NRXN complex (Connor et al., 2017b; K. Lee et al., 2013; Pettem et al., 2013a). Notably, there was an increase in perisomatic but not dendritic GABAergic synapses in MDGA1 KO mouse CA1 pyramidal neurons (Connor et al., 2017b), paralleling the results of loss of NL2 on repressing perisomatic synapses (Poulopoulos et al., 2009). In vitro experiments revealed that overexpression or sparce knockdown of MDGA1 decreased or enhanced inhibitory synapses, respectively, without affecting excitatory synapse number (Pettem et al., 2013a). Although interacting with all NLs, MDGAs interact most strongly with NL1 and NL2, with the affinity of MDGAs for NL3, NL4 and NL5 being approximately 10- to 20-fold weaker (Elegheert et al., 2017), suggesting that MDGA1 mainly suppresses NL2-meidated inhibitory synapses. By contrast, excitatory synapses were specifically enhanced on CA1 pyramidal neuronal dendrites in S.R. layer in *Mdga2*$^{+/-}$ mice (Connor et al., 2016a). In vivo experiments demonstrated that MDGA2 suppresses both inhibitory and excitatory synapse function by blocking the interaction of NL1-NRXN and NL2-NRXN. MDGA1 can compensate for lack of MDGA2 in blocking inhibitory synapses, which is supported by the results of knockdown of MDGA1 in MDGA2 lacking neurons (Connor et al., 2016a). In co-culture experiments, MDGA2 strongly suppressed NL2-meidated inhibitory synapse development (Elegheert et al., 2017). MDGA2 co-localizes with MDGA1 in most neurons, but MDGA2 is not sufficient to suppress inhibitory synapses possibly due to the lower expression level of MDGA2 compared with MDGA1 (Connor et al., 2019). In addition, we recently found that conditional knockout of MDGA2 in CA1 pyramidal neurons selectively reduced the density and suppressed

the function of excitatory synapses on pyramidal neurons in the mature hippocampus (X. Wang et al., 2024).

Interestingly, MDGAs may also act as actuators at glutamatergic synapses in addition to their roles as synapse repressors. Specifically, KD of MDGA1 or MDGA2 in mice impaired AMPAR EPSCs or NMDAR EPSCs, respectively (Bemben et al., 2023). This suggests that basal glutamatergic currents were decreased in the absence of MDGAs. However, another study found that KO of MDGA1 or MDGA2 enhanced AMPAR currents in mouse hippocampal slices. Specifically, MDGA2 KD decreased the mobilization of NL1 and GluA2-containing AMAR at synapses, suggesting more AMPARs were trapped when MDGA2 was reduced which corresponded with an increase in NRXN-NL binding. (Toledo et al., 2022).

Placed within the context of current models suggesting that MDGAs act as synapse suppressors through binding to neuroligins, these results suggest that the presence of MDGAs at a particular synapse will determine which subtype (excitatory or inhibitory) will develop. Accordingly, the presence of MDGA1 at excitatory synapses would limit the conversion of this synapse to an inhibitory synapse by sequestering the inhibitory synapse promoting neuroligin, NL2. Conversely, the presence of MDGA2 would sequester NL1 preventing the excitatory organizing effects of this isoform. Further experiments are required to determine the actuating effects of MDGAs on glutamatergic function. The possibility remains that glutamatergic receptor promoting effects may manifest in a dose-dependent manner, with the relative amount of MDGAs at synapses determining if they are promoting or suppressing glutamate synapse function.

1.5.4 The structure of MDGA-NL complex

Each MDGA monomer ectodomain forms a rigid triangular structure, stabilized by interactions between Ig1 and FnIII7 domains, which spans the NL dimers with Ig1-2 tandems, forming a 2:2 arrangement to prevent NRXN binding (Elegheert et al., 2017; Gangwar et al., 2017) (Figure 6). More specifically, Ig1 binds to one NL monomer and Ig2 binds to the other and the second MDGAs monomer binds to the NL dimer on the opposite side with symmetrical interactions (Gangwar et al., 2017). The Ig1 domain of MDGA1 was used to show that MDGA1 competes with NRXN by binding to the same region on NL2 (J. A. Kim et al., 2017).

Interestingly, recent research showed that MDGA1 can adopt both compacted triangular and more elongated forms and both states can bind to NL2. In the elongated open state, the interaction sites (Ig1-Ig2) for NLs are largely independent to the rest of the MDGAs molecule, leading to binding sites for other potential partners become possible. On the other hand, Ig4-Ig5 elbow, far away from Ig1-Ig2, is highly conserved, indicating that it may interact with an as-yet-unknown partner. In the compact form, this conserved region faces inwardly toward the center of NL-MDGA complex thus accessibility is restricted. In addition, the SSA is far from the NL-MDGA binding interface but can sterically clash with Ig6 in the compacted form of MDGA1 but less so with the elongated form. SSB in NL1 is located close to the Ig1-Ig2 binding interface, which can disrupt the NL-MDGA interaction due to direct steric hindrance (H. Lee et al., 2023) (Figure 7).

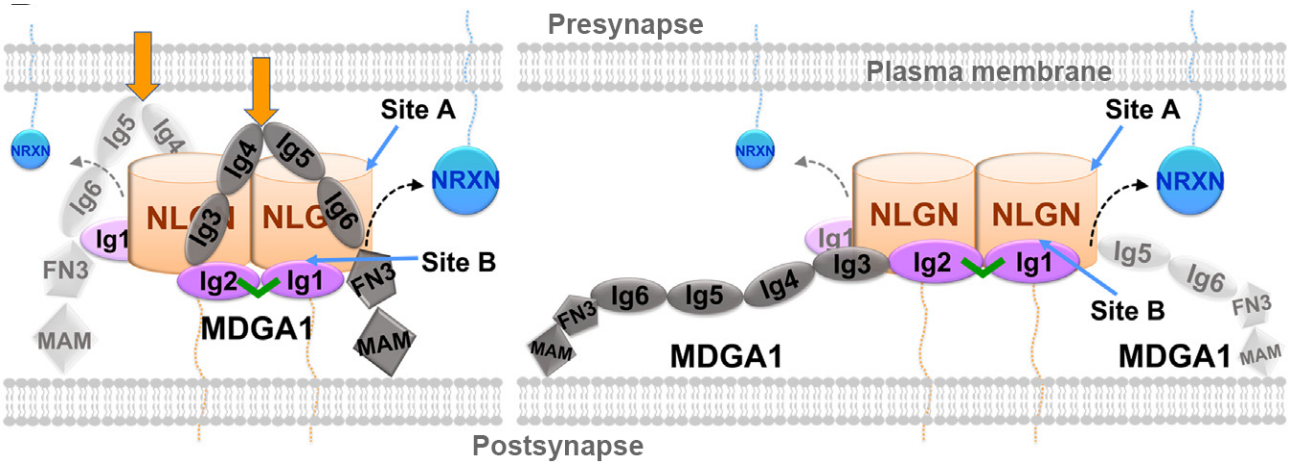

Figure 7. MDGA1 interacts with NLs.

Possible conformations of MDGA1 interacting with NLs located in the synaptic cleft. The compact triangular conformation (left) is shown. Orange arrows point to the region (Ig4-Ig5) which is highly conserved. The interdomain disulfide bond between Ig1-Ig2 is shown in green. The elongated conformation is shown (right). The NL2-interacting domains Ig1-Ig2 are highlighted in purple for MDGA1. NL SSA and SSB are discussed in the text. Image is modified from (H. Lee et al., 2023).

NL-MDGA crystal structure analysis showed that NL has two interaction sites called site I and site II, while NL-NRXN interactions only use site I (Elegheert et al., 2017). MDGAs prevent NL-NRXN complex formation through direct steric hindrance as the MDGA binding site on site I overlaps with the NL-NRXN binding interface (Elegheert et al., 2017). Accordingly, mutating five amino acids into alanine in site II prevents NL from binding to MDGAs without affecting NL-NRXN interactions (Figure 8). This NL ΔSite II model allows for the specific disruption of the NL-MDGA interaction without compromising other potential functions of MDGAs. Furthermore, site I and site II are highly conserved in MDGAs and NLs, indicating that there is a common binding pattern between all NLs and MDGAs, extending the functional range of the NL-MDGA

interaction code (Elegheert et al., 2017). Interestingly, NL2-MDGA interactions are not altered in NL2 containing SSA due to the extended distance between SSA and site I/site II. SPR further confirms that SSA does not perturb the interaction of NL2-MDGA (Elegheert et al., 2017).

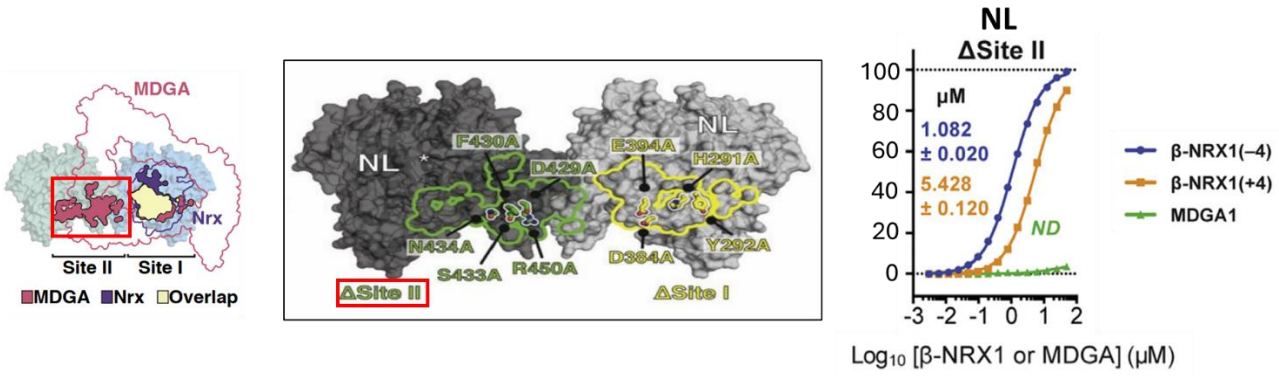

Figure 8. NL Δsite II blocks the binding of NL and MDGAs.

MDGA and NL bind at two sites, site I and site II, the MDGAs and NRXN share the NL site I interface, whereas Site II is unique to the NL-MDGA interaction. In vitro experiments showed that when the 5 amino acids in site II were mutated to alanine (Ala) ($NL^{\Delta Site\ II}$), the binding of NL and MDGA could be specifically blocked but allows binding of NRXN to NL. Image is modified from (Elegheert et al., 2017).

1.5.5 The brain function of MDGAs

Precise regulation of NL-NRXN signaling by immunoglobulin superfamily (IgSF) family MDGAs is vital to E/I balance, as genetic reduction or loss of function of MDGAs is linked to neurodevelopmental disorders (Elegheert et al., 2017). For example, in humans, intronic SNPs in MDGA1 are associated with schizophrenia (Kähler et al., 2008; Li et al., 2011), and loss-of-function truncation of MDGA2 is linked to autism spectrum disorder (ASD) (Bucan et al., 2009). In rodents, constitutive knockout of MDGA1 leads to cognitive deficits (Connor et al., 2017b) and deletion of MDGA2 results in perinatal death (Connor et al., 2016b). Administration of D-cycloserine, a co-agonist of NMDAR, can ameliorate the impaired memory and restore LTP

deficits in *Mdga1*$^{+/-}$ but not *Mdga1*$^{-/-}$ mice (Ojima et al., 2024). As early detection and diagnosis of NDDs is important for successful treatment, one recent study assessed the developmental behavioral phenotypes of *Mdga2*$^{+/-}$ mouse models from birth to weaning. They found that *Mdga2*$^{+/-}$ mice showed delayed development of motor and exploratory behaviors and deficits in grip strength consistent with developmental alterations observed in some forms of NDDs (Fertan et al., 2023).

1.6 Animal model and its advantages

As introduced above, NL-MDGA crystal structure analysis showed that NL has two interaction sites called site I and site II, while NL-NRXN interactions only use site I (Elegheert et al., 2017). MDGAs prevent NL-NRXN complex formation through direct steric hindrance as the MDGA binding site on site I overlaps with the NL-NRXN binding interface (Elegheert et al., 2017). Accordingly, mutating five amino acids into alanine (because alanine can disrupt the hydrogen bonds and electrostatic interactions) in NL site II prevents NL from binding to MDGAs without affecting NL-NRXN interactions. This NL ΔSite II model allows for the specific disruption of the NL-MDGA interaction without compromising other potential functions of MDGAs.

The site II domain of NL2 is located in the extracellular region and responsible for binding to MDGA proteins. The five key amino acids in spatial proximity are mutated into alanine. The side chain of alanine is only -CH3, without any charged or polar groups, which can eliminate side chain functional groups (such as charge and hydrogen bonds) and eliminate the interaction of the original amino acids. These mutations can directly block the bonding interface because alanine mutations remove the electrostatic or hydrophobic interactions required for MDGA binding, preventing the formation of complexes. There are some differences between NL2ΔSite II model

and other mutation models. In NL2 whole-body KO mice, all NL2 functional deficiencies lead to reduced inhibitory synapses, epilepsy, social deficits. In NL2 point mutation (such as R451C) model, it may partially disrupt multiple interactions leading to complex phenotype (social disorder with abnormal synaptic function). In NL2ΔSite II model, there is enhanced inhibitory transmission (due to the relief of MDGA inhibition), but no developmental defects. Although MDGA1 and MDGA2 are highly homologous (~60% sequence similarity), the 5-alanine mutation may have different effects on their binding. MDGA1 preferentially interacts with NL2. The affinity of MDGA2 for NL2 is relatively low. Thus, NL2ΔSite II may be more likely to affect the binding with MDGA1. MDGA1 mainly regulates PV+ INs (fast inhibition) and its absence leads to a significant increase in inhibitory input around the PNs cell body (mIPSCs frequency ↑). MDGA2 may better regulate SOM+ INs (slow inhibition) and its absence leads to enhanced dendritic inhibitory input at the distal end of PNs (mIPSCs amplitude ↑).

There are many advantages of this NL2ΔSite II mice over traditional knockout or overexpression transgenic mice. Firstly, point mutation transgenic mice preserve the natural regulation of genes by introducing a single or several base changes at a specific site, better reflecting the impact of human genetic variation on physiological and disease processes, which makes the study more reliable and more biologically significant. Secondly, compared to knockout or overexpression transgenic mice, point-mutant transgenic mice can accurately mimic specific mutations observed in human genetic diseases, providing the opportunity for in-depth research into the precise mechanisms by which these diseases occur and avenues for potential treatments. Thirdly, compared to knockout or overexpression transgenic mice, the preparation process of point mutant transgenic mice is relatively simple and rapid, because it specifically changes one or several bases rather than performing complex operations to knock out or overexpress large segments of

genes. Moreover, NL2ΔSite II model directly targets the NL2-MDGA interaction axis to avoid developmental compensation or lethal phenotypes caused by extensive NL2 KO, and more accurately simulate abnormal synaptic inhibition related to ASD. Also, retaining the synaptic localization and basic functions of NL2 while only disrupting its regulatory modules is suitable for studying the impact of specific signaling pathways on behavior. This model highly simulates the core symptoms of human ASD. The phenotypes (increased anxiety, increased fear memory and impaired social memory) are highly consistent with the behavioral characteristics of human ASD patients, especially the ASD subgroups related to NLGN2 gene mutations or MDGA1/2 abnormalities. This point mutation model is applicable to mechanism-behavior transformation research. The target can be verified through pharmacology such as $GABA_AR$ modulators or genetic intervention such as MDGA1/2 conditional KO, promoting the development of precision treatment strategies. Therefore, point mutation transgenic mice have become an important tool to explore the mechanisms of genetic diseases and develop new treatment strategies.

The unique feature of this NL2ΔSite II model is five key amino acids of NL2 Site II mutated to alanine, specifically blocking the binding of MDGA1/2, but not affecting NRXN-NL2 or other interactions such as gephyrin. In the traditional overexpression model, non-physiological high expression may lead to incorrect localization of NL2 (such as in axons or non-synaptic regions). It is impossible to distinguish whether NL2 functions is MDGA-dependent or non-dependent. Compared to overexpression model, mutant NL2 is expressed under the control of a natural promoter, maintaining spatiotemporal specificity. Only the MDGA-NL2 interaction is disrupted, while the other functions of NL2 are retained. Overexpression may saturate postsynaptic scaffold proteins (such as gephyrin), while the NL2ΔSite II model only enhances inhibitory synapses through MDGA dissociation, which is closer to the real disease mechanism.

1.7 Aims, Hypothesis and Predictions:

We designed NL2 site II point mutation (NL2ΔSite II) transgenic mice and hypothesized that unbinding of NL2 and MDGAs can enhance inhibitory synaptic transmission, disrupt the E/I balance, and affect behaviors in mice which correlate with neurodevelopmental disorders (Figure 9). To advance our understanding of the roles of NL-MDGA interactions, I have developed four aims: **Aim1:** To construct and verify the NL2ΔSite II animal model. **Aim2:** To explore the effect of NL2ΔSite II on synapse density and function within the hippocampal CA1 region. **Aim3:** To investigate whether the NL2ΔSite II model demonstrates physiological changes related to NDDs. **Aim4:** To determine the changes in behavioral outputs in NL2ΔSite II animals and their relevance to NDDs.

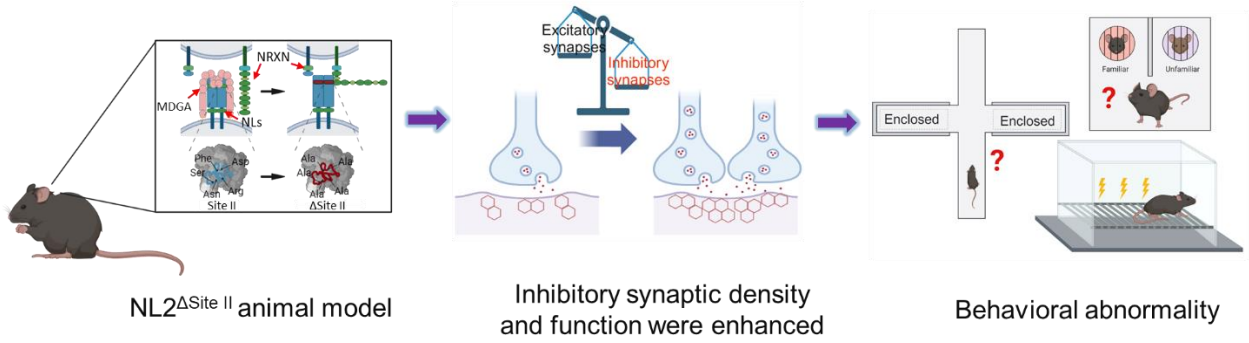

Figure 9. NL2ΔSite II transgenic mice and hypothesis.
Unbinding of NL2 and MDGAs can enhance inhibitory synaptic transmission, disrupt the E/I balance, and affect behaviors in mice which correlate with neurodevelopmental disorders.

Given previous results establishing the role of NL2 in GABAergic synapse development, and that MDGAs act as suppressors of NL2-mediated synapse development, I hypothesize that point mutations that prevent NL2-MDGA binding will increase inhibitory synapse density and

function in pyramidal neurons. I predict that GABAergic inputs onto neurons in which NL2 is no longer bound to MDGA will be upregulated. Furthermore, as mutations in NLs or MDGAs contribute to NDDs such as ASD and SCZ, I hypothesize that the NL2ΔSite II model will share physiological, behavioral and genetic markers for these disorders. I predict this point mutation model mouse will show abnormal behaviours consistent with human phenotypes identified in NDDs.

By conducting behavioral tests, electrophysiological recordings, bioinformatics and molecular biology experiments on this transgenic mouse model, we will attempt to uncover the role of MDGA-NL interactions in regulating E/I balance and determine how perturbation of these interactions contributes to the development of neurodevelopmental disorders. This research is expected to provide critical new insights into the nature of synapse development and how loss of these MDGA-NL interactions perturbs these processes. This work will lay the foundation for new therapeutics that target key aspects of the pathogenesis of neuropsychiatric and neurodevelopmental disorders and provide a scientific basis for the prevention and treatment of related diseases.

Chapter 2 Methods and Materials

2.1 Subjects

2.1.1 Acquisition of transgenic mice

2.1.1.1 NL2$^{Mut/Mut\ flox/flox}$ mice

The NL2$^{Mut/Mut\ flox/flox}$ mice were constructed by Beijing Biocytogen Gene Biotechnology Co., LTD. Transgenic mice specifically mutated five key amino groups encoding the binding site of NL2 and MDGA1. Specific mutations were made to the 5 key amino acids at the binding site II of NL2 and MDGA1 in exon 6 of the gene sequence, thereby blocking the binding of NL2 and MDGA1. In the conditionally knocked-in NL2 mutant transgenic mice, exons 3-7 between the two loxP sites represent the exons of the normal NL2 gene with the introns removed, and there is a terminator on the right side of the 3'UTR that causes transcription termination, thus enabling these transgenic mice to express the normal NL2 protein. When this mouse undergoes the process of injecting Cre virus or hybridizing with Cre tool mice to express Cre recombinase, and deletes the 3-7 exon sequence between the loxP sites, and expresses the subsequent sequence containing the mutated exon 6, the 5 key amino acids at the Stie II in the expressed NL2 protein will mutate to alanine (Asp407Ala, Phe408Ala, Ser411Ala, Asn412Ala and Arg428Ala), and will not bind to MDGAs. Specifically, this was achieved by mutating 9 DNA bases in exon 6 (A234C, T236C, T237C, T246G, C248T, A249G, A250C, C297G and C298G). The mutant mice were confirmed through genetic identification and DNA sequencing. After DNA extraction, the samples were sent to Qingke Biotechnology Co., Ltd. for sequencing to confirm that the NL2 mutation was successfully introduced.

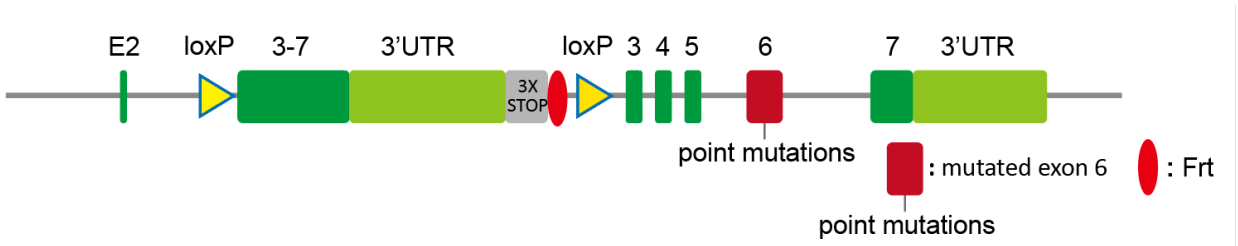

Figure 10. Genetic structure diagram of NL2Mut/Mut flox/flox mice.

2.1.1.2. NL2$^{Mut/Mut}$ mice

Hybridization strategies of transgenic mice with NL2ΔSite II: NL2$^{f/f}$ mice were hybridized with CMV-Cre tool mice (genotype CMV-Cre$^{+/-}$, https://www.jax.org/strain/006054) to produce the NL2 site II point mutant (NL2ΔSite II) whole-body knock-in heterozygous mouse (genotype NL2$^{Mut/+;}$ CMV-Cre$^{+/-}$). Secondly, the progeny was hybridized with WT mice to produce NL2ΔSite II heterozygotes (genotype NL2$^{Mut/+}$) and further hybridized with NL2$^{Mut/+}$ mice to obtain NL2ΔSite II homozygous mutant mice (genotype NL2$^{Mut/\ Mut}$). The NL2 protein expressed systemically in these mice all had the aforementioned mutations and did not bind to the MDGA1 protein.

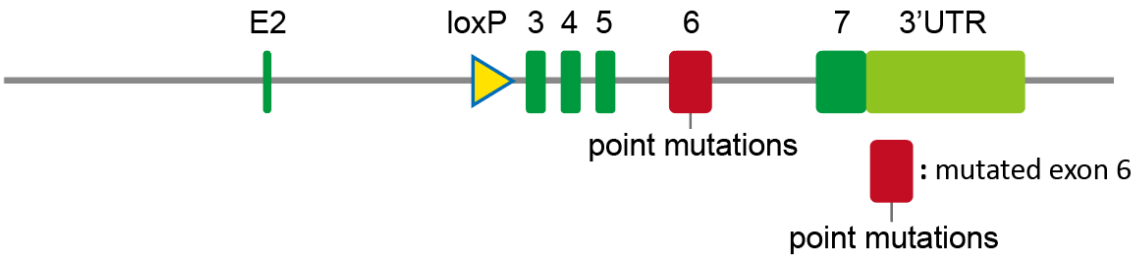

Figure 11. Genetic structure diagram of NL2Mut/Mut mice.

2.1.1.3. MDGA1$^{-/-}$ mice

The conditional MDGA1 knockout transgenic mice through traditional embryonic stem cell transgenesis technology. The targeting plasmid was purchased from the European Transgenic Mouse Collection (EUCOMM). Specifically, the MDGA1 gene was inserted with the Frt-Lacz-Frt marker fragment, thereby blocking the expression of MDGA1. Therefore, the MDGA1 knockout mice were the first to be targeted for deletion. In addition, LoxP sequences were inserted on the left side of exon 5 of MDGA1 and on the right side of exon 6 of this transgenic mouse. Therefore, when this transgenic mouse was crossed with the ROSA26-FLPO tool mouse to remove the Frt-Lacz-Frt fragment and restore the expression of MDGA1, a conditionally knockout MDGA1 floxed mouse could be obtained.

Figure 12. The genetic structure diagram of MDGA1-/- mice.

2.1.1.4. MDGA1$^{flox/flox}$ mice

The MDGA1$^{flox/flox}$ conditional knockout mice were obtained by crossing the aforementioned MDGA1$^{-/-}$ mice with the ROSA26-FLPO tool mice. The Frt-Lacz-Frt fragment was excised through hybridization with the FLPO tool mice, allowing for normal expression of MDGA1. Meanwhile, the LoxP sequences inserted on the left side of exon 5 and the right side of exon 6 of MDGA1 remained intact. Therefore, it became an MDGA1 conditional knockout mouse.

This mouse can be injected with a virus expressing the specific tissue or cell Cre recombinase, or be crossed with Cre tool mice to achieve the specific knockout of this gene.

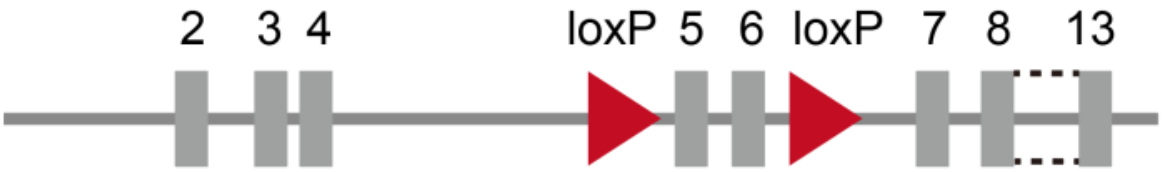

Figure 13. The genetic structure diagram of MDGA1flox/flox mice.

2.1.1.5. MDGA2$^{flox/flox}$ mice

The C57BL/6J background MDGA2$^{flox/flox}$ mice were generated by Biocytogen Pharmaceuticals Co., Ltd (Beijing, China). The generation of MDGA2$^{flox/flox}$ mice was as previously described (J. Kim et al., 2022). LoxP sequences were inserted on the left and right side of exon 2 of MDGA2.

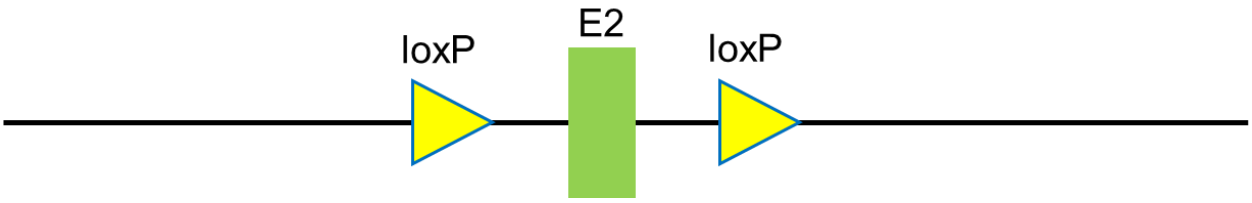

Figure 14. The genetic structure diagram of MDGA2flox/flox mice.

2.1.1.6. MDGA1 $^{flox/flox}$ MDGA2$^{flox/flox}$ mice

Double flox mice were obtained by hybridizing MDGA1$^{flox/flox}$ mice with MDGA2$^{flox/flox}$ mice.

2.1.1.7. CMV-Cre mice

Rationale: The CMV-Cre germline knock-in mouse is a widely used tool mouse for systemic and constitutive gene knockout. Cre recombinase is continuously expressed in all cells throughout the body, including germ cells, and is driven by the cytomegalovirus (CMV) promoter. The main application of CMV-Cre mice is to conditionally delete the target genes with flanked loxP (loxP loci on both sides) in all tissues to achieve systemic knockout.

Generation Strategy: Usually, the CMV-Cre expression cassette is inserted into the "safe harbor" sites in the mouse genome (such as Rosa26 or Hprt sites) to ensure that it does not affect the functions of other genes. Design the vector which is composed of CMV promotor, Cre recombinase cDNA, PolyA signal and screening markers such as neoR. Then target the embryonic stem cell (ES). Insert the CMV-Cre-neoR into the safe harbor site. The vector was transfected into mouse ES cells and integrated into the genome through homologous recombination. Successfully recombinant ES cells were screened using G418 (neoR resistance) and verified by PCR or Southern blot. Next, prepare chimeric mice. The verified ES cells were injected into blastocysts and transplanted into the uteruses of pseudopregnant female mice. After birth, chimerism is confirmed through coat color or genotype testing. Chimeras were mated with wild-type mice to screen for germline transmission of CMV-Cre mice (F1 generation). Finally, do strain purification and validation. NeoR was removed in FLP/ deleter mice to avoid interfering with gene expression. NeoR was removed in FLP/ deleter mice to avoid interfering with gene expression.

2.1.2 The rearing of mice

Five to six mice of the same sex were kept in each standard plastic mouse cage at the Animal Laboratory Center of City College of Zhejiang University with SPF grade housing and the

temperature was maintained at 24±2℃, with the relative humidity maintained at 40%-60%. The animals had access to water and food *ad libitum* and they were maintained on a 12/12 hour light/dark cycle. All experimental procedures described in this article were approved by the Animal Care Committee of Zhejiang University (No. ZJU20220294).

Experimental grouping: 8-12-week-old and weighing 20-26 grams male mice in the same cage and litter were used as control and experimental groups.

2.2 PCR and Sanger sequencing detection of NL2ΔSite II successful knock-in

PCR method: The mice used for breeding are usually kept 3 per cage (1 male and 2 females) and tail clips were harvested and genotyped when the pups were 28 days old. 400 μL 50 mM NaOH solution was added into a centrifuge tube containing mouse tail or toe and heated at 100 ℃ for 20 min using a thermostat. After cooling to room temperature, 40 μL 1 M Tris-HCl buffer with a pH of 6.8 was added to the tube, centrifuged at 4 ℃ (12,000 rpm, 5 min), and the 100 μL supernatant was absorbed into a new tube and stored at 4 ℃. Mixed solution was prepared in sterilized 1.5 mL centrifuge tubes according to the mixing system, the single mixed sample system is shown in Table 1. The successful knock-in was then identified by PCR (NL2: forward-5` to 3`: TGGTAACTGGGGAGGTGACCTAGAA, reverse: TGTTGGACACACTTTCCAAGAAGCC; CMV-Cre: forward-5` to 3`: CAGAACCTGAAGATGTTCGC, reverse: CCTGATCCTGGCAATTTCGG), amplification systems of PCR are shown in Table 2. And knock-in was further confirmed by southern blot analysis. More specifically, 2 g agarose was weighed into a conical bottle and 100 mL 1 x TAE was added. The mixture was heated for 1 min, shook and reheated for 30 s, which was repeated

twice. When there are no crystalline particles in the solution, the mixture was cooled to below 60 ℃, 3μL nucleic acid red dye was added and shaken well. The gel solution was quickly poured into the gel tray where the comb is located, the bubbles were removed, and the gel solution was solidified for 30 minutes. Once the gel had set, the comb was lifted upright with both hands. The gel hole was oriented towards the negative end of the horizontal electrophoresis tank, and DNA marker and PCR product 5μL each were added. The voltage was set to a constant voltage of 120 V, and the time was set for 30 min. After the electrophoresis, the gel was put into the gel imager and the experimental data was saved.

Table 1. PCR reaction system of Green Taq Mix（Total volume: 20 μL）

Reaction component	Volume（μL）
10 μM Primer-F	0.5
10 μM Primer-R	0.5
ddH2O	7
Green Taq Mix	10
Template DNA	2

Table 2. PCR reaction process

Step	Temp	Time	Cycles
1	95℃	3 min	1
2	95℃	15 sec	32
3	62℃	20 sec	

4	72℃	1 kb/min	
5	72℃	7 min	1
6	4℃	hold	1

Sanger sequencing method: Sanger sequencing was used to verify whether the NL2ΔSite II was successfully knocked in. Sanger sequencing is also known as “chain termination method”, an approach for determining the nucleotide sequence of DNA. This method was developed by English biochemist Frederic Sanger and his colleagues in 1977. In addition, RNAseq is a technique used to study the composition and quantity of all RNA molecules in a cell or tissue. PCA is a commonly used data dimensionality reduction technique, which transforms the original data into a set of new variables that are linearly independent in each dimension through linear transformation. This process helps extract the features that best distinguish the differences between the two groups.

The mouse tail and brain tissue were stored in 1.5mL centrifuge tubes, then quickly frozen in liquid nitrogen and stored at -80℃. DNA was extracted and amplified with high-fidelity DNase (Takara, # RR047A) (amplification system is the same as above) and stored at -80℃. Total RNA was extracted using TRIzol reagent, quantified by spectrophotometer (Thermo Scientific NanoDrop 2000), and reverse-transcribed into cDNA using HiFiScript cDNA synthesis kit, and stored at -80℃. Then these samples were sent to TsingkeBiotechnology Co., LTD, primers (NL2: forward-5`-3`: GGGAGCTACCTATGTGTGGCTTAGG, reverse-5`-3`: CCTGGCAGTGGTGGTAGAAAGTGTA) were used for sanger sequencing of DNA and cDNA of each group. NL2 corresponding to 9 mutant base pairs was observed on SnapGene.

2.3 Immunohistochemistry

The Western Blot and immunostaining techniques are often used to examine synapse density in hippocampus. Both methods identify specific proteins present in the tissue sample by using antibodies that attach themselves to the antigens. Visualizing these key interactions can be achieved using a fluorophore (creating a fluorescent signal) or enzyme (producing a chromogenic signal).

The mice were anesthetized by intraperitoneal injection of 1% pentobarbital (10 mL/kg), when the pinch reflex disappeared, mice were considered anesthetized successfully. After exposing the thoracic heart, a needle was inserted into the left ventricle from the apex of the heart and fixed. After cutting the right auricle, a peristaltic pump was used to slowly pump iced 1× PBS (4 mL/min) into the heart. After 5 min, the liver color of mice turned yellow confirming successful perfusion, after which iced 4% PFA (pH 7.4) was pumped into the mice to fix the tissue (5 mL/min). The brains were collected and post-fixed in 4% PFA in a 15 mL centrifuge tube at 4 ℃ for 24 hours. To dehydrate the brains, they were stored in 15% sucrose for 24 hours, until the brains sunk to the bottom, and in 30% sucrose for 24 hours, until the brains sunk to the bottom. The dehydrated mouse brains were taken out and carefully placed on filter paper to remove the surface liquid, then coated with OCT (Sakura, #4583) and placed on a freezer for quick freezing.

The location of the hippocampus (Bregma~-1.7 mm to ~-2.8 mm) was determined according to the stereotaxic map of Paxinos and Franklin in mouse coronal section. The brain slices (40 μm) were placed into a 12-well plate containing antifreeze and stored at -20 ℃. Then the brain sections were removed from the antifreeze, rinsed with 1×PBS for 5 min, which was repeated 3 times. Subsequently, the brain sections were placed into 48-well plates (one slice per well) with

200 μL blocking buffer per well and incubated at 37℃ for 1 hour. Each well was subsequently rinsed 3 times with 200μL 1× PBS for 5 min. The liquid in the well plate was discarded, and 150 μL of the primary antibody working solution was added to each well to ensure slices infiltration. Then the slices-containing plate was incubated overnight in a 4 ℃ on a shaker. The next day, the primary antibody solution was discarded and 200μL 1× PBS was added into each well and rinsed for 10 min. Next, 150 μL of the secondary antibody working solution was added into each well, and the slices-containing plate was incubated in a dark room at 37℃, away from light, for 2 h. The secondary antibody solution was discarded, 200μL 1× PBS was added into each well and rinsed for 10 min. The brain slices were spread out on the microscope slides (Citotest, #188105W) and dried away from light for 10 min. After there was no obvious moisture, the slices were coverslipped using DAPI sealant (SouthernBiotech, #0100-20). Then, the specimen was sealed with transparent nail oil to prevent the fluorescence fading with water and stored in a 4 ℃ dark box.

There were 3-5 mice in each group in the control group and the experimental group. 3 brain slices were taken from each mouse and confocal microscope (Zeiss, Germany) was performed under the same parameter setting. A 63x/1.4NA oil mirror was used, an image of 1024 × 1024 pixels is obtained at a scan frequency of 200 Hz, with a pixel size of 90.19 nm× 90.19 nm. In confocal 3D imaging, a vertical step of 0.05-0.1μm is used to obtain a continuous image of the Z-axis plane. Finally, ImageJ software was used to observe and quantify the fluorescence area, quantity and colocalization of antibody.

2.4 Western blotting

Bilateral hippocampi of mice were collected and weighed using ten-thousandth balance. PMSF and protease inhibitor mixture were added into Syn-PER synaptic protein extraction reagent. This reagent was added into a 1.5 mL centrifuge tube at 10 μL/1 mg. The homogenizer was used to homogenize the samples on ice at the highest speed 5-10 times until there were no obvious tissue fragments (ultrasound is not recommended to prevent excessive cell membrane breakage and membrane protein integration into the supernatant). The tube was centrifuged at 4℃ to 1,200 g for 10 min, then the supernatant (2/3 volume of synaptic protein extraction reagent) was taken into a new 1.5mL EP tube, and centrifuged again at 4C° to 15,000g for 20 min. After all supernatants were discarded, 100 μL Syn-PER was added to the re-suspend precipitated synaptic protein. After complete dissolution, the protein concentration was determined by BCA (Beyotime, # P0010S). 5 × loading buffer and Syn-PER buffer were added into tubes and underwent a mixed metal bath at 55 C° for 10 min (to prevent aggregation and denaturation of most synaptic membrane proteins after boiling). After thawing at 4 C°, the protein samples were bathed in a metal bath at 60 C° for 5 min, centrifuged at 4 C° (12,000 rpm, 4 min), and then used for sampling. The protein (~ 20 μg) was isolated by TRIS-SDS-PAGE 15-well gel with 6%-8% gradient gels and run at 80V constant pressure electrophoresis. 120 V constant pressure electrophoresis was completed after about 50 min. The SDS-PAGE gel was cut to the required size and placed in the sandwich plate. Using the wet transfer method, 260 mA constant flow was applied during transferring at 4 ℃ for 90 minutes. Then the PVDF membrane was removed and washed in a horizontal shaker with 1× TBST (Solarbio, TBS, #T1087, Tween80, # T8220) at room temperature for 5 min. After transferring, the PVDF membrane was blocked with 5% BSA (Sigma, HZB0148) TBST blocking buffer (at least 1

min of vortex oscillation when it was prepared in advance) at 25 rpm on a horizontal shaking table for 1 h. The film was then rinsed 4 times with 1× TBST for 10 min. The PVDF membrane was cut according to desired protein position. The 5% BSA TBST solution diluted with the primary antibody was added to the membrane, and the primary antibody was incubated overnight at 10 rpm in a horizontal shaker at 4℃, ensuring that the incubation time was not less than 10 h. The next day, the membrane was washed with 1× TBST solution on the shaker for 3 times, 10 min each time. The secondary antibody was diluted with 5% BSA 1×TBST solution and incubated at 25 rpm on a horizontal shaker at room temperature for 1 h. The membrane was washed with 1x TBST solution on shaker for 3 times, 10 min each time. The target strip was developed using Odyssey CLx film scanner. The vector images were exported at 300 Dpi, and the adjustable Odyssey CLx zip package was saved. The strip gray value was quantified by ImageJ and statistics was performed by Graphpad.

The primary antibodies for inhibitory synapse data were as follows: anti-GAD65 (mouse IgG2a, 1:25, Developmental Studies Hybridoma Bank, #AB528264), anti-vGAT (mouse IgG3, 1:2000 for western blotting, 1:500 for immunohistochemistry, Synaptic System, #131011), anti-gephyrin (mouse IgG2b, 1:1000 for immunohistochemistry, NeuroMab, #75-443). The primary antibodies for excitatory synapse data were as follows: anti-vGLUT1 (Guinea pig, 1:500 for immunohistochemistry, 1:2000 for western blotting, Synaptic Systems, #135304), anti-PSD95 (mouse IgG1, 1:1000 for western blotting, NeuroMab, #75-348). Secondary antibodies used were toward the appropriate species and conjugated to Alexa-488, Alexa-568, Alexa-647 (1:1000; Invitrogen) for immunohistochemistry, IRDye 800 (1:5000, LI-COR biosciences), DyLight 800, DyLight 680 (1:5000, Cell Signaling) for western blotting.

2.5 Behavioural Assays

GABAergic inhibitory interneurons fine tune spatial memory formation in the hippocampus. Notably, E/I imbalances in the hippocampus disrupt the proper formation of place fields, which constitute the cellular memory trace for places within a given spatial context (Andrews-Zwilling et al., 2012; Cutsuridis & Hasselmo, 2012; Murray et al., 2011). Several behavioral tests allow for a thorough discussion of behavioral changes associated with altered synaptic function that are well validated. For example, open field tests measure mobility and anxiety, Y-maze tests measure spatial working memory, the elevated plus maze test monitors anxiety, fear-conditioning tests measure learning and memory, three-chamber interaction tests monitor sociability and social memory, NOR measures cognitive function and memory and rotarod test assays motor coordination and balance ability.

In 1950s, the relationship between the hippocampus and episodic memory was first identified when a patient called H.M. suffered from amnesia after bilateral removal of his hippocampus (Scoville & Milner, 1957). Despite retaining normal levels of intelligence, H.M. displayed profound deficits in certain forms of memory, including anterograde contextual and semantic memory impairments. It is now known that the hippocampus is essential for both the memory encoding and retrieval processes (Davachi & DuBrow, 2015). Intriguingly, the hippocampal CA2 region is responsible for social recognition memory, whereas the CA1 region plays a greater role in contextual memory formation (Tzakis & Holahan, 2019).

Acquiring information and using it to navigate complex relationships is required for normal performance in social situations. Thus, one must have the ability to deduce the emotions and

intentions of others, predict their actions and respond to changes in the social environment (Banker et al., 2021).

ASD patients demonstrate social deficits as a core behavioral feature. For example, patients with ASD often have difficulties in keeping appropriate physical distance from other people (Kennedy & Adolphs, 2014), indicating impaired conceptualizations of interpersonal space. Interestingly, the presence of 'social place-cells' in hippocampus have been detected, which may represent both one's own and others' positions in space (Omer et al., 2018). The hippocampus also plays a pivotal role in spatial reasoning predicted on the function of 'place cells', neurons that selectively fire at particular spatial locations within an environment (O'Keefe & Dostrovsky, 1971). In real-world scenarios, hippocampal activity is vital for the cognitive representation of distances between real-world locations (Morgan et al., 2011). Moreover, the hippocampus has been heavily implicated in episodic memory, spatial learning and contextual fear (Fanselow & Dong, 2010). Taken together, these data support that cognition predicated on intact hippocampus function may be compromised under conditions in which synaptic connectivity and function deviates from the norm.

Anxiety is an emotional state that results in defensive behaviors when animals are faced with aversive stimuli, which is important for survival. According to epidemiological reports, there is higher incidence rates of fear- and anxiety-based disorders in women than men (McLean et al., 2011; Tolin & Foa, 2006). The hippocampus has been associated with regulating fear and anxiety by interacting with multiple brain regions including PFC, amygdala, hypothalamus, and the nucleus accumbens (Bannerman et al., 2004; Ghasemi et al., 2022). For example, the hippocampus inhibits the HPA axis, the major stress pathway in the brain. Accordingly, lesions of the

hippocampus impairs hormonal stress response regulation (Dedovic et al., 2009). In turn, increase levels of stress hormones results in hippocampal dysfunction (Herman et al., 2005).

Pathological anxiety is characterized by excessive and persistent fear when faced with threats or nonthreatening stimuli (Graham & Milad, 2011). Both physiological and pathological (innate/learned) fear/anxiety are associated with altered hippocampal activity. Pavlovian fear conditioning is a classic model for studying fear and anxiety. The hippocampal subregions are crucial to process contextual fear information, among which DG, CA1 and CA3 have been implicated in contextual fear acquisition, and the DG and CA1 support contextual fear memory retrieval (Bernier et al., 2017; Morellini et al., 2017). Through long range projections changes in the excitability of CA1 neurons affect the activity of other brain areas (e.g. PFC, amygdala, hypothalamus, and nucleus accumbens) involved in fear and anxiety (Cenquizca & Swanson, 2007; Loureiro et al., 2016; Swanson, 1981; Tannenholz et al., 2014).

Contextual fear conditioning using aversive electric footshock is commonly used to assess hippocampal function in spatial (context fear) and nonspatial (cued fear) memory. In this task, the animal is placed in a chamber where they receive a mild electric footshock, signaled by a brief tone within the cued paradigm. When subsequently returned to the same chamber the animals will freeze, with the time spend immobile (freezing) indicative of memory strength (J. J. Kim & Fanselow, 1992). Genetic, pharmacological, and lesion manipulations of the hippocampus all induce deficits in contextual fear (Fanselow & Dong, 2010).

Anxiety and memory impairments are important aspects of ASD. Studies have shown that patients with ASD often experience higher level of anxiety, exacerbating memory difficulties (Leachman et al., 2024). Thus, in designing and conducting behavioral experiments, particular attention should be paid to anxiety and memory impairments in patients with ASD.

Identifying cellular and molecular mechanisms and neural circuits that regulate hippocampal activity in emotion is beneficial for targeted drug discovery for treating of brain disorders.

At least 12 male mice aged 8-12 weeks in each group were selected for behavioral analysis which took place from 9 a.m. to 6 p.m. Before the behavioral experiments, the mice were handled and stroked for 5-10 minutes every day for at least 7 days. Before the daily tests, each group of mice was put into the behaviour room to get familiar with the environment in advance for at least 1 hour. The apparatus and cages were washed with ethanol to remove any residual odors.

2.5.1 Open field test

A cubic open box (40 cm× 40 cm× 40 cm) was used as an open field. The mice were placed in the box, facing the wall, along the bottom center, and allowed to move freely for 10 minutes. During this period, Ethovision software recorded the mouse activity and tracked total travel distance, and quantified the frequency and time of entering and leaving the center of the open field (20 cm×20 cm×20 cm).

2.5.2 Novel object recognition

The experiment is mainly divided into three stages: adaptation period, familiarity period and testing period. For the adaptation period, the same experimental device and placement method as the open field was used. The mouse was allowed to move freely for 10 minutes to adjust to the environment. For the familiarity period, two identical objects (A1 and A2) were installed and

secured in the box, ensuring that the objects were placed in the same position relative to the chamber. The mice were placed in the center of the bottom edge facing away from the object, and the number of explorations of the mice for each object for 10 minutes was observed and recorded. Exploration was defined as the number of times the mouse's nose or mouth touched the object and the number of times it explored within 2-3 cm of the object. For the testing period, 1 h after the end of the familiarity period was chosen as the time interval for the short-term memory test. One of the objects was replaced with different shapes, and the mouse was placed into the box according to the above method, the number of explorations of the mouse was observed and recorded for each object for 10 minutes.

2.5.3 Three-Chamber test

An open-air rectangular box (60 cm× 40 cm× 22 cm) was used as the three-box experimental equipment. It was divided into 3 identical chambers by 2 partitions with channels (4 cm× 4 cm× 4 cm) in the middle of each partition, thus allowing the mice to move freely in the box. The middle is the starting area, while there is one cylindrical cage in the middle (7.5cm in radius and 20cm in height) of the left and right rooms respectively. During the adaptation period, each mouse was placed into the middle chamber to explore all three chambers for 5 min. For the sociability test, after 5 min, the test mouse was placed in the middle chamber. The first stranger-stimulus mouse (Stranger1) was placed in the left cage, with the right (Cage only) empty. The entry time, frequency and sniffing frequency of mice in the three areas were observed and recorded within 10 minutes. For the social novelty test, after 10 min, this test mouse was placed in the middle chamber and the second stimulus mouse (Stranger2) was placed in the right empty cage. The test mouse was then allowed to explore freely for another 10 min. Exploration was defined as

the number of times the mouse's nose or mouth touched the cage and the number of times it explored within 2-3cm of the cage).

2.5.4 Elevated plus maze (EPM)

The EPM consists of two open arms and two closed arms, which are oriented in the shape of a cross. The intersection part is the central area. Each mouse was placed in the central area, and the activity track of the mice within 10 minutes, the number of times they entered each area and the stay time within each arm of the maze were recorded.

2.5.5 Y maze

A polypropylene wall with three arms (30 cm× 5 cm× 15 cm) was used as the experimental equipment. The bottom was called the starting arm, the right was the novelty arm, and the left was the other arm. For the spontaneous alternation task (which tests spatial working memory), each mouse was placed in the center of the bottom edge with their back to the wall of the starting arm. Within 8 minutes, the spontaneous alternations index was calculated manually according to the sequence and frequency of entering each arm by each mouse. For the novel arm exploration experiment, it is mainly divided into two stages: the training period and detection period. In the first stage, the novel arm was closed with a partition, and each mouse was placed in the center of the bottom edge facing away from the wall of the starting arm. The number of explorations into the other two arms within 5 minutes was observed and recorded. One hour later, the second stage of the experiment was carried out. The novel arm was opened, and each mouse was put back into

the experiment. The number of visits to each arm within 5 minutes was recorded, so as to compare the index of visits to the novel arm in each group.

2.5.6 Rotarod test

This task is divided into two stages: the training period and the experimental period. In the first stage (training), the mice were placed on a rotating rod at a constant speed of 5 rpm/min for 5 min. In the second stage (experimental), the mice were placed on a rotating rod and accelerated from 5 rpm/min to 60 rpm/min in 5 minutes. The mice were tested twice a day. The test interval was 1 hour. The latency to fall from the rod was recorded.

2.5.7 Contextual fear conditioning

During fear acquisition, each mouse was placed into the conditioning chamber (60 cm× 60 cm × 60 cm, Harvard Apparatus) for a total of 300 s. After 120 s exposure in the chamber, a 2 s, 0.5 mA foot-shock was delivered through the grid floor. This process was repeated two more times which started at 180 s and 240 s respectively. The freezing (absence of movement, except respiration) percentage was recorded. During fear memory retrieval, each mouse was placed back in the same chamber 24 and 72 hours later, and the freezing percentage was recorded.

2.6 Ex vivo slice electrophysiology recording

In addition, electrophysiology (whole-cell patch clamp) was used to examine synaptic transmission. mPSCs are spontaneous synaptic events that are generated by ongoing spontaneous

exocytosis (without presynaptic action potentials) of single (or more) synaptic transmitter vesicle(s) (Chiang et al., 2021; Gordleeva et al., 2023; Wierenga & Wadman, 1999). mEPSCs or mIPSCs are evoked by vesicular release of glutamate or GABA neurotransmitters, respectively.

The generation mechanism of EPSC can be divided into the following key steps: 1) APs arriving leads to depolarization of presynaptic neurons. Voltage-gated calcium channels (VGCCs, such as CaV2.1) are open and Calcium influx the presynaptic neurons. Calcium triggers the fusion of synaptic vesicles with the plasma membrane and glutamate is released into the synaptic cleft. The released glutamate diffuses into the postsynaptic membrane and binds to two types of ionic receptors (AMPARs and NMDARs). AMPARs mediate rapid Na^+/K^+ permeability and generate a rapid ascending phase (early component) of EPSC. NMDARs mediate the slow $Ca^{2+}/Na^+/K^+$ permeability and generate the continuous phase (late component) of EPSC.

To resolve the effects of NL2ΔSite II on dynamics of synaptic transmission, mEPSCs and mIPSCs from neurons within hippocampal slices were recorded. The amplitude of mPSCs reflects the "strength" (amount of current) flowing through postsynaptic receptors, and the frequency of mPSCs reflects the number of spontaneously active synapses or their neurotransmitter release probability (Wierenga & Wadman, 1999). PPR is used to study synaptic transmission and synaptic plasticity. Two short spaced pulses (stimuli) act on the neuron successively, and by comparing the postsynaptic current (or potential) caused by the two pulses, information about the probability of presynaptic release and the postsynaptic response can be obtained. PPR is calculated by the ratio of the postsynaptic response caused by the second pulse (P2) to the postsynaptic response caused by the first pulse (P1), namely: PPR=P2/P1. PPR value can reflect the change of presynaptic release probability. PPR > 1 indicates the enhanced response of the second pulse, which is called PPF. If PPR < 1, the response of the second pulse is diminished, which is called PPD. Intrinsic

Excitability refers to the ability of neurons to spontaneously generate electrical activity in the absence of external stimuli. Measuring intrinsic excitability usually involves the membrane potential change (The changes of cell membrane potential were recorded to observe the reaction of cells under different conditions), action potential threshold (Determine the minimum stimulus intensity required to trigger an action potential), discharge frequency (Measures how often a cell generates an action potential in response to sustained stimulation). Ramp and step stimulation are two commonly used electrophysiological techniques for measuring intrinsic excitability of cells. Ramp stimulation refers to the way in which the current or voltage is gradually increased or decreased. This approach can help to study how cells respond to different stimulus intensities, especially for measuring threshold and excitability changes in action potentials. By gradually increasing the stimulus, the starting point and range of the cell's response can be more precisely determined (Szabó et al., 2021). Step stimulation refers to the mode of stimulation in which the current or voltage changes suddenly to a fixed value and is maintained for a period of time. This method is often used to measure the input-output relationship of cells (that is, the relationship between the intensity of the stimulus and the frequency of the action potential). By applying different intensities of step stimulation, the discharge frequency and excitability characteristics of cells can be assessed (Brookings et al., 2012).

Male $NL2^{Mut/Mut}$ mice and WT littermates (8-10-week-old) or Mdga1 and Mdga2 double KO and control mice were anesthetized with isoflurane and underwent transcardial perfusion with iced slicing solution (saturated with 95% O2 and 5% CO2) consisting of (in mM): 235 Sucrose, 1.25 NaH2PO4, 2.5 KCl, 0.5 CaCl2, 7 MgCl2, 20 Glucose, 26 NaHCO3, and 5 Pyruvate (pH 7.3, 310 mOsm). The brain was rapidly removed and quickly immersed in the iced oxygenated slicing solution. 300 μm coronal (for mPSCs) slices containing hippocampus were sectioned in cold

slicing solution using the VT1200S Vibratome (Leica, Germany). The slices were subsequently transferred to and incubated in ACSF (saturated with 95% O2 and 5% CO2) consisting of (in mM): 26 NaHCO3, 2.5 KCl, 126 NaCl, 20 D-glucose, 1 sodium pyruvate, 1.25 NaH2PO4, 2 CaCl2 and 1 MgCl2 (pH 7.4, 310 mOsm), for 30 min at 34℃ and recovered for at least 1 hour at 25℃ before recording. Subsequently, a single brain slice was transferred to the recording chamber with continuous perfused oxygenated ACSF (2 mL/min) for electrophysiological experiments.

Whole-cell recordings of CA1 pyramidal neurons were performed using the MultiClamp 700B amplifier. For mEPSC recordings, neurons were voltage clamped at -70 mV. 1 μM tetrodotoxin (TTX) and 100 μM picrotoxin (PTX) were added into the bath solution to block action potentials and GABAergic inhibitory synaptic currents respectively. The pipette resistance was 3-5 MΩ and filled with an intracellular solution containing (in mM): 130 Cs-methanesulfonate, 5 NaCl, 1 MgCl2, 10 HEPES, 0.2 EGTA, 572 2ATP-Mg, 0.1 GTP-Na and 5 QX314 with pH adjusted to 7.3-7.4 by CsOH and osmolarity was adjusted to 285 mOsm with sucrose. For mIPSC recordings, neurons were voltage clamped at -70 mV. 20 μM CNQX (6-Cyano-7-nitroquinoxaline-2,3-dione), 20 μM APV (D-(-)-2-Amino-5-phosphonopentanoic acid) and 1 μM TTX added to the bath solution to block excitatory synaptic transmission and action potentials. The pipette resistance was 3-5 MΩ and filled with solution containing (in mM): 100 CsCl, 30 cesium methanesulfonate, 5 NaCl, 1 MgCl2, 10 HEPES, 0.2 EGTA, 2 ATP-Mg, and 0.1 578 GTP-Na. The pH was adjusted to 7.3-7.4 with CsOH and osmolarity was adjusted to mOsm with sucrose. mPSC events were rejected if the amplitude was < 7.5 pA. Analysis for amplitude and frequency was conducted using MiniAnalysis software. For paired-pulse ratio recording, pyramidal neurons were clamped at 0 mV in the presence of 20 μM CNQX, 20 μM APV, and the patch electrodes were filled with Cs-methanesulfonate pipette solution. A concentric bipolar stimulating electrode was placed in the

stratum radiatum to evoke IPSCs in CA1 pyramidal cells. Paired stimuli were delivered with different inter-stimulus intervals (25, 50, 100, and 200 ms). The ratios were calculated as 2nd IPSC/1st IPSC. To evoke APs, cells were recorded in current-clamp step and a ramp protocol. In case of step protocol, APs were evoked with 1 s long square-pulse current injections from 0 to 250 pA in 50 pA increments. A current ramp protocol of varying slopes (0 to 250 pA over 1 s) was also used to evoke AP firing. (Thouta et al., 2022; X. Wang et al., 2024). The patch electrodes were filled with K-gluconate pipette solution containing (in mmol/L), 130 K-gluconate, 5 NaCl, 1 MgCl2, 10 HEPES, 0.2 EGTA, 2 MgATP, and 0.1 NaGTP. The pH was adjusted to 7.3–7.4 with KOH and osmolarity was adjusted to 285 mOsm with sucrose. The AP threshold was identified at the point where the AP was initiated and showed a > 10-fold change in the rate of rise. AP amplitude was calculated as the maximum voltage during the spike minus the spike threshold voltage.

TTX, PTX, APV, and CNQX were from Tocris unless otherwise specified. Stock solutions of PTX and CNQX were made by dissolution in dimethyl sulfoxide. Stock solutions of TTX and APV were made in sterilized ddH2O. TTX targets voltage-gated sodium channels and can irreversibly block the generation of action potentials and inhibit the release of neurotransmitters in presynaptic neurons. PTX is a non-competitive antagonist of $GABA_A$Rs, blocking inhibitory postsynaptic currents (IPSCs). CNQX competitively antagonizes glutamate binding sites to block AMPAR-mediated fast excitatory synaptic currents (EPSCs). APV competitively antagonize glutamate binding sites and selectively block NMDAR-mediated slow EPSC components.

2.7 Bioinformatics

Bioinformatics involves the use of computers and mathematical methods to collect, process, analyze and interpret large amounts of biological data generated by RNAseq. Combining RNAseq and bioinformatics amplifies our ability to study biological processes such as gene expression and transcript variation. GO is a standardized bioinformatics tool used to describe the function of genes and proteins. The GO vocabulary is organized into three main categories: molecular functions, cellular components, and biological processes. These terms can help researchers conduct a deeper analysis of gene function and advance the understanding of gene regulatory networks in different biological systems. DEGs are often used to describe genes whose expression levels differ significantly under different conditions, such as control and experimental groups. DEG analysis helps identify genes associated with specific biological processes or diseases. The Pearson correlation coefficient is a statistical method that measures the strength and direction of the linear relationship between two variables. It ranges from -1 to 1, where 0 means no correlation, 1 means a completely positive correlation, and -1 means a completely negative correlation.

Transcriptome data in this study were obtained from the GEO database (https://www.ncbi.nlm.nih.gov/geo). PCA, a mathematical algorithm that reduces the dimensionality of the data and concentrated on the most significantly associated genes (Ringnér, 2008), was performed to distinguish the $NL2^{+/+}$ and $NL2^{Mut/Mut}$ using principle components 1 (PC1) and 2 (PC2). All DEGs analyses were carried out employing the DESeq2 package in the R environment (Love et al., 2014). Differences with p value < 0.05 and log2 |fold change|> 1 were considered significant. The DEGs were identified using online Venn diagrams drawing tool (http://bioinformatics.psb.ugent.be/webtools/Venn/). Pearson correlation analysis was used to predict the correlation of $NL2^{Mut/Mut}$ and NDDs (SCZ, ASD and TLE); when the $|R| \geqslant 0.95$, $P \leqslant$

0.01, it was considered a positive correlation. The differential genes were then analysed using GO (DAVID https://david.ncifcrf.gov/) on the mice genome. All analyses were performed using the clusterProfiler R package (Yu et al., 2012). The dataset downloaded from the GEO database (GSE201624, GSE81501, GSE112663, GSE198403 and GSE122228) were used to predict the $NL2^{Mut/Mut}$-related diseases.

2.8 Stereotaxic Surgery and Viral Injection

For stereotaxic surgery, the mice were deeply anesthetized with 2% pentobarbital sodium and fixed in a stereotaxic frame (RWD, China). An incision was made in the midline of the scalp, and a craniotomy was performed above the hippocampus region. The virus AAV2/9-CaMKIIα-CRE-P2A-mCherry-WPRE-hGH-pA (1.26×10^{11} vg/mL, 1:20, 200 nL, PT-0739, BrainVTA, China) or the control virus: AAV2/9-CaMKIIα-mCherry-WPRE-hGH-pA (2.57×10^{11} vg/mL, 1:20, 200 nL, PT-0108, BrainVTA, China) was injected bilaterally into the hippocampus, area CA1 (ML, ± 1.7 mm; AP, − 2.15 mm; DV, − 1.23 mm) through a pulled-glass micropipette with a 10–20 μm tip diameter connected to a 10 μL microliter syringe (Hamilton Co., USA). The AAV was delivered using a stereotactic injector (Pump 11 Elite, Harvard Apparatus, USA) at a rate of 50 nL/min. After injection, the micropipettes were left in place for an additional 10 min to allow for diffusion before the pipette was slowly withdrawn.

2.9 Statistical analysis

Data in this study were presented as mean ± SEM and analyzed with GraphPad Prism 9.5.1 (GraphPad Software Inc, USA). For data with more than one independent variable, two-way ANOVA with post-hoc Bonferroni's t-test was used. Student's t test was used to compare

differences between two groups. Each experiment was performed with at least three independent biological replicates, and $p < 0.05$ was considered to be statistically significant.

Chapter 3 Results

PROJECT1: 3.1 Successful preparation and verification of NL2 site II point mutation mice

3.1.1 Construction and breeding of $NL2^{Mut/Mut}$ transgenic mice

To accurately examine how NL2 and MDGAs regulate synaptic activity, the NL2 site II point mutation (NL2ΔSite II) mice were generated. The mouse NL2 gene is located on chromosome 11 and the total length is about 14.9 kilobase (Kb). The gene ID is 216856. The transgenic design is based on the transcript (NM_198862) because it is the predominant transcript according to the NCBI. Five of the amino acids that are required for NL2/MDGA1 interactions were mutated to alanine at site II, located on exon 6 (Asp407Ala、Phe408Ala、Ser411Ala、Asn412Ala and Arg428Ala). The conditional NL2 point mutation ($NL2^{Mut/Mut\ flox/flox}$) mice were made by inserting a fragment (>5 kilo base pairs (Kb)) including exon3 to exon7 (where introns are removed), 3`UTR, 3 terminators and Neo gene, which are floxed by two loxP sites. Both the 5' and 3' loxP sites were inserted into the non-conserved sequence of intron2-3 (Figure 15A). When there is no Cre recombinase, the transcription stops at the terminator genes, leading to normal gene expression. Next, the $NL2^{Mut/+}$, CMV-$Cre^{+/-}$ mice were obtained by crossing the $NL2^{Mut/Mut\ flox/flox}$ mice and CMV-Cre mice. These $NL2^{Mut/+}$, CMV-$Cre^{+/-}$ mice were then crossed with C57BL/6J wild type (WT) mice which have the same genetic background to obtain $NL2^{Mut/+}$ mice and eliminate CMV-$Cre^{+/-}$. Following this, the $NL2^{Mut/+}$ mice were crossed to produce $NL2^{+/+}$ (WT) and homozygous $NL2^{Mut/Mut}$ littermates (Figure 15B).

3.1.2 To determine the successful knock-in of mutations in NL2ΔSite II in mice by PCR and sanger sequencing.

PCR was used to determine the successful knock-in of mutations in NL2ΔSite II in mice. After knock-in, one loxP site will remain in the gene, thus, the forward and reverse primers are designed at both sides of loxP. PCR gel imaging reveals that the 354bp single band is in $NL2^{Mut/Mut}$ mice, 290bp single band is shown in $NL2^{+/+}$ mice and 290bp and 354bp bands are simultaneously shown in $NL2^{Mut/+}$ mice (Figure 15C). These results suggest that the mutant gene is successfully knocked-in at the genome level.

To further investigate whether the bases are mutated in NL2 transgenic mice, the brain tissue and tail samples were prepared to undergo Sanger sequencing (Figure 15D). The results indicate that either in brain or tail tissue, 9 mutation peaks (A234C， T236C, T237C, T246G, C248T, A249G, A250C, C297G and C298G) were observed in $NL2^{Mut/Mut}$ mice, normal base peaks were shown in $NL2^{+/+}$ mice, and both normal peaks and mutation peaks were shown in $NL2^{Mut/+}$ mice.

To further explore the transcription level in NL2 point mutation mice, the total RNA of brain and tail of mice were extracted using TRIzol methods. The extracted RNA was reverse transcribed to cDNA with high fidelity and underwent Sanger sequencing. Since the NL2 gene is not transcribed in the tail of mice, no PCR products were detected in cDNA of tails. The cDNA sequencing results from the brain indicate that 9 mutation base peaks were shown in $NL2^{Mut/Mut}$ mice, normal base peaks were observed in $NL2^{+/+}$ mice, and both mutation and normal base peaks were shown in $NL2^{Mut/+}$ mice (Figure 15E).

3.1.3 To detect whether the expression levels of synaptic organizers were affected due to this point mutation.

Next, the RNA-seq was used to detect whether the expression levels of synaptic organizers were affected due to this point mutation. Before the analysis of differences between groups, it is particularly important to conduct parallel tests for biological replication. The sample repeatability in WT and $NL2^{Mut/Mut}$ was good (Figure 16A). The correlation coefficients in both the WT group and the $NL2^{Mut/Mut}$ group were high, while the correlation coefficients between the groups were low, indicating that the biological replication effect was good and further analysis could be carried out (Figure 16B). Also, we distinguished $NL2^{+/+}$ and $NL2^{Mut/Mut}$ by PCA (Figure 16C). The PCA of the transcriptome profiles indicated that the WT mice and $NL2^{Mut/Mut}$ are clearly distinct from each other, recommending the samples for further analysis. The RNA expression level of Mdga1, Mdga2, Nlgn1, Nlgn2, Nlgn3, Nrxn1, Nrxn2 and Nrxn3 were comparable between $NL2^{+/+}$ and $NL2^{Mut/Mut}$ mice (Figure 16D-F).

Finally, the above results show that the NL2 point mutation was successfully knocked-in and transcribed into mRNA in the brain of mice, which successfully verifies the preparation of NL2 point mutation mice at both genome and transcription levels.

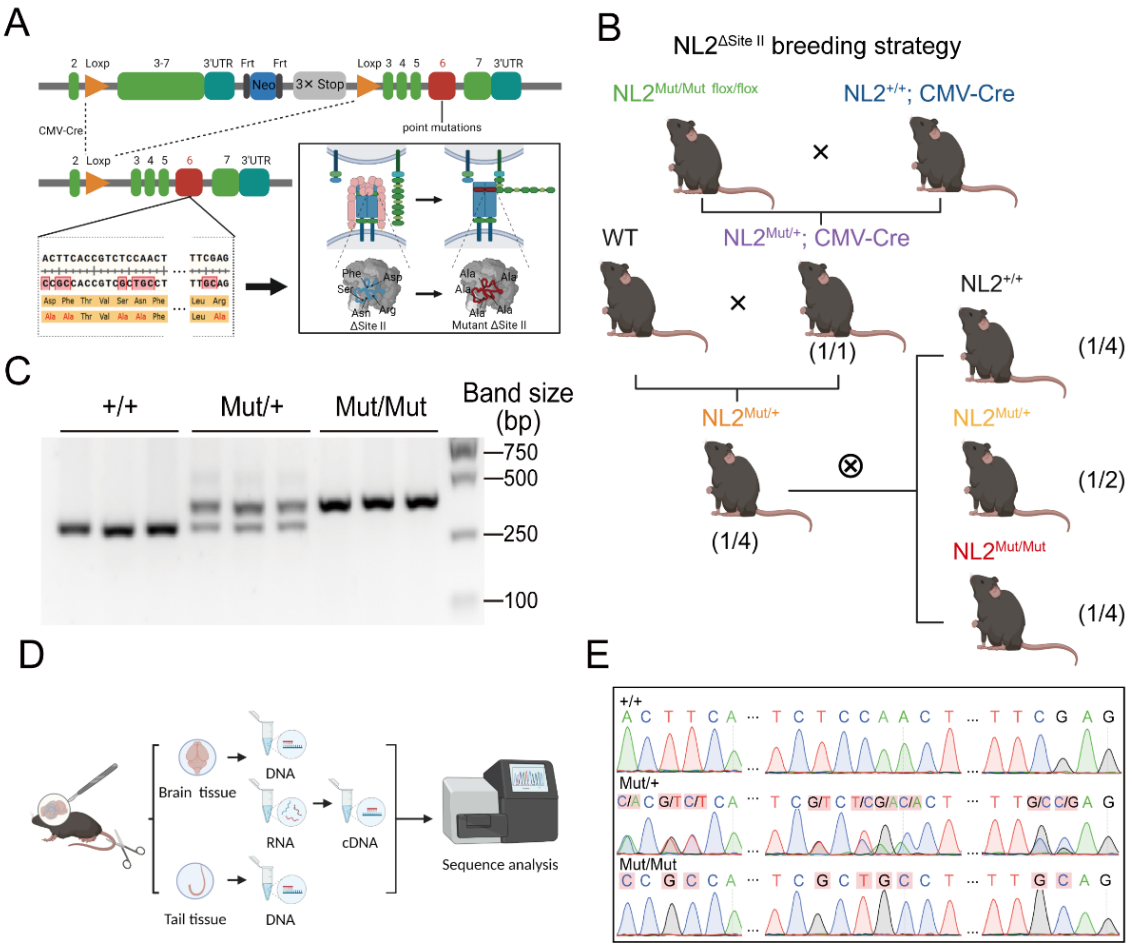

Figure 15. Preparation and detection of NL2ΔSite II mice.

(A) The diagram of the knock-in of NL2ΔSite II, mRNA transcription and protein expression. (B) The schema of breeding strategy of NL2ΔSite II mice. (C) PCR imaging shows that the bands of $NL2^{Mut/Mut}$ (n=3), $NL2^{Mut/+}$ (n=3) and $NL2^{+/+}$ (n=3) are 354bp, 354/290bp and 290bp, respectively. (D) The flow chart of Sanger sequencing experiments. (E) The graph of Sanger sequencing results. The 9 base peak mutations are detected in both DNA and cDNA samples of $NL2^{Mut/Mut}$ (n=3) mice, double peaks of mutant and normal bases are detected in $NL2^{Mut/+}$(n=3) mice, and the normal base peaks are detected in the corresponding position in $NL2^{+/+}$ (n=3).

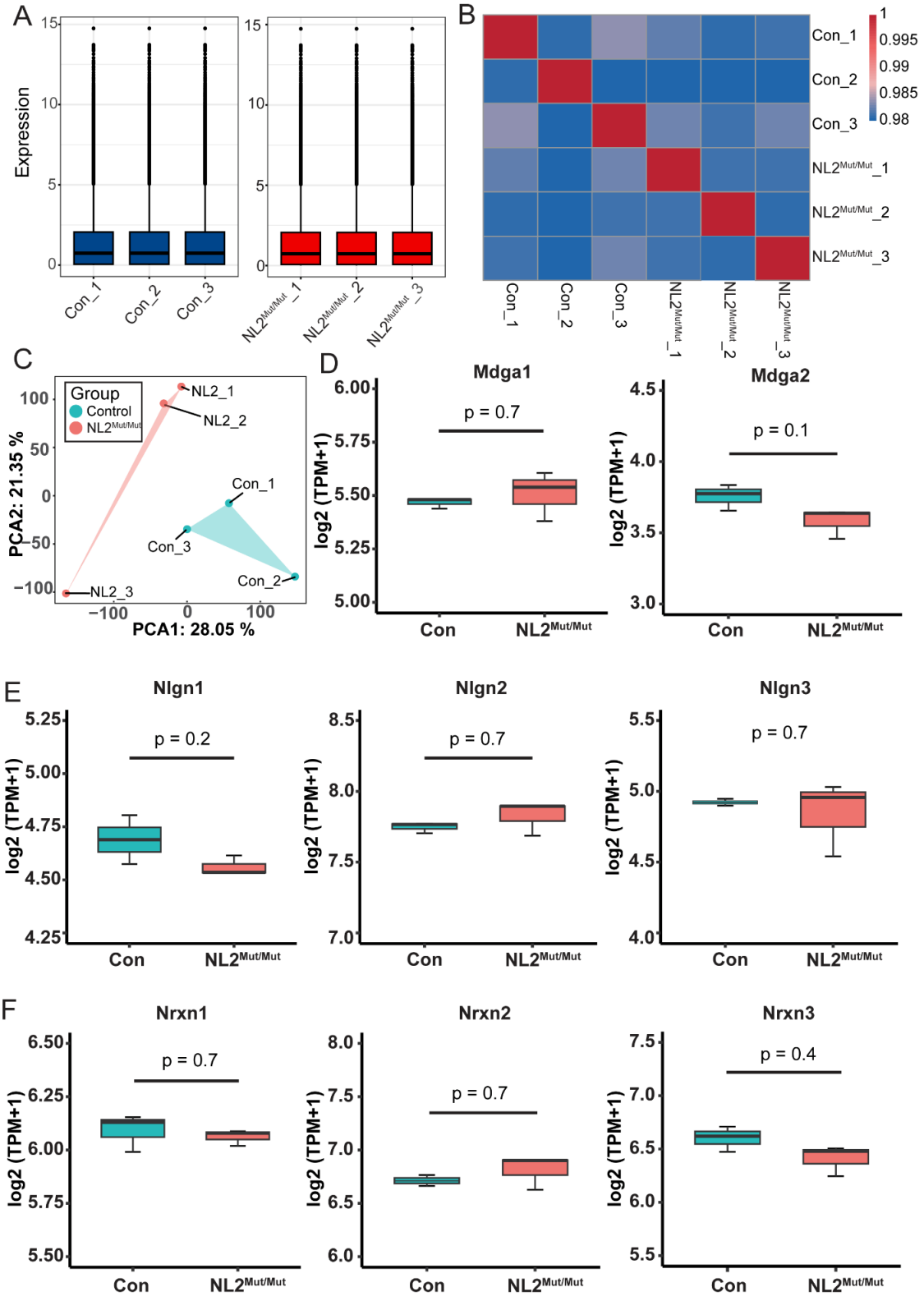
A
Expression
Con_1
Con_2
Con_3
NL2Mut/Mut_1
NL2Mut/Mut_2
NL2Mut/Mut_3
B
1
0.995
0.99
0.985
0.98
C
Group
Control
NL2Mut/Mut
PCA2: 21.35 %
PCA1: 28.05 %
D
Mdga1
Mdga2
p = 0.7
p = 0.1
log2 (TPM+1)
Con
NL2Mut/Mut
E
Nlgn1
Nlgn2
Nlgn3
p = 0.2
p = 0.7
F
Nrxn1
Nrxn2
Nrxn3
p = 0.7
p = 0.4

Figure 16. The synaptic protein expression levels in WT (control) and NL2Mut/Mut mice using RNAseq.

(A) Boxplots showing the sample repeatability in control and $NL2^{Mut/Mut}$. (B) Heatmap showing the correlation coefficient between control and $NL2^{Mut/Mut}$. (C) PCA of the samples. Principal component 1 (x axis) is accountable for 28.05% of the variability of the samples and principal component 2 is accountable for 21.35% of the variability of the samples (y axis). The boxplots show the expression profile of Mdga1 and Mdga2 (D), Nlgn1, Nlgn2 and Nlgn3 (E) and Nrxn1, Nrxn2 and Nrxn3 (F) in control and $NL2^{Mut/Mut}$ mice.

3.2 NL2ΔSite II specifically upregulates inhibitory synapse function

3.2.1 To explore the change of synaptic function in NL2ΔSite II mice by RNA sequencing.

To gain a deeper comprehension of the change of synaptic function in NL2ΔSite II mice, we performed RNAseq analysis using the hippocampal tissues from the NL2 $^{+/+}$ and NL2$^{Mut/Mut}$ mice (Figure 17A). Specifically, we identified 971 DEGs (adjusted $p < 0.05$, 539 up and 432 down) in the NL2$^{Mut/Mut}$ group compared to NL2 $^{+/+}$ group (Figure 17B). GO and Syn GO pathways analysis revealed that DEGs of CC were involved in postsynaptic membrane, postsynaptic density, postsynaptic specialization, etc. BP analysis revealed that the DEGs were markedly enriched in processes found within the postsynapse, including GABAergic synaptic transmission, among others (Figure 17C-F).

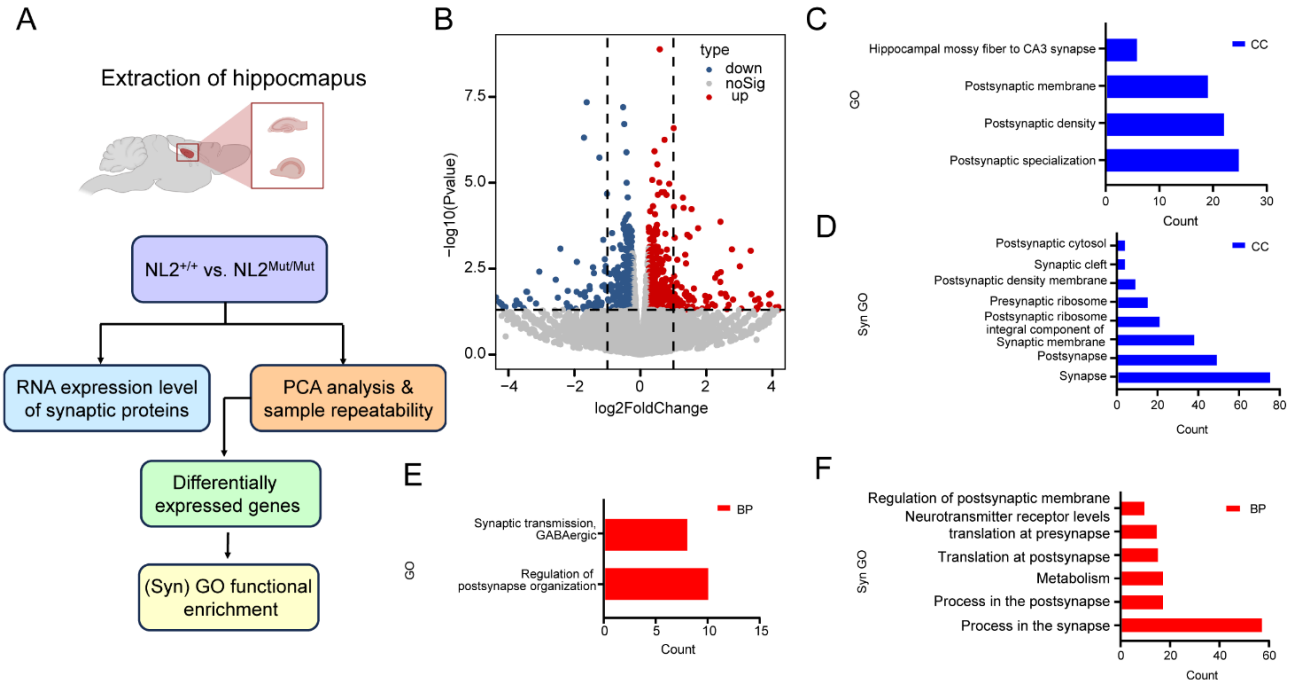

Figure 17. NL2ΔSite II specifically upregulates inhibitory synapse function within pyramidal neurons in the CA1 region of mouse hippocampus.

(A) Flow chart of the experiments. (B) The volcano plot showing the DEGs in the hippocampus with significantly increased (red) or decreased (blue) expression ($p < 0.05$, $|\log2|>1$) compared between the control and $NL2^{Mut/Mut}$. GO (C and E) and syn GO (D and F) analysis showing the DEGs in cellular component and biological process between control and $NL2^{Mut/Mut}$.

3.2.2 To explore the change of synaptic function in NL2ΔSite II mice by electrophysiology.

To further confirm that the NL2ΔSite II contributes to synapse function in CA1, acute brain slices were prepared, and whole-cell patch clamp was performed to record mIPSCs (Figure 18A) and mEPSCs (Figure 18D). The frequency (Figure 18B) of mIPSCs was significantly increased in $NL2^{Mut/Mut}$ mice compared to $NL2^{+/+}$ mice without affecting amplitude (Figure 18C), whereas the frequency (Figure 18E) and amplitude (Figure 18F) of mEPSCs were not altered in $NL2^{Mut/Mut}$ mice compared to $NL2^{+/+}$ mice, reflecting that NL2ΔSite II increases inhibitory synaptic function but does not affect excitatory synaptic function. Accordingly, NL2ΔSite II results in selective upregulation of inhibitory synapse function without detectably altering excitatory synapses.

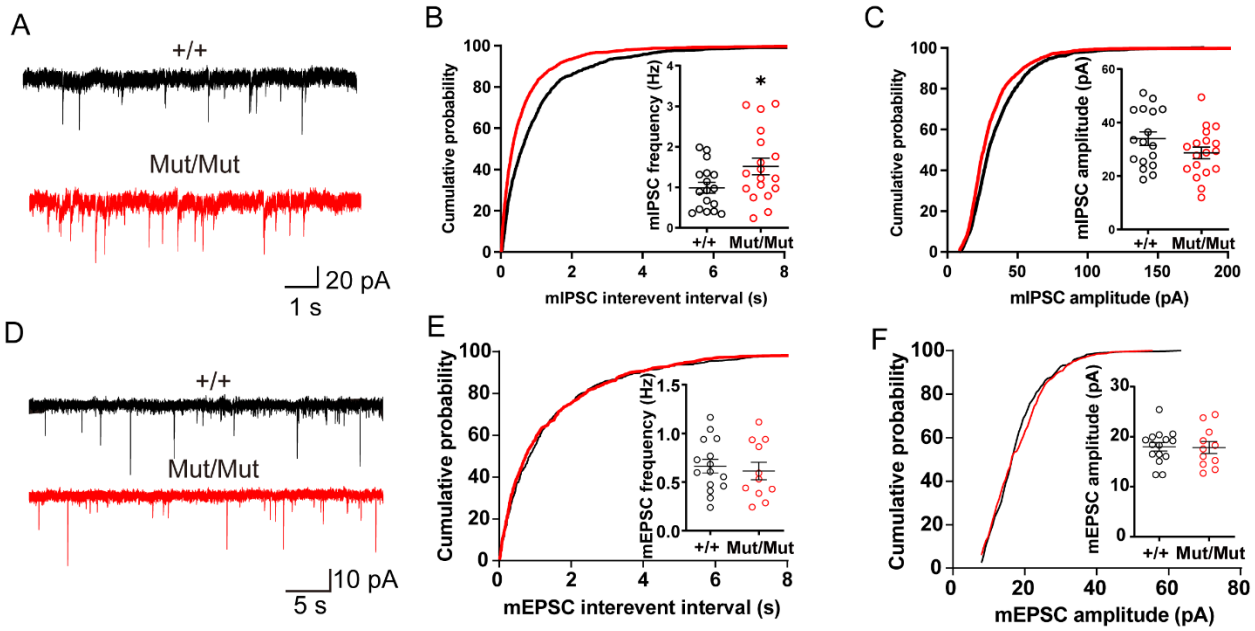

Figure 18. NL2ΔSite II specifically upregulates inhibitory synapse function of pyramidal neurons in hippocampal CA1 region of mice.

(A) Representative traces of the mIPSCs. The mIPSC frequency (B) and amplitude (C) of pyramidal neurons in $NL2^{Mut/Mut}$ mice (n=16 neurons from 3 mice) were significantly increased compared to that in $NL2^{+/+}$ mice (n=18 neurons from 3 mice). ($NL2^{+/+}$ vs. $NL2^{Mut/Mut}$, frequency: 1.85±0.20 vs. 3.64±0.65, *$p<0.05$; amplitude:30.11±1.00 vs. 35.64±1.91, $p>0.05$). (D) Representative traces of mEPSCs. There is no significant difference in mEPSC frequency (E) or amplitude (F) in pyramidal neurons in $NL2^{Mut/Mut}$ mice (n=11 neurons from 4 mice) and $NL2^{+/+}$ mice (n=15 neurons from 4 mice). ($NL2^{+/+}$ vs. $NL2^{Mut/Mut}$, frequency: 0.66±0.07 vs. 0.61±0.09, $p=0.67$; amplitude: 17.99±0.86 vs. 17.83±1.19, $p=0.91$).

3.3 NL2ΔSite II upregulates inhibitory synapse density in hippocampal CA1 of mice.

3.3.1 To detect the glutamatergic pre-synaptic transmission in NL2ΔSite II mice.

The increased frequency of mIPSCs suggests that NL2ΔSite II may selectively enhance the function or density of glutamatergic pre-synaptic terminals in CA1. However, no differences were found in PPF (Figure 18A, B), suggesting that the increased frequency of mIPSCs was not due to changes in neurotransmitter release probability. We next assessed whether the mature PNs of NL2ΔSite II demonstrate changes in synaptic density.

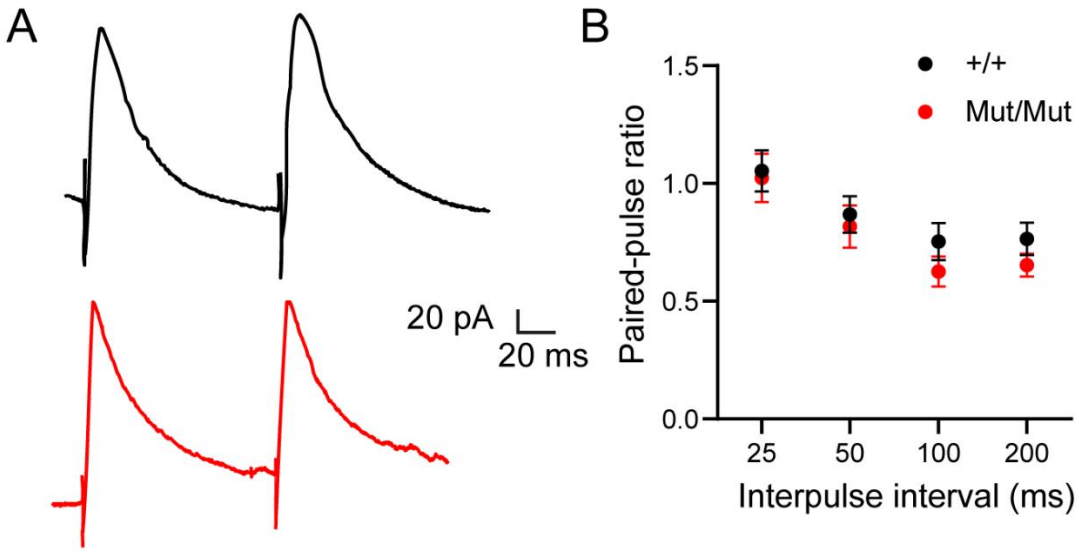

Figure 19. NL2ΔSite II does not alter the PPR in CA1, a presynaptic function assay.

(A) Representative traces of paired-pulse stimulation at a 100 ms. (B) PPR is normal in NL2ΔSite II mice. n = 13 neurons, from 3 mice for WT (+/+) group; n = 11 neurons from 2 mice for NL2ΔSite II ($NL2^{Mut/Mut}$) group; P = 0.1594; F (1, 88) = 2.014; two-way ANOVA.

3.3.2 To anatomically explore the change of density of inhibitory synapse and excitatory synapse in NL2ΔSite II mice.

To investigate whether only NL2ΔSite II can induce E/I imbalance, the membrane proteins of hippocampal lysates (P2) were collected. Western blots were employed to quantitatively evaluate the variation of inhibitory and excitatory synapses in hippocampus (Figure 20A and Figure 21A). The gray value of the inhibitory synaptic markers VGAT (Figure 20Ai) and gephyrin (Figure 20Aii) antibodies significantly increases in $NL2^{Mut/Mut}$ mice compared to $NL2^{+/+}$ mice, reflecting that NL2ΔSite II in mice increases inhibitory synapse density. However, the gray value of the excitatory presynaptic marker vesicular glutamate transporters 1 (VGluT1) (Figure 21Ai) and the excitatory postsynaptic marker PSD-95 (Figure 21Aii) are not affected in $NL2^{Mut/Mut}$ mice compared to $NL2^{+/+}$ mice, suggesting that NL2 point mutation in mice does not alter excitatory synapse density.

Previous studies have established that NL2-MDGA1 interactions are prominent in hippocampal CA1 pyramidal neurons (Chih et al., 2006; Ullrich et al., 1995; Vogt et al., 2018), and hence this research focuses on the CA1 brain region. Immunostaining was employed to explore the distribution pattern of the inhibitory presynaptic marker GAD65 (Figure 20B) and excitatory presynaptic marker VGluT1 (Figure 21B). The area of GAD65 significantly increases in CA1 SP, SR and SLM, but remained constant in SO (Figure 20Bi) in $NL2^{Mut/Mut}$ mice compared to $NL2^{+/+}$ mice, whereas the area of VGLuT1 (Figure 21Bi) is not altered in $NL2^{Mut/Mut}$ mice compared to $NL2^{+/+}$ mice. This further supports that NL2ΔSite II enhances inhibitory synapse density without affecting excitatory synapse density.

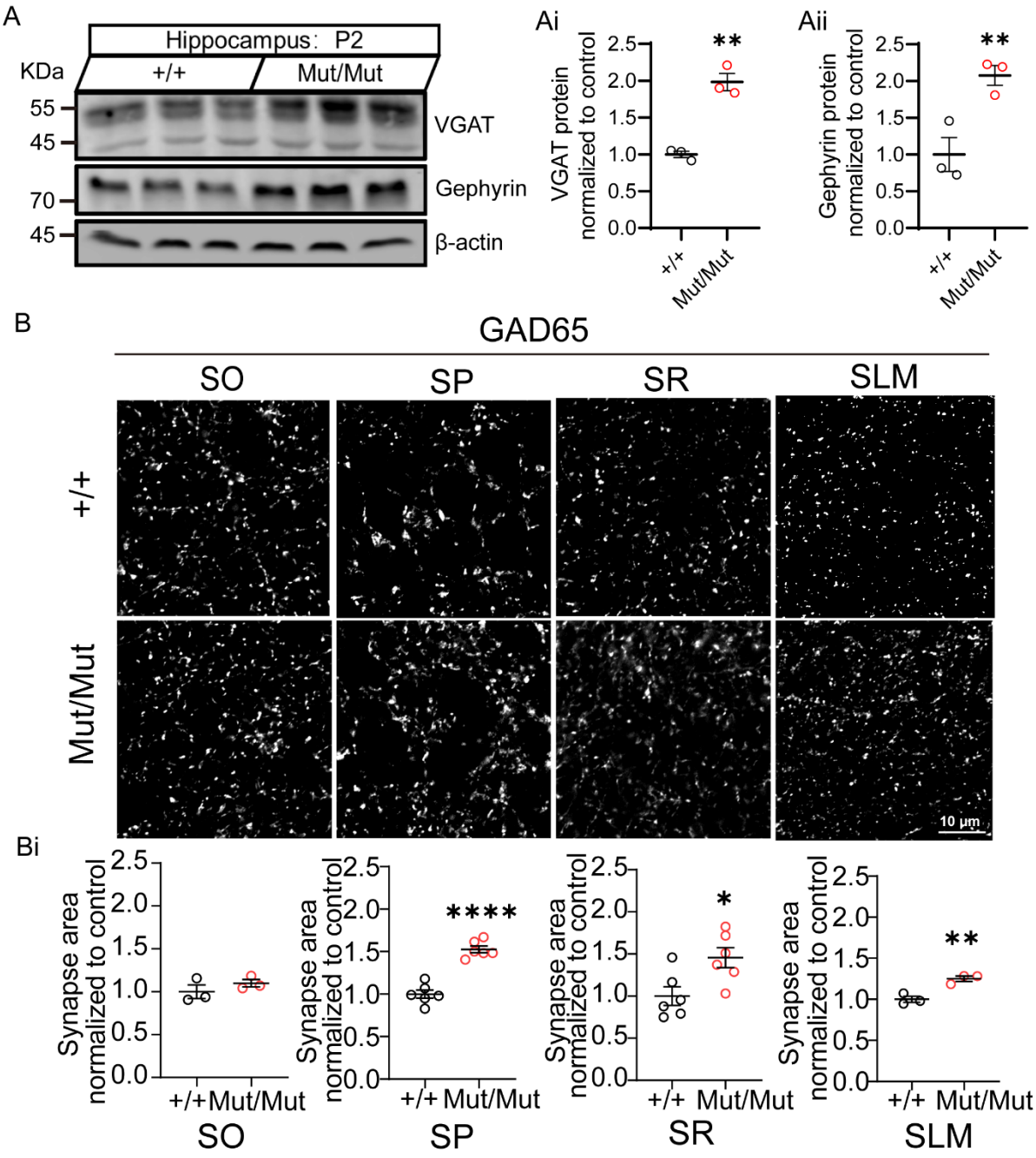

Figure 20. NL2ΔSite II specifically upregulates inhibitory synapse density in pyramidal neurons in hippocampal CA1 of mice.

(A) Western blot image of VGAT and gephyrin in membrane protein lysates of hippocampus. The band gray values of VGAT (Ai) and gephyrin (Aii) in $NL2^{Mut/Mut}$ mice (n=3) were significantly

increased relative to $NL2^{+/+}$ mice (n=3). ($NL2^{+/+}$ vs. $NL2^{Mut/Mut}$, VGAT: 1.00±0.04 vs. 1.98±0.12, **p<0.01; Gephyrin:1.00±0.23 vs. 2.08±0.13, **p<0.01). (B) The immunostaining images of GAD65 (white) in SO, SP, SR and SLM layers. Scale bar=10 μm. The immunofluorescence area of GAD65 in SP, SR and SLM but not SO (Bi) layers is significantly increased in $NL2^{Mut/Mut}$ mice (n=6) relative to $NL2^{+/+}$ mice (n=6). ($NL2^{+/+}$ vs. $NL2^{Mut/Mut}$, the immunofluorescence area of SO: 1.00±0.08 vs. 1.10±0.04, p=0.3361; the immunofluorescence area of SP: 1.00±0.05 vs. 1.53±0.04, ****p<0.001; the immunofluorescence area of SR: 1.00±0.11 vs. 1.46±0.12, *p<0.01; the immunofluorescence area of SLM: 1.00±0.04 vs. 1.25±0.03, **p<0.01). All the western blot and immunostaining data were normalized to controls. Means are represented as mean ±S.E.M. Two-tailed unpaired student`s t-test is performed.

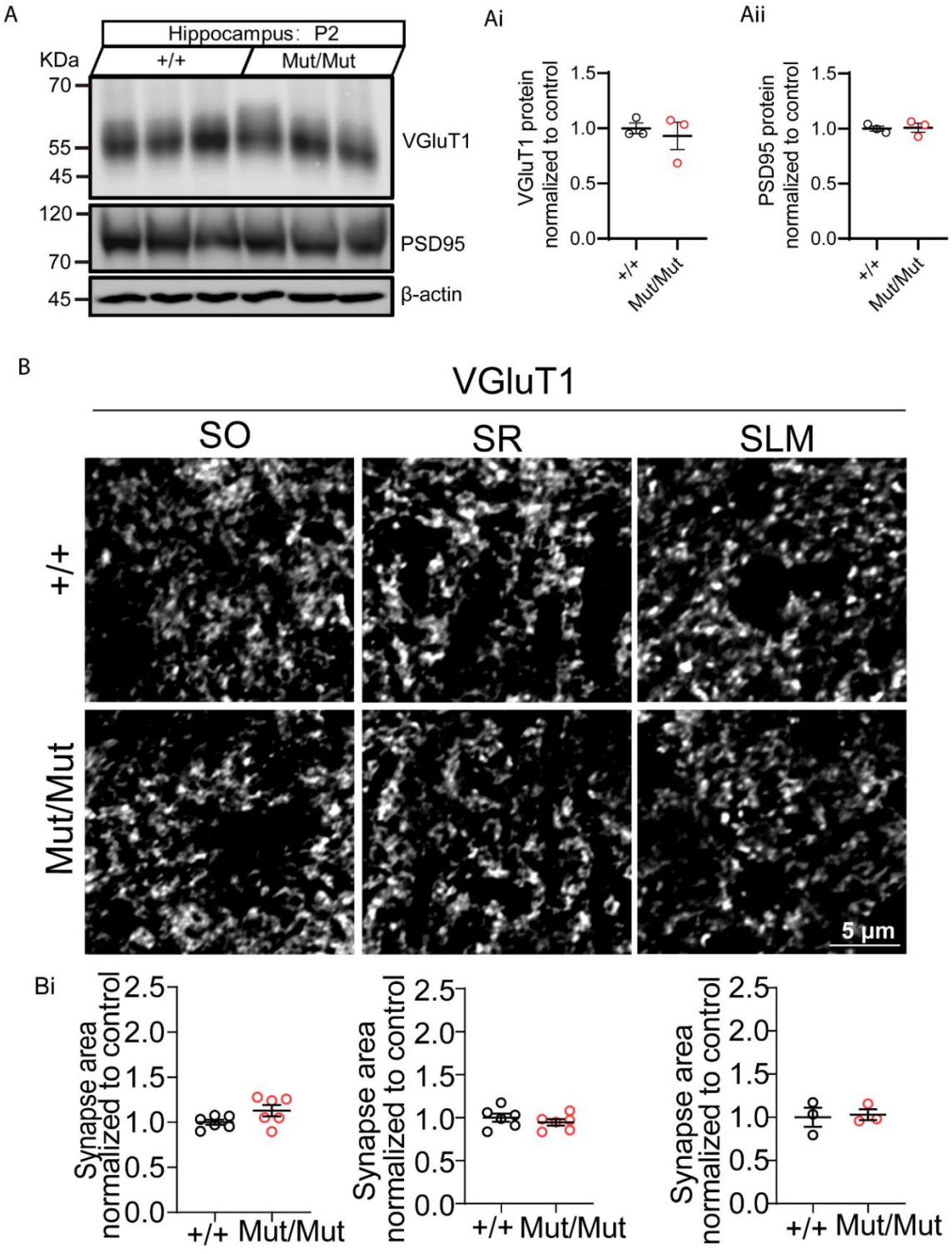
A
Hippocampus: P2
KDa
+/+
Mut/Mut
70
55
45
120
70
45
VGluT1
PSD95
β-actin
Ai
VGluT1 protein normalized to control
1.5
1.0
0.5
0.0
+/+
Mut/Mut
Aii
PSD95 protein normalized to control
1.5
1.0
0.5
0.0
+/+
Mut/Mut
B
VGluT1
SO
SR
SLM
+/+
Mut/Mut
5 µm
Bi
Synapse area normalized to control
2.5
2.0
1.5
1.0
0.5
0.0
+/+ Mut/Mut
Synapse area normalized to control
2.5
2.0
1.5
1.0
0.5
0.0
+/+ Mut/Mut
Synapse area normalized to control
2.5
2.0
1.5
1.0
0.5
0.0
+/+ Mut/Mut

Figure 21. NL2ΔSite II does not affect excitatory synapse density in pyramidal neurons in hippocampal CA1 of mice.

(A) A western blot image of VGLUT1 and PSD95 in membrane protein lysates of hippocampus. There is no significant difference of band gray values of VGLUT1 (Ai) and PSD95 (Aii) between $NL2^{Mut/Mut}$ mice (n=3) and $NL2^{+/+}$ mice (n=3). ($NL2^{+/+}$ vs. $NL2^{Mut/Mut}$, VGLUT1: 1.00±0.04 vs. 0.93±0.12, p=0.63>0.05; PSD95: 1.00±0.02 vs. 1.01±0.04, p=0.88>0.05). (B) The immunostaining images of VGLUT1 (white) in SO, SR and SLM layers. Scale bar=5 μm. There is no significant difference in immunofluorescence area of VGLUT1 in SO, SR and SLM (Bi) layers between $NL2^{Mut/Mut}$ mice (n=6) and $NL2^{+/+}$ mice (n=6). ($NL2^{+/+}$ vs. $NL2^{Mut/Mut}$, the immunofluorescence area of SO: 1.00±0.03 vs. 1.13±0.06, p=0.0905; the immunofluorescence area of SR:1.00±0.05 vs. 0.95±0.04, p=0.3910; the immunofluorescence area of SLM: 1.00±0.11 vs. 1.03±0.06, p=0.8160).

3.4 NL2ΔSite II model is highly correlated with the shank3$^{-/-}$ NDD model

3.4.1 Shank3-/- NDD model is related to NL2ΔSite II model.

The flow chart of the experiment is shown in Figure 22A. To investigate which diseases are related to NL2ΔSite II model, the transcriptome data of different diseases models were compared with NL2$^{Mut/Mut}$ (Figure 22B). Mutations in Shank3, which codes for a synaptic scaffolding protein enriched in the postsynaptic density of excitatory synapses and contributes to the formation, maturation, and maintenance of synapses, is associated with SCZ and ASD (Huang et al., 2023; Zhou et al., 2016). Interestingly, the Pearson's r of transcriptome data of NL2$^{Mut/Mut}$ and shank3$^{-/-}$ is 0.606, indicating that NL2ΔSite II is positively correlated with shank3$^{-/-}$ related diseases. 61 genes overlapped between NL2$^{Mut/Mut}$ and shank3$^{-/-}$ (Figure 22C). These common genes were enriched in biological pathways including cellular catabolic processes, immune system processes, ameboidal-type cell migration, learning and memory and synaptic plasticity (Figure 22D). To specifically understand the relationship between NL2$^{Mut/Mut}$ and shank3$^{-/-}$ in these biological pathways, we performed at Pearson correlation analysis. Consistently, NL2$^{Mut/Mut}$ and shank3$^{-/-}$ are positively correlated, among which the genes Trafd1, Camk2b, Zc3h18, Nop53 and Pacsin3 overlapped (Figure 22E-I).

3.4.2 To probe the relationship between BTBR T+tf/J mouse model and NL2ΔSite II model.

To further probe the relationship between our model and existing models of NDDs, we next compared the BTBR T+tf/J mouse, which demonstrates physiological and behavioral features consistent with an ASD-like phenotypes (Meyza & Blanchard, 2017; Mizuno et al., 2020). We also used KA-induced to model features of temporal lobe epilepsy (TLE) is a commonly occurring co-morbidity with ASD. KA is a potent glutamate analog that, through driving overexcitation within

neural networks, generates epileptic-like insults in rodent models (Kienzler-Norwood et al., 2017; Rusina et al., 2021).

Comparisons between our model and the BTBR T+tf/J mouse revealed that 282 genes were shared between $NL2^{Mut/Mut}$ and this model for ASD (Figure 23A). These genes were concentrated in biological pathways including positive regulation of reactive oxygen species metabolic processes, synaptic transmission, GABAergic signaling, negative regulation of neuron death, regulation of macromolecule biosynthetic processes and synaptic organization (Figure 23B). Further Pearson correlation results revealed that there was modest correlation between $NL2^{Mut/Mut}$ and BTBR-related ASD (Figure 23C-F).

3.4.3 To probe the relationship between TLE mouse model and NL2ΔSite II model.

When comparing the TLE model, 198 genes were identified as shared between $NL2^{Mut/Mut}$ and mice in which TLE was induced (Figure 24A). These genes were concentrated in biological pathways linked to regulation of neurogenesis, cognition, calcium ion transport, regulation of lipid metabolic processes and synapse organization (Figure 24B). Further Pearson correlation results suggested that there was low correlation between $NL2^{Mut/Mut}$ and KA-induced TLE (Figure 24C-E). Additionally, the $NL2^{Mut/Mut}$ was not highly correlated with MeCP-related RTT (Good et al., 2021; Ip et al., 2018) or FXS (Figure 22B).

A

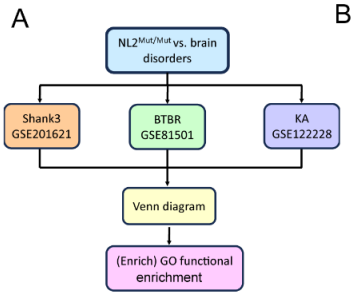

B

Sample Information

GSE	Model	Number	Method	Cor.
GSE201621	Shank3	5 vs 5	RNA-seq	0.606
GSE81501	BTBR	4 vs 4	RNA-seq	-0.131
GSE112663	Mecp	4 vs 4	RNA-seq	-0.049
GSE198403	Fraigle x	3 vs 3	RNA-seq	0.005
GSE122228	KA	3 vs 3	RNA-seq	0.112

C

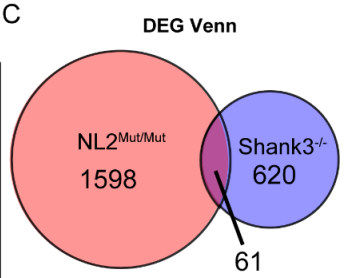

D

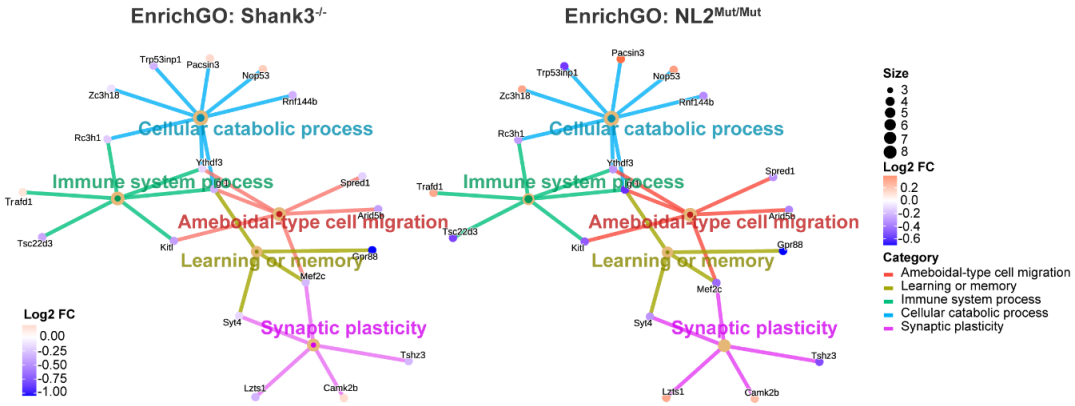

E

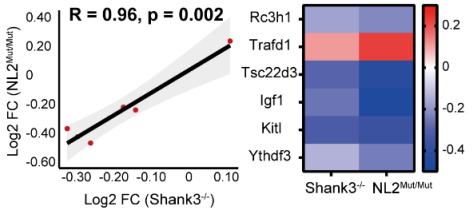

F

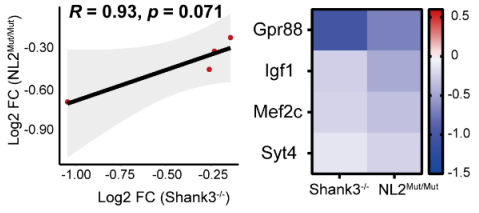

G

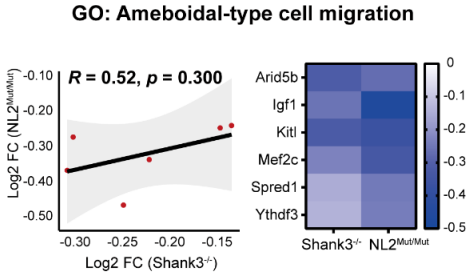

H

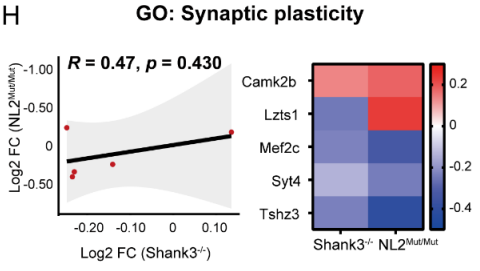

I

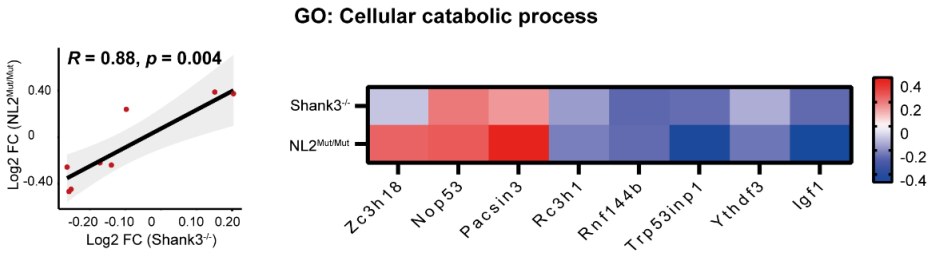

Figure 22. Comparison between NL2ΔSite II and shank3-/- model.

(A) Flow chart of the experiments. (B) Sample information for disease models and Pearson correlation. (C) Venn diagram showing the number of shared and unique genes between $NL2^{Mut/Mut}$ and $shank3^{-/-}$ mice, a total of 61 DEGs were identified. (D) Enrich GO regulatory network of $NL2^{Mut/Mut}$ and $shank3^{-/-}$. The size of the point indicates the connectivity. The greater the point is, the greater the connectivity is. Upregulated genes are depicted in orange, while downregulated genes are represented in purple. Pearson analysis showed the correlation between $NL2^{Mut/Mut}$ and $shank3^{-/-}$ and related gene heatmaps in immune system process (E), learning or memory (F), ameboidal-type cell migration (G), synaptic plasticity (H) and cellular catabolic process (I).

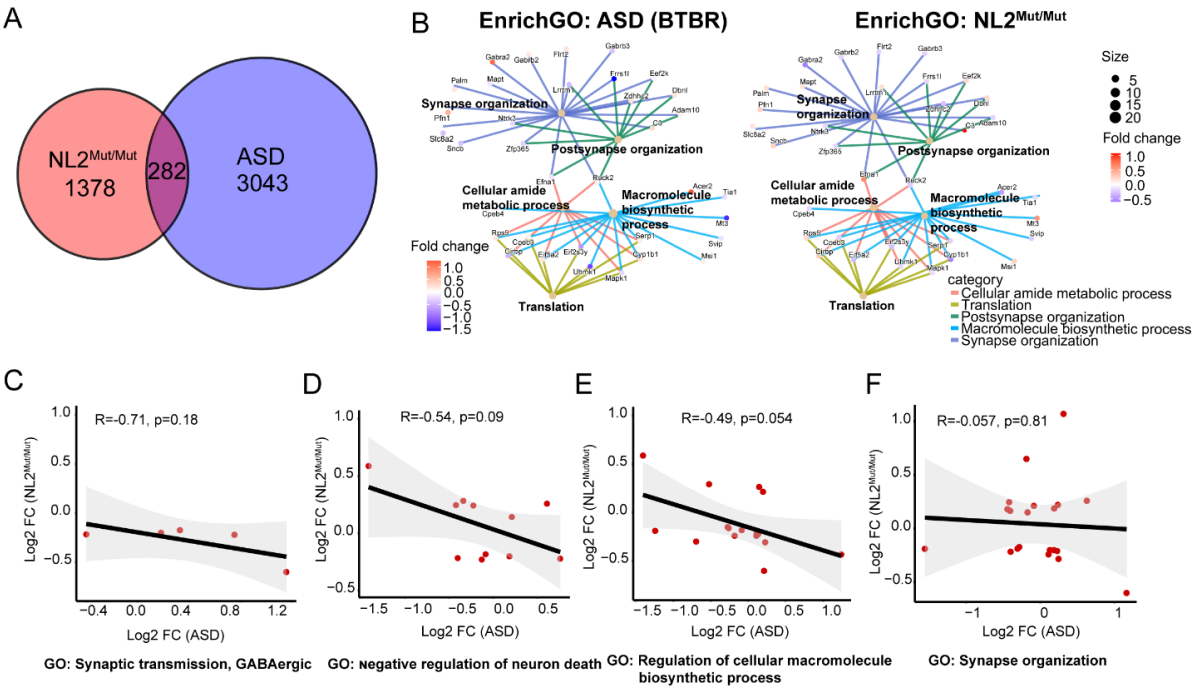

Figure 23. Comparison of NL2ΔSite II and ASD.

(A) Venn diagram showing the number of shared and unique genes between NL2$^{Mut/Mut}$ and ASD mice, a total of 282 DEGs were identified. (B) Enrich GO regulatory network of NL2$^{Mut/Mut}$ and ASD. The size of the point indicates the connectivity, with a larger point indicating greater connectivity. Upregulated genes are depicted in orange, while downregulated genes are represented in purple. Pearson analysis showed the correlation between NL2$^{Mut/Mut}$ and ASD in GABAergic synaptic transmission (C), negative regulation of neuron death (D), regulation of cellular macromolecule biosynthetic processes (E) and synapse organization (F).

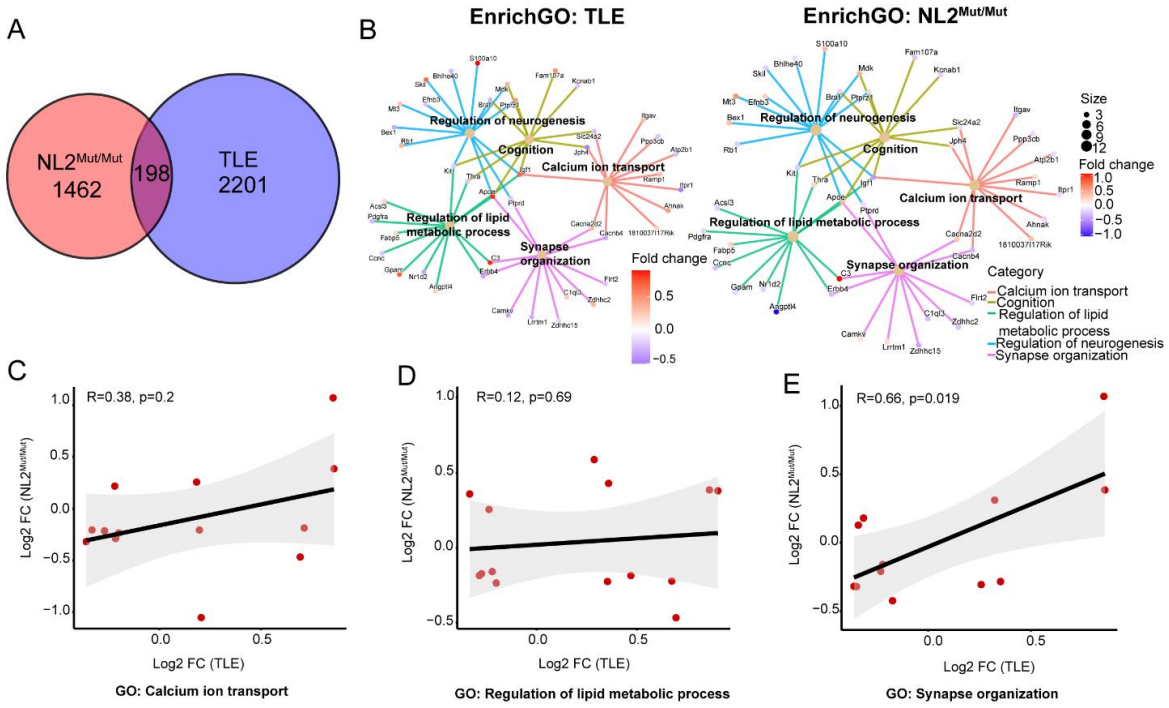

Figure 24. Comparison of NL2ΔSite II and TLE.

(A) Venn diagram showing the number of shared and unique genes between NL2$^{Mut/Mut}$ and TLE mice, a total of 198 DEGs were identified. (B) Enrich GO regulatory network of NL2$^{Mut/Mut}$ and TLE. The size of the point indicates the connectivity, with a larger point indicating a greater degree of connectivity. Upregulated genes are depicted in orange, while downregulated genes are represented in purple. Pearson analysis showed the correlation between NL2$^{Mut/Mut}$ and TLE in calcium ion transport (C), regulation of lipid metabolic process (D) and synapse organization (E).

3.5 NL2ΔSite II results in increased anxiety, enhanced fear memory and impairment in social memory

3.5.1 NL2ΔSite II results in enhanced anxiety behavior in mice.

Mutations and altered expression of NL2 and its binding partners are associated with neuropsychiatric and cognitive illnesses including autism, anxiety and schizophrenia(Ali et al., 2020). To explore whether the uncoupling of MDGAs and NL2 results in behavioral abnormalities in mice, the open field test (Figure 25A), elevated plus maze (Figure 25E), rotarod test (Figure 25H), novel object recognition test (Figure 26A), three chamber test (Figure 26B and C), Y maze (Figure 26D) and contextual fear conditioning (Figure 26E) were conducted to evaluate the anxiety, motion coordination, social ability, and learning and memory capacity in the KI model.

Firstly, the open field task was used to assess basal levels of anxiety. Open field results revealed that the time in center (Figure 25B), the number of entries into the center (Figure 25C) and the total travel distance (Figure 25D) in $NL2^{Mut/Mut}$ mice were significantly decreased compared to that in $NL2^{+/+}$ mice. Elevated plus maze results demonstrated that the time spent (Figure 25F) and number of entries (Figure 25G) in open arms in $NL2^{Mut/Mut}$ mice were also significantly decreased compared to that in $NL2^{+/+}$ mice. These results indicate that $NL2^{Mut/Mut}$ mice show higher anxiety-like behavior. The rotarod results reveal that as the training time increases, the motor coordination of both groups of mice markedly improved (Figure 25I), indicating that NL2ΔSite II in mice does not affect the motor coordination and balance ability.

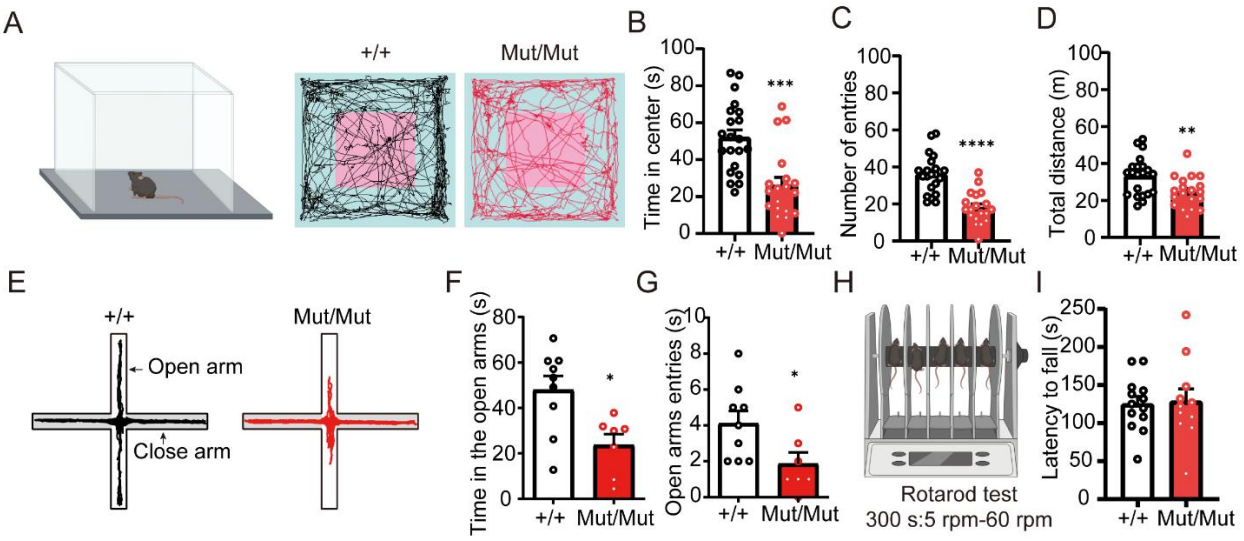

Figure 25. NL2ΔSite II enhances anxiety-like behavior in mice.

The mice underwent tests for anxiety-related behavior tests and mobility. Means are represented as mean ±S.E.M. Two-tailed unpaired student`s t-test was performed to test for differences between groups. (A) The schematic diagram of open field test and tracks of $NL2^{Mut/Mut}$ (red) and $NL2^{+/+}$(black). The time spent in center (B), the number of entries into the center (C) and the total distance travelled (D) are shown. $NL2^{Mut/Mut}$ mice demonstrate a decrease in the time spent in the arena center, the number of entries into the center, and total distance travelled compared to $NL2^{+/+}$ mice. ($NL2^{+/+}$ (n=21) vs. $NL2^{Mut/Mut}$ (n=19), time spent in center: 51.94±4.174 vs. 26.03±4.355, ***p<0.001; number of entries to the center:35.95±2.290 vs. 18.05±1.965, ****p<0.001; total distance:33.24±2.275 vs. 24.56±1.916, **p<0.01). (E) The schematic diagram of elevated plus maze and tracks of $NL2^{Mut/Mut}$ (red) and $NL2^{+/+}$(black). The time spent in the open arms (F) and the number of entries into the open arms (G) are shown. $NL2^{Mut/Mut}$ (n=7) mice demonstrate a decrease in the time spent in the open arms and a decrease in the number of entries into the open arms compared to $NL2^{+/+}$(n=9) mice. ($NL2^{+/+}$ vs. $NL2^{Mut/Mut}$, time spent in the open arms: 47.94±6.142 vs.23.70±4.771, *p<0.05; the number of entering the open arms: 4.11±0.696 vs.1.857±0.634, *p<0.05). (H) The schematic diagram of rotarod test. (I) There is no significant difference in the delayed drop time of either $NL2^{+/+}$ (n=13) or $NL2^{Mut/Mut}$ (n=11) groups. ($NL2^{+/+}$ vs. $NL2^{Mut/Mut}$, latency to fall:125.1±9.846 vs. 128.5±16.320, p>0.05).

3.5.2 NL2ΔSite II results in enhance fear memory and impaired social memory in mice.

Next, social behaviors and learning and memory function were measured. The novel object recognition test was conducted to evaluate object discrimination and learning and memory capacity. The discrimination index (The time spent with the novel object/the total object exploration time x 100%) (Figure 26Ai) in $NL2^{Mut/Mut}$ mice was comparable to that in $NL2^{+/+}$ mice. Next, the three-chamber test was performed to evaluate the social function of mice. The detection index is divided into two stages, the sociability during training (Figure 26B) and social memory during testing (Figure 26C). During training, both $NL2^{+/+}$ and $NL2^{Mut/Mut}$ mice show similar social preference (Figure 26Bi-Bii). During testing, the $NL2^{Mut/Mut}$ mice showed no social preference between new and familiar mice (Figure 26Ci-Cii), suggesting NL2ΔSite II impairs social memory in mice.

In addition, to further investigate the influence of the interaction of MDGAs and NL2 to the capacity of learning and memory, behavioral experiments that are highly correlated with hippocampus function were performed. First, the Y maze was conducted to evaluate the spatial discrimination and working memory of mice. Compared to $NL2^{+/+}$mice, $NL2^{Mut/Mut}$ mice show no significant difference in the spontaneous alternation index (Figure 26Di), and the discrimination index was also intact (Figure 26Dii), indicating that hippocampus-mediated spatial exploration capacity and working memory were intact in male $NL2^{Mut/Mut}$ mice. Next, contextual fear conditioning was performed to evaluate learning and memory ability of mice. During training, the freezing level was measured before footshocks and after three footshocks. The freezing percentage of the two groups of mice increased along with the increase in the number of footshocks (Figure 26E), indicating that the pain learning ability and pain sensitivity were normal in $NL2^{Mut/Mut}$ mice. During testing, the freezing percentages 24 hours and 72 hours after footshocks were measured. Either 24 hours or 72 hours after footshocks, the freezing percentage of $NL2^{Mut/Mut}$ mice was

increased relative to $NL2^{+/+}$ mice (Figure 26Ei), suggesting that fear memory was significantly enhanced in $NL2^{Mut/Mut}$ mice. Cumulatively, NL2ΔSite II increases anxiety and fear memory, impairs social memory but does not affect the motor coordination, social preference, spatial exploration capacity and working memory of mice.

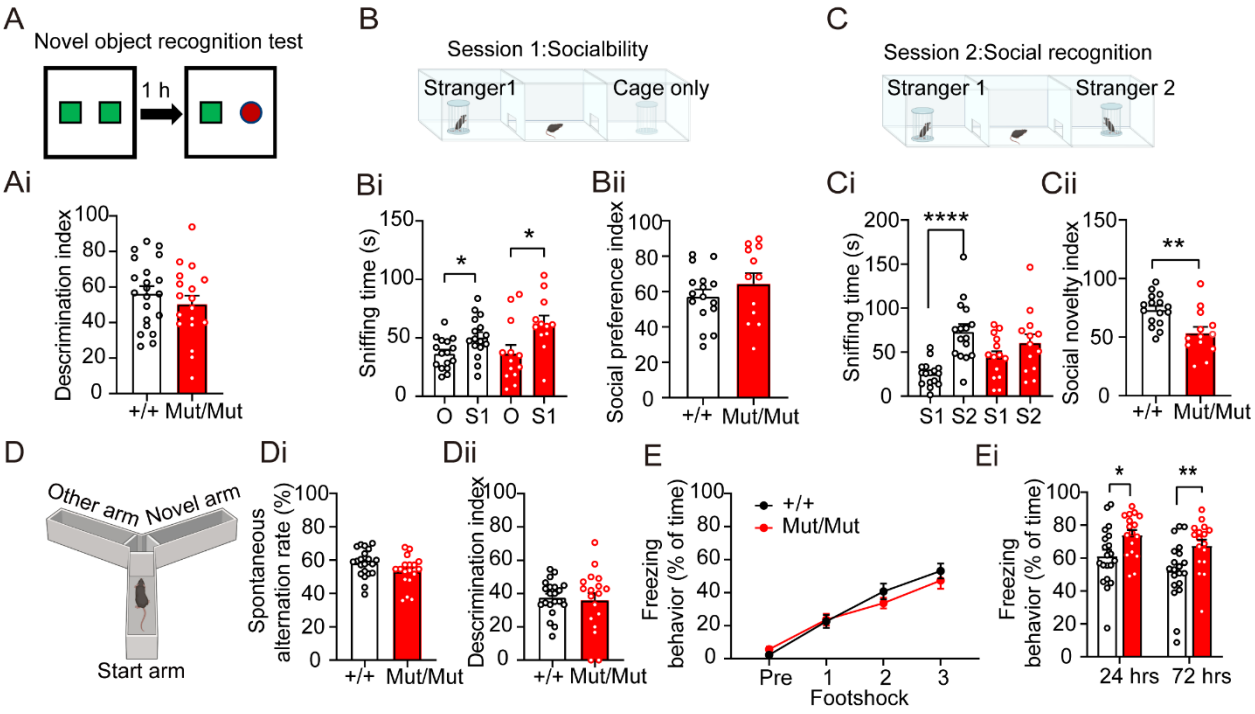

Figure 26. NL2ΔSite II impairs social memory and enhances the fear memory.

Mice underwent the novel object recognition test, three-chamber test, Y-maze and contextual fear conditioning test. Means are represented as mean ±S.E.M. Two-tailed unpaired student`s t-test were performed. (A) The schematic diagram of novel object recognition test. (Ai) There is no significant difference of novel object discrimination index in both $NL2^{+/+}$ (n=21) and $NL2^{Mut/Mut}$ (n=18) groups of mice. ($NL2^{+/+}$ vs. $NL2^{Mut/Mu}$, novel object discrimination index: 56.42±4.056 vs. 50.27±4.912, p=0.3359). (B) The schematic diagram of the training (first stage) of three-chamber test. The time spent in the left and right regions (Bi) and social preference index (Bii) are shown. The time spent in the strange mice (S1) in both $NL2^{+/+}$ (n=16) and $NL2^{Mut/Mut}$ (n=12) groups of mice is significantly higher than that in the empty cage (O). There is no significant difference of

social preference index between the two groups of mice. ($NL2^{+/+}$ time spent in O vs. S1: 36.51±3.298 vs.50.56±4.354, *p<0.05; $NL2^{Mut/Mut}$ time spent in O vs. S1: 36.43±7.900 vs. 62.35±6.769, *p<0.05; $NL2^{+/+}$ vs. $NL2^{Mut/Mut}$ social preference index: 57.32±3.917 vs. 64.33±6.125, p=0.3234). (C) The schematic diagram of the testing (second stage) of three-chamber test. The time spent in the left and right regions (Ci) and social novelty index (Cii) are shown. There is no significant difference between the time spent in S1 and the new strange mice (S2) in $NL2^{Mut/Mut}$ (n=12) mice. However, the $NL2^{+/+}$ mice (n=16) spent significantly more time with S2. Accordingly, the social novelty index of $NL2^{Mut/Mut}$ mice is significantly decreased compared to $NL2^{+/+}$ mice. ($NL2^{+/+}$, time spent in S1 vs. S2:25.44±3.437 vs.73.33±8.405, ***p<0.001; $NL2^{Mut/Mut}$, time spent in S1 vs. S2: 47.39±6.943 vs. 63.99±10.13, p=0.1904; $NL2^{+/+}$ vs. $NL2^{Mut/Mut}$ social novelty index: 73.32±3.370 vs. 55.52±5.361, **p<0.01). (D) The schematic diagram of the Y-maze, which is classified into novel arm, start arm and other arm. (Di) The spontaneous alteration rate of $NL2^{Mut/Mut}$ (n=18) mice is comparable to that of $NL2^{+/+}$ (n=21) mice. (Dii) There is no significant difference of the exploration time of novel arm between the two groups of mice. ($NL2^{+/+}$ vs. $NL2^{Mut/Mut}$ spontaneous alteration rate: 58.11±1.802 vs. 53.14±2.180, p=0.0844. $NL2^{+/+}$ vs. $NL2^{Mut/Mut}$ the exploration time of novel arm:37.68±2.283 vs. 35.99±4.353, p=0.7223). (E) The freezing level of two groups of mice increases as the number of footshocks increases in contextual fear acquisition. (Ei) During the contextual fear retrieval, the freezing level of $NL2^{Mut/Mut}$ (n=17) mice is significantly increased compared to $NL2^{+/+}$ (n=20) mice at 24 hours and 72 hours after footshocks training. (The freezing level of $NL2^{+/+}$ vs. $NL2^{Mut/Mut}$ before footshocks: two-way ANOVA, genotype $F_{1,140}$=0.63, p=0.43; The freezing level of $NL2^{+/+}$ vs. $NL2^{Mut/Mut}$ at 24 hours after footshocks: Two- tailed unpaired student`s t-test: 61.08±3.937 vs.73.87±3.149, *p<0.05; The freezing level of $NL2^{+/+}$ vs. $NL2^{Mut/Mut}$ at 72 hours after footshocks: Two- tailed unpaired student`s t-test: 52.28±4.056 vs. 67.46±3.653, **p<0.01).

PROJECT2: 3.6 Adult knockout of Mdga1 and Mdga2 increases the excitability of CA1 pyramidal neurons.

Most studies to date have focused on studying MDGA1 or MDGA2 (Connor et al., 2019). Accordingly, MDGA1/2 DKO mice can be used to address key questions surrounding functional compensation or how these proteins operate in tandem (or opposition) to regulate synapses. To date, no studies have elucidated the neuronal effects of MDGA1/2 DKO in vivo. Previous studies have shown that KD of *Mdga1* in *Mdga2* heterozygous KO cells increased the frequency of mIPSCs, suggesting that MDGA1 is able to functionally compensate for loss of MDGA2 at inhibitory synapses (Connor et al., 2016a). However, this experiment was conducted in cell cultures and residual levels of MDGA2 due to the use of heterozygous KO cells confounds interpretation of these findings. Therefore, a critical question remains as to what will happen within neural circuits when both MDGA1 and MDGA2 are knocked out? To begin to address this, I explored basal characteristics of cellular properties and synapse function in hippocampal brain slices extracted from MDGA1/2 DKO mice to examine neuronal intrinsic excitability, and mIPSC and mEPSC characteristics in this novel mouse line.

I first sought to determine whether combined Mdga1 and Mdga2 deficiency alters neuronal properties, including intrinsic excitability, RMP and input resistance (Rin) of CA1 pyramidal neurons. AAV2/9-CaMKII-Cre-mCherry or AAV2/9-CaMKII-mCherry was administered to 5–6 week-old $Mdga1^{f/f}Mdga2^{f/f}$ mice. Whole-cell patch-clamp recordings were made to measure the excitability of virus infected CA1 PNs using ex vivo slice electrophysiology 4–5 weeks later. APs in virus-infected CA1 PNs were induced by injecting depolarizing currents in incremental steps (Δ = 50 pA, 1 s duration).

As shown in Figure 27 A and B, the AP firing rate was significantly greater in the MDGA1/2 DKO (Cre) mice when compared to control (Ctrl) mice, while the Rin and RMP remained unaltered (Figure 27 C and D). This data indicates that CA1 PNs are more excitable in MDGA1/2 DKO mice as demonstrated by the elevated AP frequency in response to injected current. To confirm this results, another protocol was applied to measure neuronal firing upon the injection of ramped depolarizing currents (Figure 27 E). Consistent with the previous result, AP numbers recorded in virus infected CA1 PNs in MDGA1/2 DKO mice were significantly increased compared to control mice (Figure 27 F). These results suggest that dual reduction of MDGA1/2 renders CA1 PNs are more hyperactive relative to neurons containing both MDGA1 and MDGA2.

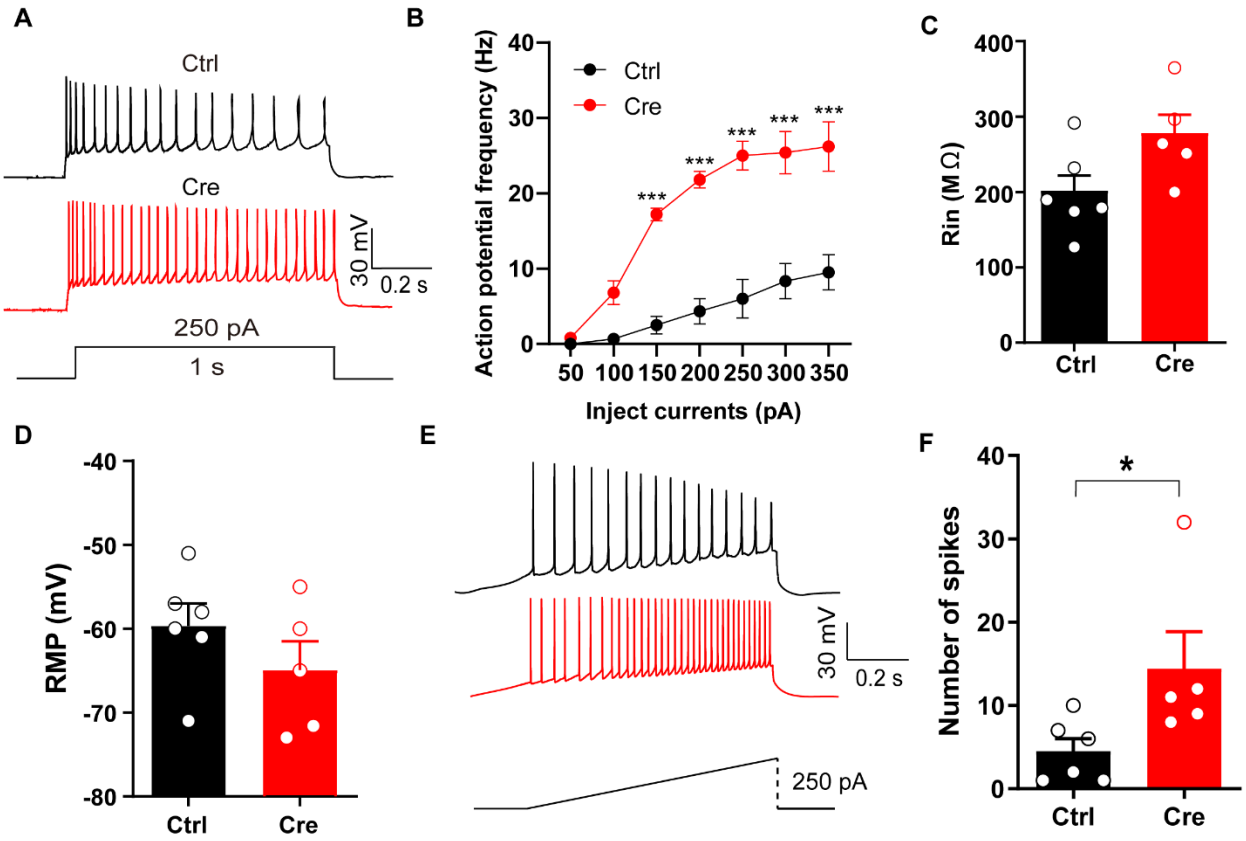

Figure 27. Adult knockout of Mdga1 and Mdga2 in hippocampal CA1 pyramidal neurons elevates neuronal excitability.

(A) Representative traces of AP firing in response to injection of current in neurons from control (Ctrl) and CA1-MDGA1/2 DKO (Cre) mice. (B) MDGA1/2 DKO in CA1 PNs increases the number of APs relative to the injected current strength. n = 6 neurons, 2 mice for control (Ctrl) group; n = 5 neurons, 2 mice for MDGA1/2 DKO (Cre) group; $p < 0.0001$; $F(1, 154) = 19.79$; two-way ANOVA. (C) MDGA1/2-deficiency in CA1 PNs had no effect on the input resistance (Rin). n = 6 neurons, 2 mice for control (Ctrl) group; n = 5 neurons, 2 mice for MDGA1/2 DKO (Cre) group; $p = 0.0591$, unpaired t test. (D) MDGA1/2 deficiency in CA1 PNs had no effect on RMP. n = 6 neurons, 2 mice for control (Ctrl) group; n = 5 neurons, 2 mice for MDGA1/2 DKO (Cre) group; $p = 0.2499$, unpaired t test. (E) Representative spiking traces showing the firing of CA1 PNs upon the injection of a depolarizing current ramp (0–250 pA, 1 s). (F) Summary plots of AP numbers with ramped depolarizing current injected into CA1 PNs, as in E. n = 6neurons, 2 mice for control (Ctrl) group; n = 5 neurons, 2 mice for MDGA1/2 DKO (Cre) group; $p= 0.0493$, unpaired t test.

3.7 Adult Mdga1 and Mdga2 knockout in hippocampal CA1 pyramidal neurons increases excitatory but decreases inhibitory synaptic strength.

3.7.1 Adult Mdga1 and Mdga2 knockout in hippocampal CA1 pyramidal neurons decreases the amplitude of mIPSC without changing the frequency.

Next, I examined the impact of dual loss of MDGA1 and MDGA2 on synaptic function. Whole-cell voltage-clamp recordings were made in CA1 PNs in acute brain slices from MDGA1/2 DKO and control mice. As shown in Figure 28A, compared with controls, combined MDGA1 and MDGA2 reduction had no effect on mIPSC frequency but significantly decreased the amplitude of mIPSCs (Figure 28B, C), relative to control neurons. Consistent with these effects, no shift in

frequency curves (Figure 28B) and a significant leftward shift in the cumulative probability curve of the mIPSC amplitude (Figure 28C) were found, respectively.

3.7.2 Adult Mdga1 and Mdga2 knockout in hippocampal CA1 pyramidal neurons increases the amplitude of mEPSC without changing the frequency.

Additional exploration of effects on excitatory transmission onto CA1 PNs was assayed by recording mEPSCs. As shown in Figure 29A, MDGA1/2 DKO did not detectably change the mean and cumulative probability curve of mEPSC frequency (Figure 29B) but increased the mean or cumulative probability curve of mEPSC amplitude (Figure 29C).

Further analysis of mIPSC and mEPSC kinetics (decay, rise time, halfwidth and 10%-90% slope; Figure 28D–G and Figure 29D–G) showed that the MDGA1/2 DKO mice increased the decay time in mIPSCs. The extended decay time may reflect slower clearance of unbinding of GABA from postsynaptic $GABA_A$ receptors or altered receptor kinetics. This prolongation may be a compensatory response to the reduced mIPSC amplitude noted above. For mEPSC, a significant increased in the 10%-90% slope was detected in MDGA1/2 DKO mEPSCs compared to control mice. This finding is consistent a more rapid postsynaptic depolarization upon glutamate release which may, in part, explain the hyperactivity phenotype noted above MDGA1/2 DKO neurons. Other kinetics of mIPSCs and mEPSCs in CA1 PNs were not altered by late Mdga1 and Mdga2 double knockout.

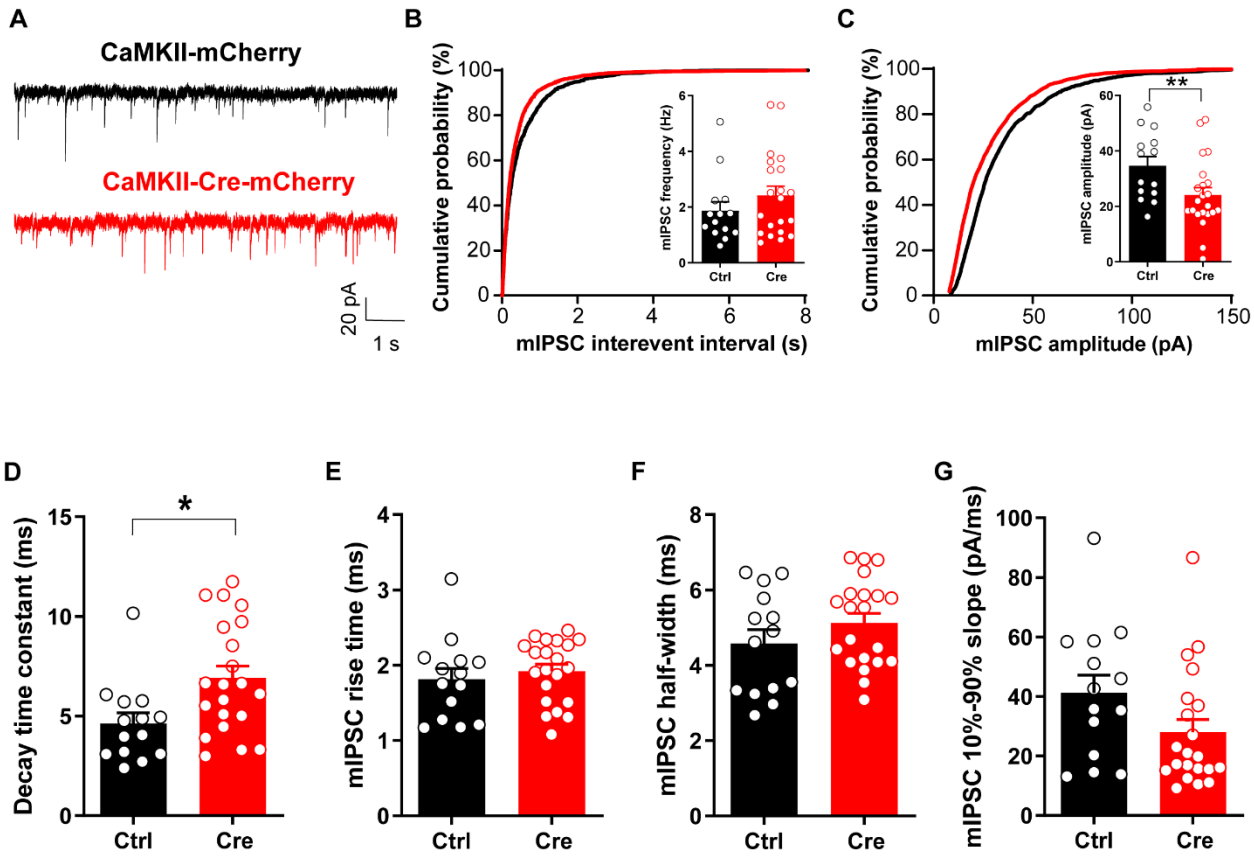

Figure 28. Adult knockout of Mdga1 and Mdga2 in hippocampal CA1 pyramidal neurons decreased inhibitory synaptic strength.

(A) Representative mIPSC traces in CA1 pyramidal neurons. (B) No significant differences were found between MDGA1/2 DKO (Cre) neurons and control (Ctrl) neurons in mIPSC frequency. n = 14 neurons, from 3 mice for Ctrl, n = 21 neurons, from 5 mice for Cre; P = 0.1272, unpaired t test. (C) MDGA1/2 DKO (Cre) neurons exhibit a significant decrease in mIPSC amplitude compared with control (Ctrl) neurons; P = 0.0089, unpaired t test. n = 14 neurons, from 3 mice for Ctrl, n = 21 neurons, from 5 mice for Cre. This increase results in a leftward shift in the cumulative probability curve corresponding to reduced inter-event intervals. (D-G) Comparison of kinetics (decay time, rise time, half-width and 10%-90% slope) between mIPSCs in CA1 control (Ctrl) neurons and MDGA1/2 DKO (Cre) neurons. n = 14 neurons, from 3 mice for Ctrl, n = 21 neurons, from 5 mice for Cre. Decay time: P = 0.0128, others: P > 0.05, unpaired t test.

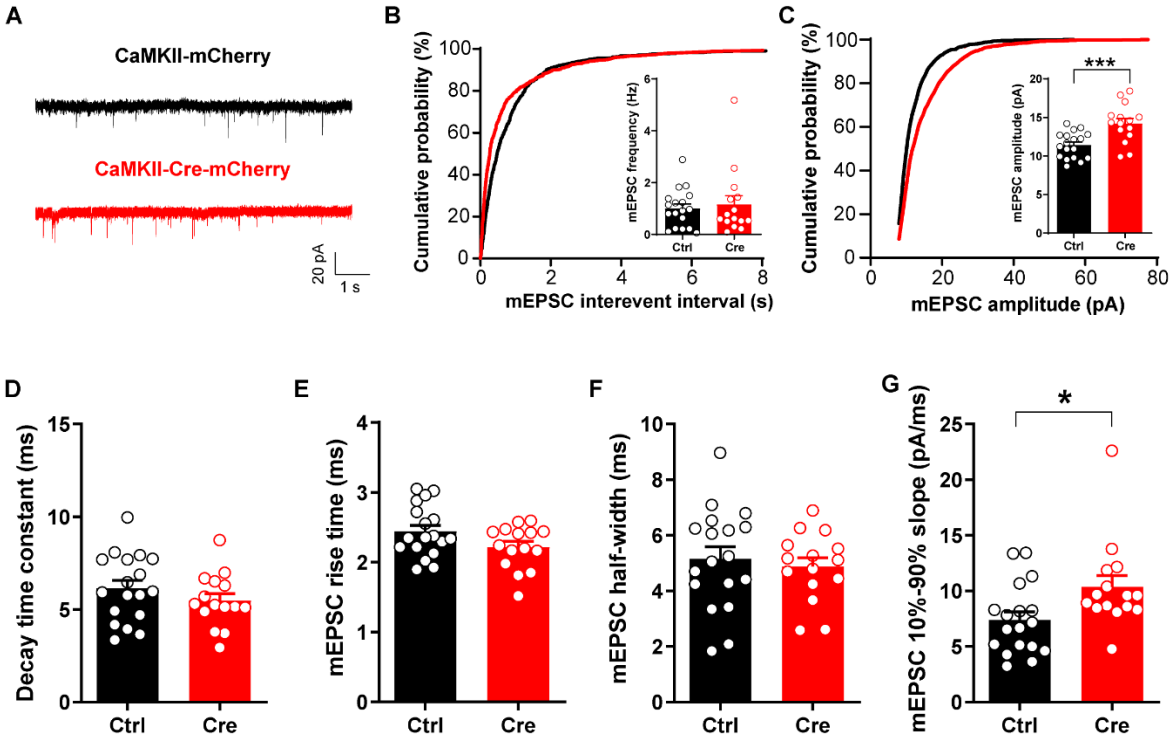

Figure 29. Adult KO of Mdga1 and Mdga2 in hippocampal CA1 pyramidal neurons elevates excitatory synaptic strength.

(A) Representative mEPSC traces in CA1 pyramidal neurons. (B) No significant differences were found between MDGA1/2 DKO (Cre) neurons and control (Ctrl) neurons in mEPSC frequency. n = 18 neurons, from 3 mice for Ctrl, n = 19 neurons, from 3 mice for Cre. P = 0.6533, unpaired t test. (C) MDGA1/2 DKO (Cre) neurons exhibit a significant increase in mEPSC amplitude compared with control (Ctrl) neurons; n = 18 neurons, from 3 mice for Ctrl, n = 19 neurons, from 3 mice for Cre. P = 0.0005, unpaired t test. This increase results in a rightward shift in the cumulative probability curve corresponding to increased inter-event intervals. (D-G) Comparison of kinetics (decay time, rise time, half-width and 10%-90% slope) between mEPSCs in CA1 control (Ctrl) neurons and MDGA1/2 DKO (Cre) neurons. n = 18 neurons, from 3 mice for Ctrl, n = 19 neurons, from 3 mice for Cre. 10%-90% slope: P = 0.0215, others: P > 0.05, unpaired t test.

Chapter 4 Discussion

4.1 Decoding the significance of NL2/MDGA interactions.

In this study, we prepared a new transgenic animal model to study the synaptic function of NL2 by mutating the key structural site where NL2 binds to MDGA proteins (NL2ΔSite II). The transgenic mouse model was validated at the gene and mRNA transcription levels. As shown in Figure 15A, conversion of five amino acids to alanine was optimal for obtaining a clear binding differential and the resulting cellular phenotype.

Importantly, multiple NL2 variants have been discovered in human patients with schizophrenia, autism and anxiety disorders and several mouse models of these variants in human mimic associated psychiatric phenotypes (Ali et al., 2020). For example, the R215H point mutation (D.-Y. Jiang et al., 2018; Sun et al., 2011) and de novo nonsense mutation (Y147*) (Parente et al., 2017) in NL2 were found in patients with schizophrenia and ASD, respectively. Furthermore, two homozygous R215H KI mouse lines were generated, which showed reduced expression of mature NL2 protein and limited glycosylation, mimicking the loss-of-function of constitutive KOs (D.-Y. Jiang et al., 2018; Sun et al., 2011). Conversely, this NL2ΔSite II mouse model may mimic the NL2 OE model due to the impairment of the interaction between NL2 and MDGAs, biasing NL2 binding towards presynaptic NRXNs. At the transcription level, NLs, NRXNs and MDGAs are not affected (Figure 16D-F).

Studies have shown that mutations in several of the interaction partners of NL2 at inhibitory synapses including NRXNs (Kasem et al., 2018), MDGAs (R. Wang et al., 2019), S-SCAM (Koide et al., 2012) and the IgSF9b (Schizophrenia Working Group of the Psychiatric Genomics Consortium, 2014) are risk factors for the onset of mental disorders. Therefore, the

animal model in the current study further contributes to the analysis of NL2 variants and potential additional mutations, which are essential for understanding the full extent and clinical impact of altered function of synapse organizers in brain disorders.

It is important to note that this NL2 point mutation may affect the binding of other key proteins. For example, hevin (high endothelial venule protein), also known as SPARCL1, is secreted by astrocytes and can promote synapse development by targeting the NL-NRXN complex which is also blocked by MDGAs. This synaptogenesis-dependent induction of hevin is antagonized by SPARC (Figure 30). Hevin contains a follistatin-like (FS) domain and an extracellular calcium-binding (EC) domain. To evaluate whether MDGAs and hevin compete for NL2 binding, point mutation of NL2 was tested to determine if it disrupts the binding of MDGA as well as hevin (Fan et al., 2021). As shown in Figure 31, NL2 Mut1, 3 and 4 can disrupt the binding of MDGA1 while Mut2 cannot. Hevin FS domain can bind to Mut2 but cannot bind to Mut1, 3 and 4. Therefore, the hevin FS domain competes with MDGA1 for binding NL2. However, our point mutations on NL2 are D407A, F408A, S411A, N412A and R428A, which are different from Mut1, 3 or 4. Whether this point mutation can affect the binding of hevin remains unknown. Accordingly, functional experiments need to be performed to explore how hevin affects MDGA1-NL2 interactions.

Additionally, protein-protein interactions need to be assessed to test if our mutations further modify other NL2 interactions. Several notable interactions have been identified, including SPARC which competes with hevin for binding to the NL2-NRXN complex (Fan et al., 2021). Similar to MDGA, γ-protocadherin can also bind to NL2 which appears to block NL-NRXN3 binding (Steffen et al., 2021). Finally, thrombospondin-1 can bind to NL1 which is blocked in the

presence of MDGA (Elegheert et al., 2017). Further experiments are required to determine if NL2 point mutation affects the binding of these proteins.

MDGA1 can bind to presynaptic amyloid precursor protein (APP) in CA1 SLM to impair GABAergic synapse maintenance (J. Kim et al., 2022). In the MDGA1/2 DKO model, the APP singling pathway is completely out of control. This may lead to $GABA_AR$ internalization and increased AMPAR phosphorylation thus decrease and increase inhibitory synaptic transmission and excitatory synaptic transmission, respectively.

The receptor tyrosine kinases like TrkB are a NL2-dependent regulator of gephyrin clustering. The ligand of TrkB is brain-derived neurotrophic factor (BDNF). The interaction of BDNF and TrkB can trigger the release of Ca^{2+} from internal Ca^{2+} stores like endoplasmic reticulum (ER) and thereby activate CaMKII (A. I. Chen et al., 2011; Wüstner et al., 2024). This serve as a rationale that the inhibitory synaptic transmission is increased and the increased concentration of Ca^{2+} may activate downstream signaling pathway in the NL2ΔSite II model.

In the NL2ΔSite II mice, the synaptic NL2 aggregation maybe enhanced and the extrasynaptic NL2 localization maybe decreased. NL2-NRXN-gephyrin complex is no longer inhibited because it cannot bind to MDGAs. For example, immunofluorescence studies have shown that in MDGA1 KO mice, the density of synaptic puncta of NL2 in the hippocampus increased by approximately 40% (Connor et al., 2019). Also, the NL2 protein levels maybe increased. The Aβ -like region of NL2 can be cleaved by ADAM10 (Suzuki et al., 2012), uncoupling MDGA-NL2 binding may cover this cutting site thus protecting NL2 from being cut, leading to more NL2.

NL2ΔSite II completely destroys the combination of MDGA1/2 and NL2, the binding affinity decreased by more than 90%, as confirmed by surface plasmon resonance experiments (J. A. Kim et al., 2017). Releasing the inhibition of MDGAs on NL2 leads to the continuous activation of the NL2-gephyrin-neurexin pathway (Gangwar et al., 2017). The NL2ΔSite II mutation mimics the state of MDGA1/2 deletion but only targets the NL2 pathway. The absence of MDGA1 or MDGA2 also leads to an increase in NL2 synaptic aggregation to a degree similar to that of the NL2ΔSite II, but the frequency increase of mIPSC is more significant. This indicates that MDGA1 or MADGA2 not only regulates its synaptic localization by binding to NL2 but may also affect the presynaptic release probability through other indirect pathways (Connor et al., 2019). Furthermore, MDGA1/2 is generally regarded as a negative regulatory factor of inhibitory synapses, but the electrophysiology results of MDGA1/2 DKO model suggests that MDGA1/2 may indirectly regulate excitatory synapses through an unknown mechanism. MDGA1/2 DKO may trigger compensatory neural circuit remodeling such as enhancing glutamatergic synapse to counteract inhibitory synapse absence. It may also reflect the non-NL2 dependent functions of MDGAs.

In MDGA1 KO model, due to the relief of the inhibitory effect of MDGA1 on NL2, the aggregation of synaptic NL2 increases, leading to enhanced frequency of mIPSC (Connor et al., 2017a). Although the MDGA1 is absent, the interaction of NL2 and MDGA2 still exists, some NL2 is still inhibited. In MDGA1/2 DKO model, the decreased amplitude of mIPSC indicates MDGA1/2 may maintain inhibitory synaptic function through non-NL2-dependent pathways, such as directly regulating GABAAR transport. Moreover, the unchanged frequency and amplitude of mEPSC suggest that MDGA1 mainly regulates inhibitory synapses (Connor et al., 2017a). In MDGA1/2 DKO model, the amplitude of mEPSC increases. That suggests that the inhibitory input has decreased resulting in AMPAR compensatory upregulation.

The synaptic transmission in the MDGA1/2 DKO model maybe unchanged. Firstly, the synaptic transmission is not altered in MDGA1 KO and MDGA2 haploinsufficiency mice. Secondly, only the amplitude of mIPSC and mEPSC are changed in MDGA1/2 DKO model, the frequency which is related to presynaptic transmission is unaltered.

Triple KO of NL2, MDGA1 and MDGA2 can be used to further detect the function of these synaptic organizers, which can resolve the residual NL2 function interference in MDGA1/2 DKO. In the triple KO model, MDGAs regulation are completely lost, and due to the loss of NL2, the $GABA_AR$ transport system collapsed, and the gephyrin scaffold disintegrated, leading to decreased inhibitory synaptic transmission, which in turn contributing to the insertion of AMPAR and thus increased excitatory synaptic transmission.

This finding may not be specific to autism because NL2ΔSite II mice also show impaired social memory and increased fear memory which reflect the post-traumatic stress disorder (PTSD).

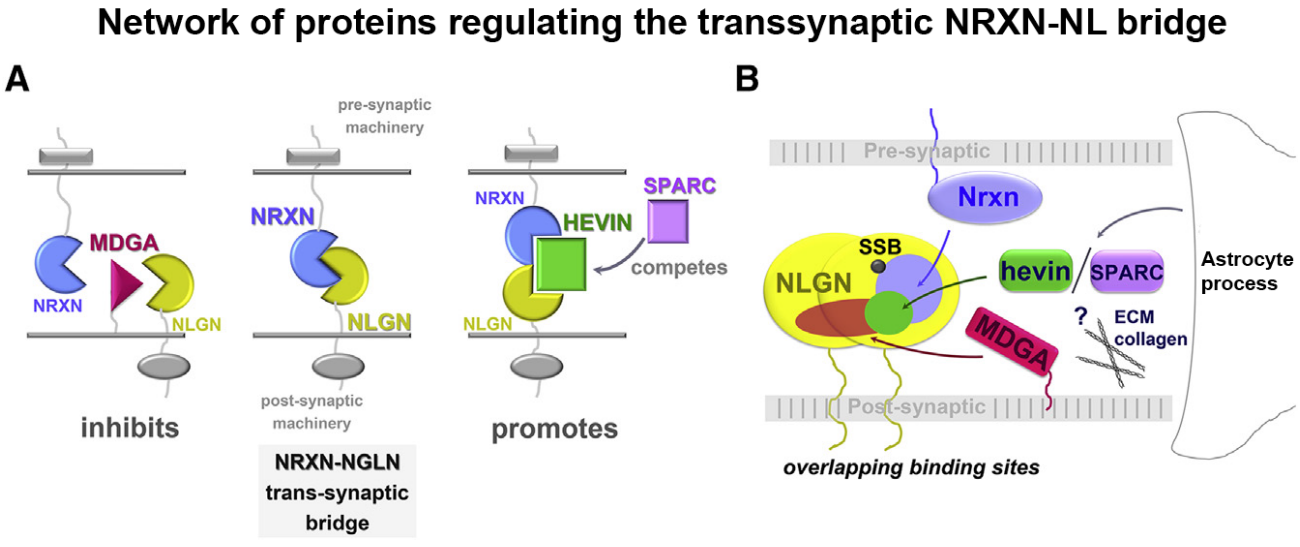

Figure 30. The NRXN-NL complex is regulated by networks of proteins.

(A) Positive (hevin) and negative (MDGA) modulators of NRXN-NL complex. (B) NLs and NRXNs from transsynaptic bridges that promote synapse development. Multiple modulators of the NRXN-NL complex compete for overlapping binding sites. The hevin FS domain binds both NRXNs and NLs via a direct interaction and competes with MDGAs for an overlapping binding site on NLs, whereas the hevin EC domain binds the ECM protein collagen. Antagonist SPARC also binds NRXN/NL, competing with hevin. Image is modified from (Fan et al., 2021).

Mutants	Mutated residues	Effect on binding to MDGA1 Ig1-Ig2
* NLGN2(+A)_Mut1	H278A, D362K, E372K	Disrupts binding to MDGA1 Ig1-Ig2
NLGN2(+A)_Mut2	F408A, R428A	Does not disrupt binding to MDGA1 Ig1-Ig2
* NLGN2(+A)_Mut3	H278A, D362, KE372K, F408A, R428A	Disrupts binding to MDGA1 Ig1-Ig2
* NLGN2(+A)_Mut4	H278A, D362A, E372A	Disrupts binding to MDGA1 Ig1-Ig2

Figure 31. NL2 mutants used in the study.

Image is modified from (Fan et al., 2021).

4.2 Inhibitory synapse function.

NL2ΔSite II phenocopies loss of MDGA1 but not MDGA2 as demonstrated by the selective effects on inhibitory synapses. Previous *in vitro* studies demonstrated that overexpression or sparce knockdown of MDGA1 reduced or elevated inhibitory synapse density, respectively (Pettem et al., 2013b). *In vivo*, the functional study of MDGAs has been limited primarily to hippocampal CA1 pyramidal cells. In *Mdga1*$^{-/-}$ mice, perisomatic inhibitory synapse density was

increased, whereas dendritic inhibitory synapses were not affected (Connor et al., 2017a). However, recent evidence showed an interaction between MDGA1 and APP negatively regulates inhibitory synapse density in CA1 SLM layer which receives SST interneuron inputs (J. Kim et al., 2022).

Functionally, studies have shown NL2 deletion (Poulopoulos et al., 2009) and MDGA1 deletion (Connor et al., 2017a) reduced and upregulated the frequency of mIPSCs, respectively. Alternatively, both constitutive and conditional knockout of MDGA2 increased the frequency and amplitude of mEPSCs (Connor et al., 2016a; X. Wang et al., 2024). This discrepancy likely is the result of the differential regulation of the NLs by MDGA1 (NL2) and MDGA2 (NL1), which would affect inhibitory and excitatory synapse development, respectively (Connor et al., 2016a).

GO analysis revealed that the differential DEG regulation between $NL2^{Mut/Mut}$ and $NL2^{+/+}$ were mainly detected in postsynaptic membrane, postsynaptic density, postsynaptic specializations, processes in the postsynapse and GABAergic synaptic transmission (Figure 17C-F). Additionally, NL2ΔSite II enhanced the frequency of mIPSCs (Figure 18A-C) without affecting mEPSCs (Figure 18D-F), which reflects gain-of function of NL2 in this animal model and further supports the idea that the binding of NL2 and MDGA1 selectively affects inhibitory synapses.

4.3 Inhibitory synapse density.

Deletion of NL2 disrupts postsynaptic clustering of $GABA_A$Rs and gephyrin not only in SP but also in SR (Panzanelli et al., 2017). Previous work has identified the parvalbumin-expressing (PV^+) GABAergic interneurons form inhibitory synapses preferentially at perisomatic sites containing NL2 homomeric dimers while SOM^+ interneurons form inhibitory synapses preferentially at dendrites containing NL2-NL3 heterodimers (Horn & Nicoll, 2018).

Overexpression of NL2 in hippocampal neurons increases gephyrin, $GABA_ARs$ and VGAT, indicating trans-synaptic enhancement of GABAergic synapses (Van Zandt et al., 2019). In *Mdga2*$^{+/-}$ mice, the punctate immunofluorescence of VGluT1 was upregulated in SR (Connor et al., 2016a), whereas following knockout of MDGA2 in adult mice, this effect extends to SO and SLM without affecting $VGAT^+$ areas in SO, SP, SR or SLM (X. Wang et al., 2024). Consistently, NL2ΔSite II resulted in increased inhibitory synapse density in SP, SR and SLM (Figure 20B) without affecting excitatory synapse density in SO, SR and SLM (Figure 21B), suggesting that diverse hippocampal interneuron networks are involved.

4.4 Bioinformatics.

Given that the growing body of data implicating alterations in the function of GABAergic synapses and neurons in a broad range of psychiatric and neurodevelopmental disorders, we compared the transcriptome data of our NL2ΔSite II model with NDDs models including SCZ, ASD, and TLE. Although SCZ and ASD are two different disorders, they share some common pathogenic genes, including shank3 (Huang et al., 2023; Zhou et al., 2016). The high Pearson's correlation between NL2ΔSite II and shank3$^{-/-}$ (Figure 22) indicate that this NL2ΔSite II model mimic gene regulation profiles of SCZ and ASD. Thus, disrupting NL2-MDGAs induced gene regulatory changes that mirror major forms of NDD. It will be important going forward to experimentally link the noted changes in transcription regulation to elevated E/I ratio at synapses in our model. Additionally, it will be critical to determine if the noted changes in transcription regulation are borne out at the level of protein expression to further refine out of the connection between disrupted NL2-MDGA1 interactions and changes in mRNA and protein production.

4.5 Behavioral impact of preventing NL2/MDGA interactions.

Our behavioral results of indicated that anxiety behaviours were increased in both the open field test (Figure 25A-D) and EPM tests (Figure 25E-G) in NL2ΔSite II mice. These findings indicate that loss of proper regulation of NL2 and corresponding shifts in E/I balance likely contribute to altered neural circuits that promote anxiogenesis. Interestingly, this also suggest that both increases and decreases in E/I balance at NL2-containing synapses may contribute to anxiety (Ali et al., 2020). For example, constitutive global knockout of NL2 results in a robust anxiety phenotype (Babaev et al., 2016). Additionally, transgenic mice with a moderate overexpression of NL2 show anxiety-like symptoms (Hines et al., 2008). Importantly, it will be instructive to investigate brain structures and synaptic function beyond the hippocampus in which NL2-mediated synaptic inhibition is observed as other brain areas and neural networks may contribute to anxiety. This need is highlighted by the discrepancies that emerged when examining the role of NL2 in specific brain regions. For example, deletion of NL2 in BLA and vHPC increased anxiety (Cruces-Solis et al., 2021), while deletion of NL2 in mPFC (Liang et al., 2015) and LS (Troyano-Rodriguez et al., 2019) reduced anxiety-like behaviours.

Interestingly, LFP recordings during the exploration of an open field suggested that the LFP power in vHPC-mPFC-BLA circuits is a better indicator for predicting anxiety than that in the individual brain regions (Cruces-Solis et al., 2021). Thus, determining the network effects may be useful for understanding how NL2 contributes to brain wide effects on susceptibility to anxiety. In addition, the conserved pain sensitivity (Figure 26E) and motor function (Figure 25I) in $NL2^{+/+}$ and $NL2^{Mut/Mut}$ mice match those observed in earlier studies indicating that both sensory function and locomotor activity were intact in the transgenic mice with a moderate overexpression of NL2 (Hines et al., 2008). Accordingly, the decreased total distance in open field test indicative of

reduced exploratory activity most likely reflects the anxiety phenotype (Babaev et al., 2016) in $NL2^{Mut/Mut}$ mice.

In terms of social behaviors, social recognition memory was impaired in $NL2^{Mut/Mut}$ mice compared to that in $NL2^{+/+}$ mice, in accord with studies indicating that gain-of-function or AAV-mediated overexpression of NL2 in hippocampus did not alter sociability but significantly impaired social recognition memory (Hines et al., 2008; Kohl et al., 2015). This finding indicates that intact NL2/MDGA interactions are required for specific aspects of social skills and that loss of this complex may selectively interfere with one's ability to recognize others in social settings, which has important implications for our understanding of social deficits in ASD. An inability to appropriately identify individuals which one has interacted with before may elevate social anxiety, contributing to the noted social withdrawal observed in some cases of autism.

Very few studies have explored the roles of NL2 in cognitive function. In the present study, the $NL2^{Mut/Mut}$ mice did not show significant differences in novel object recognition or spatial working memory in Y maze compared to $NL2^{+/+}$ mice. Some studies have shown that OE of NL2 in hippocampus impaired social memory but not sociability, disrupting hippocampal dependent spatial memory assayed by the novel object recognition test (Van Zandt et al., 2019).

Others have shown that, global deletion of NL2 and conditional knockout of NL2 in mPFC did not alter novel object recognition ability (Cao et al., 2020) or spatial memory ability in Y maze (Liang et al., 2015). Collectively, these results suggest that shifting of E/I balance in either direction has no detectable effect on cognitive processes required for novel object recognition or the Y maze. Intriguingly, the $NL2^{Mut/Mut}$ mice showed enhanced contextual fear memory (Figure 26Ei) compared to $NL2^{+/+}$ mice without affecting fear memory acquisition (Figure 26E). However, one study has shown that conditional knockout of NL2 in mPFC impairs contextual fear memory

acquisition and consolidation but not retrieval (Liang et al., 2015). Thus, the present study further refines the roles of NL2 and MDGAs in fear memory circuits, indicating an ongoing requirement for NL2 suppression within the hippocampus for normal social memory formation.

Together, these behavioral data indicate that this NL2ΔSite II animal model may serve as novel in vivo model which may help to further understand the role of NL2 in NDDs mechanisms. Directly addressing this would require the re-establishment of MDGA-mediated suppression of NL2 in our model. Alternatively, although we have identified clear changes in the transcriptome associated with our model, very little is known about how altered NL-MDGA interactions reconfigure the transcript and protein expression landscape in neurons. Further analysis is needed to understand the relationship between these alterations and the behavioral changes observed in this model.

4.6 Intrinsic excitability and basal synaptic transmission of MDGA1/2 DKO mice.

Intrinsic excitability of neurons refers to the ability of neurons to respond to stimuli. Abnormal neuronal excitability is a central feature of many NDDs. For example, neurons in patients with ASD and epilepsy often exhibit excessive excitability (Dionne et al., 2024). In patch clamp experiments, the step and ramp protocols are used to analyze the intrinsic excitability of cells. The step protocol is used to measure the current response of cells under different currents. During this test, the cells are stimulated by a series of fixed current steps, each lasting a certain amount of time. Ramp protocol is used to measure the voltage response of cells under gradually changing currents. During the ramp protocol, the cells are stimulated by a continuously varying

voltage gradient (ramp), with the voltage gradually changing from one value to another. The two protocols, when used in combination, provide a comprehensive assessment of the mechanisms underlying the intrinsic excitability of cells.

Application of the step protocol showed that the AP frequency within DKO CA1 pyramidal neurons was elevated (Figure 27B), indicating increased cell responsiveness to a specific current stimulus. This may reflect increased activation or decreased inhibition of ion channels such as sodium channels or calcium channels, resulting in neurons being more prone to generating APs.

Rin reflects the resistance of the cell membrane to current. A high Rin usually means that the cell is more sensitive to current stimulation because the same current causes a larger change in membrane potential. This makes it easier for the cells to reach the threshold of an action potential, which increases excitability. Thus, the increased excitability of DKO CA1 PNs may be partially due to increased trend of Rin (Figure 27C).

RMP refers to the potential difference between the inner and outer sides of the membrane when the cell is not stimulated and is usually negative. There was no change in the RMP in two groups (Figure 27D). This may be due to increased activity of excitatory ion channels, such as sodium channels or calcium channels, can make it easier for cells to generate APs, thereby increasing the excitability of cells. This change may not significantly affect the RMP because the RMP is primarily maintained by the potassium ion channel and the sodium-potassium pump. In the ramp protocol, the voltage increases gradually, and an increase in the number of spikes recorded (Figure 27F) indicates that the DKO CA1 PNs become more excitable over a wider range of voltages.

Since I moved from China to Canada, I was unable to continue conducting these similar experiments for NL2ΔSite II model. The expected outcomes in NL2ΔSite II model would be the action potentials are reduced in $NL2^{Mut/Mut}$ mice due to the increased inhibition.

Notably, the amplitude of mIPSCs in DKO CA1 PNs was decreased but the frequency remained unaltered. This indicates excessive activation of NL2 may trigger endocytosis of $GABA_ARs$ receptors or destabilization of postsynaptic scaffold proteins such as gephyrin. Moreover, MDGA1/2 may maintain receptor stability through non-NL2 pathways such as direct binding to $GABA_ARs$ and its absence leads to a reduction in the number of receptors. Finally, the reduction in the function or number of inhibitory postsynaptic receptors resulting in a reduction in the amplitude of the current caused by each inhibitory synaptic event. However, the constant frequency indicates no change in the inhibitory synapse number or probability of inhibitory presynaptic neurons releasing GABA. MDGA1/2 mainly acts on postsynaptic mechanisms.

In contrast, the amplitude of mEPSCs in DKO CA1 PNs was increased but the frequency remained unaltered. This may indicate inhibitory synaptic dysfunction (mIPSC↓) leads to disinhibition, triggering compensatory enhancement of excitatory synapses (homeostatic plasticity). Furthermore, MDGA1/2 may restrict the insertion of AMPARs by binding to PSD95 or NMDARs, and its absence leads to an increase in postsynaptic AMPARs. The increase in the function or number of excitatory postsynaptic receptors results in an increase in the amplitude of the current caused by each excitatory synaptic event. Similarly, the unaltered frequency indicates no change in the excitatory synapse number or probability of excitatory presynaptic neurons releasing glutamate. Importantly, the increased cell membrane excitability could enhance the response of excitatory synapses and weaken the response of inhibitory synapses through signal

integration and amplification mechanisms. This mechanism can also explain the phenomenon of increased mEPSC amplitude (Figure 29C) and decreased mIPSC amplitude (Figure 28C).

Overall, these findings indicate that simultaneous loss of MDGA1 and MDGA2 increase neuronal excitability which is associated with a simultaneous downregulation of basal inhibitory synaptic currents and upregulation of excitatory currents. This data suggests that E/I stability within neural networks is shifted towards excitation when MDGAs are reduced. Interestingly, some cases of autism are associated with increased prevalence of epilepsy, which would be predicted under conditions observed in our DKO model. Further research is required to address important questions about whether MDGA reduction renders neurons more susceptible to epileptogenic insults.

Going forward, several key questions remain that will help refine our understanding of the impact of dual loss of MDGAs. For example, loss of MDGA-based regulation may be restricted to select cellular compartments (i.e. soma vs dendrites), which will determine computational properties of neurons as temporal and spatial summation of inputs will, in part, determine cellular excitability. Additionally, changes in complement of synaptic receptors, which is the most parsimonious explanation for enhanced glutamatergic currents could reflect either a change in the density, subtype, distribution or function of glutamatergic receptors at synaptic inputs. It will be important to isolate and measure the function of these receptors and how they change as when MDGAs are absent.

Individual KO controls were not included in the DKO study, because previous studies may suggest that single KO of MDGA1 or MDGA2 has a relatively small impact on synaptic function due to the redundancy of their functions (Both MDGA1/2 can interact with NL2) (Pettem et al., 2013c). If the single KO phenotype is not significant, prioritizing DKO can more efficiently reveal

the core role of the pathway. If add single KO controls, the functional redundancy can be verified. If a single KO of MDGA1 or MDGA2 only causes a mild phenotype, while the DKO phenotype is significantly enhanced, it can be directly proved that the two have complementary or synergistic functions.

4.7 Significance and impact of this work

NL2 and MDGAs are two important synaptic organizers that play a key role in the central nervous system. NL2 is mainly involved in the formation and functional regulation of inhibitory synapses, while MDGAs regulate synaptic stability and plasticity through its interaction with NL2. In recent years, the role of NL2 and MDGAs in NDDs and psychiatric disorders has attracted considerable attention. In this study, we explored the function of NL2-MDGAs interaction to reveal their specific roles in synaptic function and neural network stability, which not only enriches the theoretical knowledge in the field of neurobiology, but also provides a new perspective for understanding the complexity of the nervous system. In particular, studying how MDGA regulates the function of NL2 could reveal the complex regulatory mechanisms of the synaptic adhesion protein network. These findings could lead to the development of novel treatments for NDDs and psychiatric disorders. For example, understanding the role of NL2 and MDGAs in ASDs and schizophrenia could provide a scientific basis for early diagnosis and intervention in these brain disorders.

Moreover, this research may also lead to the development of new drugs and improve the quality of life of patients, especially targeting the regulatory mechanism of NL2-MDGAs interaction may be a new target for the treatment of related diseases. Although this study made

some important findings, there are still some limitations. Future studies could further explore the specific roles of NL2 and MDGAs in different types of neurons, as well as their interactions with other synaptic proteins. In addition, using advanced imaging techniques and gene-editing tools, the dynamic changes and functions of these proteins can be revealed more precisely. In particular, studying the interaction of NL2 and MDGAs in different pathological states may provide new ideas for understanding and treating related diseases.

Chapter 5 Conclusion

To investigate the role of NL2 in the regulation of inhibitory synapses, a novel specific NL2ΔSite II (uncouples the binding of MDGAs and NL2) transgenic mouse model was successfully generated. This transgenic animal model was verified through analysis at the genomic and mRNA transcription levels which confirmed that NL2 was not binding to MDGAs in hippocampus of $NL2^{Mut/Mut}$ mice. Secondly, behavioral results revealed that harboring the NL2ΔSite II increased anxiety, fear memory and, impaired social memory. Thirdly, given this behavioral abnormality reflects phenotypes of neurodevelopmental disorders linked to synaptic dysfunction, I employed immunostaining and electrophysiology techniques to discover that NL2ΔSite II selectively increased the expression level of inhibitory synapse proteins (VGAT and gephyrin) and function (mIPSCs), but does not affect the expression level of excitatory synapse proteins (VGLUT1 and PSD95) or glutamatergic function (mEPSCs). Moreover, NL2ΔSite II mouse model share physiological, behavioral and genetic markers for NDDs such as ASD and SCZ. Cumulatively, our findings provide primary evidence that NL2ΔSite II specifically modulates inhibitory synapses and leads to behavioral abnormalities consistent with those observed in major neurodevelopmental disorders (Figure 32). Also, in adult mice, after KO Mdga1 and Mdga2 genes by viral injection, the excitability of PNs in hippocampal CA1 region was significantly increased. The amplitude of mEPSC increases while the frequency remains the same. Meanwhile, the amplitude of mIPSC decreased, but the frequency did not change. These results suggest that Mdga1 and Mdga2 genes play an important role in regulating synaptic transmission and excitability of pyramidal cells in hippocampal CA1 region (Figure 33).

NL2 is a cell adhesion molecule mainly distributed in inhibitory synapses (GABAergic), which regulates the formation and function of inhibitory synapses by binding to postsynaptic

scaffold proteins (such as gephyrin) and transsynaptic partners (such as neurexins, MDGAs). MDGA is negative regulatory factors of NL2 through the interaction of NL2 site II domain structure, inhibition of its interaction with neurexin, thereby restricting the maturation of inhibitory synapses. Thus, I raised key question: How does the disruption of the MDGA-NL2 interaction affect inhibitory synaptic transmission, neural network function and behavioral phenotypes? For the experimental design, select the site II domain of the NL2 protein (the known key region for binding to MDGA), and mutate five key amino acids to Alanine to disrupt its binding ability to MDGA. Gephyrin, VGAT, GAD65 are markers of inhibitory synapses, and they are used to observe the alteration of density of inhibitory synapses in mutant mice. Apart from the anatomy experiments, functional experiments like electrophysiology are employed to detect the synaptic transmission in mutant mice. Anxiety, sociability and fear memory are comorbidities of ASD, so I design the behavior experiments for the mutant mice. For the conclusion, Site II mutations disrupt MDGA-NL2 binding → release more functional NL2 → enhance inhibitory synaptic transmission and density → E/I imbalance in hippocampus → increase anxiety, fear memory and impair social deficits.

In summary, under physiological conditions, MDGA1/2 binds to NL2, restricting the excessive formation of inhibitory synapses and maintaining the E/I balance. In NL2ΔSite II model, the absence of MDGA binding frees up NL2 and promotes inhibitory synaptic formation leads to excessive circuit inhibition and anxiety and fear behavior. In MDGA1/2 DKO model, NL2 loses its "brake" and inhibitory synapses are overly pruned (due to the intervention of other regulatory factors) resulting in E/I imbalance and increase cell excitability. These models provide direct evidence for the synaptic inhibition hypothesis of ASD, suggesting that targeting this pathway may improve symptoms. Regulating the expression of MDGA1/2 or the NL2-MDGA interaction (such

as small molecule intervention) may restore the E/I balance. Stabilize the interaction by enhancing the binding of NL2-MDGA1 through allosteric modulators (such as inhibiting the self-restricting conformation of MDGA1). The advantage of small molecule strategy is high blood-brain barrier penetration, suitable for systemic administration. Peptide competitive agents can also be used. Synthesize short peptides with NL2 Site II or MDGA1 binding domains (such as 5-10 amino acids). Agonist peptide can mimic the NL2 Site II sequence and enhances MDGA1 recruitment. These can be applied to treatment of ASD, schizophrenia and epilepsy.

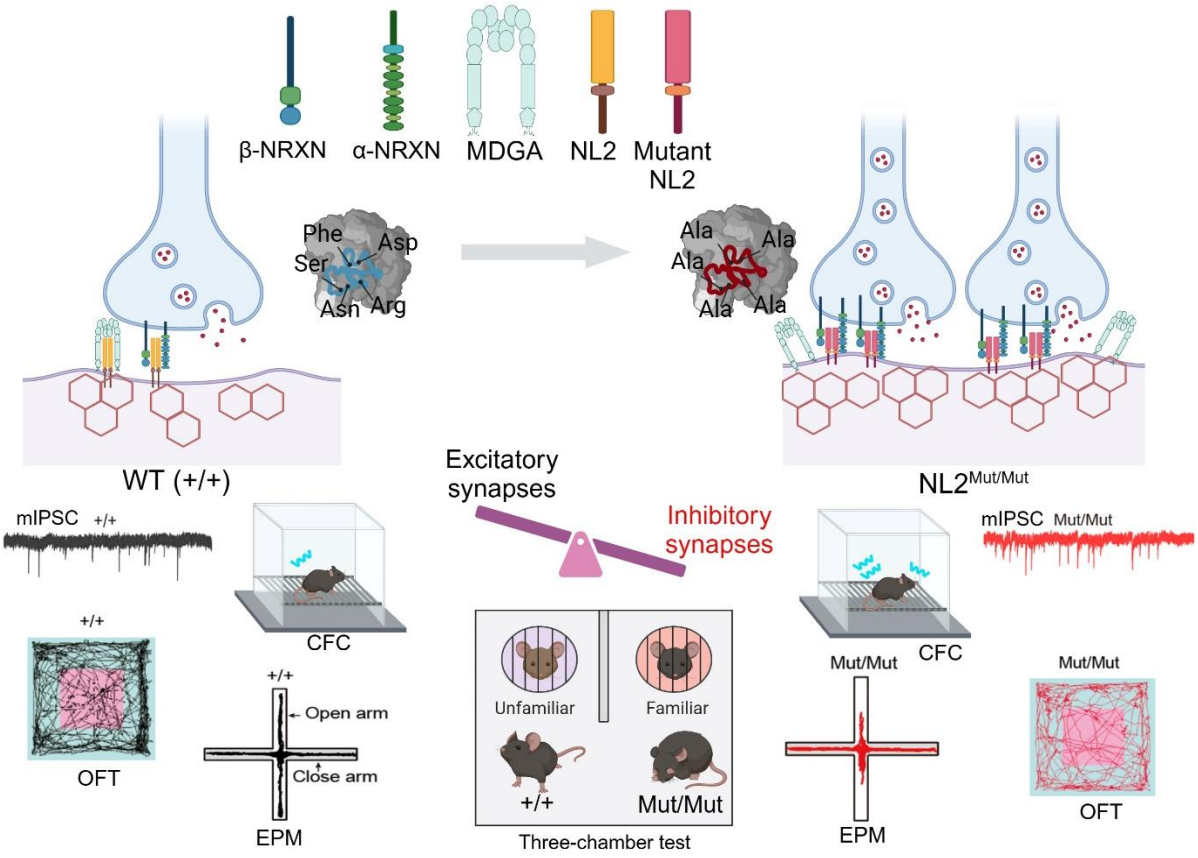

Figure 32. Summary of NL2ΔSite II research overview chart.

NL2 site II mutation blocked the binding of NL2 and MDGA in the mouse hippocampus. This mutation up-regulates the density of inhibitory synapses and enhances inhibitory transmission in hippocampal CA1 in mice. The mutation mice were observed to have increased anxiety, impaired social memory, and increased fear memory. (Image generated with BioRender.com).

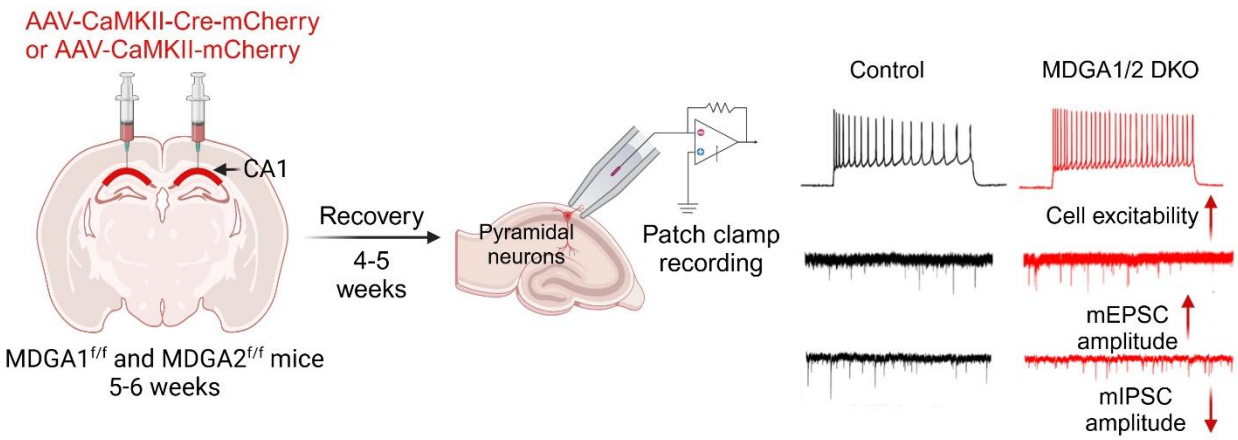

Figure 33. Summary of MDGA1/2 DKO research overview chart.

After KO Mdga1 and Mdga2 genes by viral injection, the excitability of PNs in hippocampal CA1 region was significantly increased. The amplitude of mEPSC increases while the frequency remains the same. Meanwhile, the amplitude of mIPSC decreased, but the frequency did not change. (Image generated with BioRender.com).

Chapter 6 Future outlook

The network excitability indicators including sPSCs, input/output curve and paired-pulse ratio, which measure basal synaptic transmission and changes in presynaptic release function, are necessary to further confirm the status of E/I imbalance in NL2ΔSite II mice. Also, fMRI can be used to examine which parts of the brain are critical for increased anxiety, impaired social and enhanced fear memory behavior in NL2ΔSite II mice. Optogenetics could also be used to further dissect which cell types and neural circuits are altered in the NL2ΔSite II mice and help refine treatment "targets" (cell types, brain regions and networks) for neurodevelopmental disorders.

Accordingly, we could explore the effect of interneurons in specific neural circuits in NL2ΔSite II mice and interneurons are powerful regulators of endogenous brain rhythms that mediate higher-order cognition. Interneuron immunostaining in NL2ΔSite II mice could reveal which interneurons are affected and how their connections have changed under these genetic conditions. Although MDGA1 is not expressed in interneurons in hippocampus, there could be collateral or compensatory effects of elevated inhibition of pyramidal neurons that drive corresponding changes at inhibitory inputs or excitatory inputs onto interneurons. The prediction would be that elevated inhibition on pyramidal cells may cause a compensatory downregulation of excitatory inputs onto interneurons as the system attempts to normalize E/I balance. Additionally, it would be interesting to test if pharmacologically re-setting E/I balance through either inhibition of GABAergic inputs or elevation of excitatory inputs in the hippocampus reverses anxiety phenotypes in this model. If these experiments proved successful, this could form the basis for a proof-of-concept treatment for genetic conditions in which MDGA1 function is compromised, indicating that modulating GABAergic function is a viable approach for normalizing brain function is patients harboring these mutations.

For the MDGA1/2 DKO project, to determine whether E/I balance in the network is compromised, it will be important to assess evoked synaptic transmission using input/output responses in acute hippocampal slices. Paired-pulse ratio, a measure of presynaptic function within neural networks could also be observed to determine whether neurotransmitter release possibility is changed at a network level. Important questions remain about the impacts of tandem loss of MDGA1 and MDGA2 function of cognitive function. Physiologically, this could be explored through testing whether synaptic plasticity is altered by measuring LTP at Schaffer collateral-CA1 synapses. An obvious but key experimental validation of the relative roles of MDGA1 and MDGA2 would be their singular reintroduction in the DKO model and testing for which aspects of neuronal excitability/synapse properties are restored.

Going forward, these experimental lines of investigation should further refine our understanding of the role of these rare, negative regulators of synapse development and provide further insight into the cellular nature of major neurodevelopmental disorders. The noted alterations in E/I balance detected here indicate that loss of MDGA function shifts the balance of neural network function towards a pathologized state. Reintroduction of MDGAs will further address the important question of whether reconstitution of synapse suppression resets neural networks and restores physiological and behavioural phenotypes to wildtype levels.

References

Ahmed, O. J., & Mehta, M. R. (2009). The hippocampal rate code: Anatomy, physiology and theory. *Trends in Neurosciences*, *32*(6), 329–338. https://doi.org/10.1016/j.tins.2009.01.009

Ali, H., Marth, L., & Krueger-Burg, D. (2020). Neuroligin-2 as a central organizer of inhibitory synapses in health and disease. *Science Signaling*, *13*(663), eabd8379. https://doi.org/10.1126/scisignal.abd8379

Almey, A., Milner, T. A., & Brake, W. G. (2015). Estrogen receptors in the central nervous system and their implication for dopamine-dependent cognition in females. *Hormones and Behavior*, *74*, 125–138. https://doi.org/10.1016/j.yhbeh.2015.06.010

Andrews-Zwilling, Y., Gillespie, A. K., Kravitz, A. V., Nelson, A. B., Devidze, N., Lo, I., Yoon, S. Y., Bien-Ly, N., Ring, K., Zwilling, D., Potter, G. B., Rubenstein, J. L. R., Kreitzer, A. C., & Huang, Y. (2012). Hilar GABAergic interneuron activity controls spatial learning and memory retrieval. *PloS One*, *7*(7), e40555. https://doi.org/10.1371/journal.pone.0040555

Araç, D., Boucard, A. A., Özkan, E., Strop, P., Newell, E., Südhof, T. C., & Brunger, A. T. (2007). Structures of Neuroligin-1 and the Neuroligin-1/Neurexin-1β Complex Reveal Specific Protein-Protein and Protein-Ca2+ Interactions. *Neuron*, *56*(6), 992–1003. https://doi.org/10.1016/j.neuron.2007.12.002

Asgarihafshejani, A., Honoré, È., Michon, F.-X., Laplante, I., & Lacaille, J.-C. (2022). Long-term potentiation at pyramidal cell to somatostatin interneuron synapses controls hippocampal network plasticity and memory. *iScience*, *25*(5), 104259. https://doi.org/10.1016/j.isci.2022.104259

Auyeung, B., Baron-Cohen, S., Ashwin, E., Knickmeyer, R., Taylor, K., & Hackett, G. (2009). Fetal testosterone and autistic traits. *British Journal of Psychology*, *100*(1), 1–22. Scopus. https://doi.org/10.1348/000712608X311731

Babaev, O., Botta, P., Meyer, E., Müller, C., Ehrenreich, H., Brose, N., Lüthi, A., & Krueger-Burg, D. (2016). Neuroligin 2 deletion alters inhibitory synapse function and anxiety-associated neuronal activation in the amygdala. *Neuropharmacology*, *100*, 56–65. https://doi.org/10.1016/j.neuropharm.2015.06.016

Bai, D., Yip, B. H. K., Windham, G. C., Sourander, A., Francis, R., Yoffe, R., Glasson, E., Mahjani, B., Suominen, A., Leonard, H., Gissler, M., Buxbaum, J. D., Wong, K., Schendel, D., Kodesh, A., Breshnahan, M., Levine, S. Z., Parner, E. T., Hansen, S. N., … Sandin, S. (2019). Association of Genetic and Environmental Factors With Autism in a 5-Country Cohort. *JAMA Psychiatry*, *76*(10), 1035–1043. https://doi.org/10.1001/jamapsychiatry.2019.1411

Bale, T. L., Baram, T. Z., Brown, A. S., Goldstein, J. M., Insel, T. R., McCarthy, M. M., Nemeroff, C. B., Reyes, T. M., Simerly, R. B., Susser, E. S., & Nestler, E. J. (2010). Early life programming and neurodevelopmental disorders. *Biological Psychiatry*, *68*(4), 314–319. https://doi.org/10.1016/j.biopsych.2010.05.028

Banker, S. M., Gu, X., Schiller, D., & Foss-Feig, J. H. (2021). Hippocampal contributions to social and cognitive deficits in autism spectrum disorder. *Trends in Neurosciences*, *44*(10), 793–807. https://doi.org/10.1016/j.tins.2021.08.005

Bannerman, D. M., Deacon, R. M. J., Offen, S., Friswell, J., Grubb, M., & Rawlins, J. N. P. (2002). Double dissociation of function within the hippocampus: Spatial memory and

hyponeophagia. *Behavioral Neuroscience*, *116*(5), 884–901. https://doi.org/10.1037//0735-7044.116.5.884

Bannerman, D. M., Matthews, P., Deacon, R. M. J., & Rawlins, J. N. P. (2004). Medial septal lesions mimic effects of both selective dorsal and ventral hippocampal lesions. *Behavioral Neuroscience*, *118*(5), 1033–1041. https://doi.org/10.1037/0735-7044.118.5.1033

Barnea-Goraly, N., Frazier, T. W., Piacenza, L., Minshew, N. J., Keshavan, M. S., Reiss, A. L., & Hardan, A. Y. (2014). A preliminary longitudinal volumetric MRI study of amygdala and hippocampal volumes in autism. *Progress in Neuro-Psychopharmacology & Biological Psychiatry*, *48*, 124–128. https://doi.org/10.1016/j.pnpbp.2013.09.010

Baron-Cohen, S., Auyeung, B., Nørgaard-Pedersen, B., Hougaard, D. M., Abdallah, M. W., Melgaard, L., Cohen, A. S., Chakrabarti, B., Ruta, L., & Lombardo, M. V. (2015). Elevated fetal steroidogenic activity in autism. *Molecular Psychiatry*, *20*(3), 369–376. https://doi.org/10.1038/mp.2014.48

Baron-Cohen, S., Lombardo, M. V., Auyeung, B., Ashwin, E., Chakrabarti, B., & Knickmeyer, R. (2011). Why are autism spectrum conditions more prevalent in males? *PLoS Biology*, *9*(6), e1001081. https://doi.org/10.1371/journal.pbio.1001081

Baron-Cohen, S., Tsompanidis, A., Auyeung, B., Nørgaard-Pedersen, B., Hougaard, D. M., Abdallah, M., Cohen, A., & Pohl, A. (2020). Foetal oestrogens and autism. *Molecular Psychiatry*, *25*(11), 2970–2978. https://doi.org/10.1038/s41380-019-0454-9

Bemben, M. A., Sandoval, M., Le, A. A., Won, S., Chau, V. N., Lauterborn, J. C., Incontro, S., Li, K. H., Burlingame, A. L., Roche, K. W., Gall, C. M., Nicoll, R. A., & Diaz-Alonso, J.

(2023). *Contrasting synaptic roles of MDGA1 and MDGA2* [Preprint]. Neuroscience. https://doi.org/10.1101/2023.05.25.542333

Bemben, M. A., Shipman, S. L., Nicoll, R. A., & Roche, K. W. (2015). The cellular and molecular landscape of neuroligins. *Trends in Neurosciences*, *38*(8), 496–505. https://doi.org/10.1016/j.tins.2015.06.004

Bernier, B. E., Lacagnina, A. F., Ayoub, A., Shue, F., Zemelman, B. V., Krasne, F. B., & Drew, M. R. (2017). Dentate Gyrus Contributes to Retrieval as well as Encoding: Evidence from Context Fear Conditioning, Recall, and Extinction. *The Journal of Neuroscience: The Official Journal of the Society for Neuroscience*, *37*(26), 6359–6371. https://doi.org/10.1523/JNEUROSCI.3029-16.2017

Binda, C. S., Nakamura, Y., Henley, J. M., & Wilkinson, K. A. (2019). Sorting nexin 27 rescues neuroligin 2 from lysosomal degradation to control inhibitory synapse number. *The Biochemical Journal*, *476*(2), 293–306. https://doi.org/10.1042/BCJ20180504

Birdsall, V., & Waites, C. L. (2019). Autophagy at the synapse. *Neuroscience Letters*, *697*, 24–28. https://doi.org/10.1016/j.neulet.2018.05.033

Blundell, J., Tabuchi, K., Bolliger, M. F., Blaiss, C. A., Brose, N., Liu, X., Südhof, T. C., & Powell, C. M. (2009). Increased anxiety-like behavior in mice lacking the inhibitory synapse cell adhesion molecule neuroligin 2. *Genes, Brain, and Behavior*, *8*(1), 114–126. https://doi.org/10.1111/j.1601-183X.2008.00455.x

Boivin, J. R., & Nedivi, E. (2018). Functional implications of inhibitory synapse placement on signal processing in pyramidal neuron dendrites. *Current Opinion in Neurobiology*, *51*, 16–22. https://doi.org/10.1016/j.conb.2018.01.013

Bourgeron, T. (2015). From the genetic architecture to synaptic plasticity in autism spectrum disorder. *Nature Reviews. Neuroscience*, *16*(9), 551–563. https://doi.org/10.1038/nrn3992

Brookings, T., Grashow, R., & Marder, E. (2012). Statistics of neuronal identification with open- and closed-loop measures of intrinsic excitability. *Frontiers in Neural Circuits*, *6*, 19. https://doi.org/10.3389/fncir.2012.00019

Bruining, H., Hardstone, R., Juarez-Martinez, E. L., Sprengers, J., Avramiea, A.-E., Simpraga, S., Houtman, S. J., Poil, S.-S., Dallares, E., Palva, S., Oranje, B., Matias Palva, J., Mansvelder, H. D., & Linkenkaer-Hansen, K. (2020). Measurement of excitation-inhibition ratio in autism spectrum disorder using critical brain dynamics. *Scientific Reports*, *10*(1), 9195. https://doi.org/10.1038/s41598-020-65500-4

Brunsdon, V. E. A., Colvert, E., Ames, C., Garnett, T., Gillan, N., Hallett, V., Lietz, S., Woodhouse, E., Bolton, P., & Happé, F. (2015). Exploring the cognitive features in children with autism spectrum disorder, their co-twins, and typically developing children within a population-based sample. *Journal of Child Psychology and Psychiatry, and Allied Disciplines*, *56*(8), 893–902. https://doi.org/10.1111/jcpp.12362

Bucan, M., Abrahams, B. S., Wang, K., Glessner, J. T., Herman, E. I., Sonnenblick, L. I., Retuerto, A. I. A., Imielinski, M., Hadley, D., Bradfield, J. P., Kim, C., Gidaya, N. B., Lindquist, I., Hutman, T., Sigman, M., Kustanovich, V., Lajonchere, C. M., Singleton, A., Kim, J., … Hakonarson, H. (2009). Genome-Wide Analyses of Exonic Copy Number Variants in a Family-Based Study Point to Novel Autism Susceptibility Genes. *PLOS Genetics*, *5*(6), e1000536. https://doi.org/10.1371/journal.pgen.1000536

Budreck, E. C., & Scheiffele, P. (2007). Neuroligin-3 is a neuronal adhesion protein at GABAergic and glutamatergic synapses. *The European Journal of Neuroscience*, *26*(7), 1738–1748. https://doi.org/10.1111/j.1460-9568.2007.05842.x

Burden-Gulley, S. M., & Lemmon, V. (1995). Ig superfamily adhesion molecules in the vertebrate nervous system: Binding partners and signal transduction during axon growth. *Seminars in Developmental Biology*, *6*(2), 79–87. https://doi.org/10.1016/S1044-5781(06)80017-4

Cao, F., Liu, J. J., Zhou, S., Cortez, M. A., Snead, O. C., Han, J., & Jia, Z. (2020). Neuroligin 2 regulates absence seizures and behavioral arrests through GABAergic transmission within the thalamocortical circuitry. *Nature Communications*, *11*(1), Article 1. https://doi.org/10.1038/s41467-020-17560-3

Cenquizca, L. A., & Swanson, L. W. (2007). Spatial organization of direct hippocampal field CA1 axonal projections to the rest of the cerebral cortex. *Brain Research Reviews*, *56*(1), 1–26. https://doi.org/10.1016/j.brainresrev.2007.05.002

Chen, A. I., Nguyen, C. N., Copenhagen, D. R., Badurek, S., Minichiello, L., Ranscht, B., & Reichardt, L. F. (2011). TrkB (tropomyosin-related kinase B) controls the assembly and maintenance of GABAergic synapses in the cerebellar cortex. *The Journal of Neuroscience: The Official Journal of the Society for Neuroscience*, *31*(8), 2769–2780. https://doi.org/10.1523/JNEUROSCI.4991-10.2011

Chen, X., Liu, H., Shim, A. H. R., Focia, P. J., & He, X. (2008). Structural basis for synaptic adhesion mediated by neuroligin-neurexin interactions. *Nature Structural & Molecular Biology*, *15*(1), 50–56. https://doi.org/10.1038/nsmb1350

Chiang, C.-W., Shu, W.-C., Wan, J., Weaver, B. A., & Jackson, M. B. (2021). Recordings from neuron-HEK cell cocultures reveal the determinants of miniature excitatory postsynaptic currents. *The Journal of General Physiology*, *153*(5), e202012849. https://doi.org/10.1085/jgp.202012849

Chih, B., Engelman, H., & Scheiffele, P. (2005). Control of Excitatory and Inhibitory Synapse Formation by Neuroligins. *Science*, *307*(5713), 1324–1328. https://doi.org/10.1126/science.1107470

Chih, B., Gollan, L., & Scheiffele, P. (2006). Alternative Splicing Controls Selective Trans-Synaptic Interactions of the Neuroligin-Neurexin Complex. *Neuron*, *51*(2), 171–178. https://doi.org/10.1016/j.neuron.2006.06.005

Chubykin, A. A., Atasoy, D., Etherton, M. R., Brose, N., Kavalali, E. T., Gibson, J. R., & Südhof, T. C. (2007). Activity-Dependent Validation of Excitatory versus Inhibitory Synapses by Neuroligin-1 versus Neuroligin-2. *Neuron*, *54*(6), 919–931. https://doi.org/10.1016/j.neuron.2007.05.029

Chura, L. R., Lombardo, M. V., Ashwin, E., Auyeung, B., Chakrabarti, B., Bullmore, E. T., & Baron-Cohen, S. (2010). Organizational effects of fetal testosterone on human corpus callosum size and asymmetry. *Psychoneuroendocrinology*, *35*(1), 122–132. https://doi.org/10.1016/j.psyneuen.2009.09.009

Connor, S. A., Ammendrup-Johnsen, I., Chan, A. W., Kishimoto, Y., Murayama, C., Kurihara, N., Tada, A., Ge, Y., Lu, H., Yan, R., LeDue, J. M., Matsumoto, H., Kiyonari, H., Kirino, Y., Matsuzaki, F., Suzuki, T., Murphy, T. H., Wang, Y. T., Yamamoto, T., & Craig, A. M. (2016a). Altered Cortical Dynamics and Cognitive Function upon Haploinsufficiency of

the Autism-Linked Excitatory Synaptic Suppressor MDGA2. *Neuron*, *91*(5), 1052–1068. https://doi.org/10.1016/j.neuron.2016.08.016

Connor, S. A., Ammendrup-Johnsen, I., Chan, A. W., Kishimoto, Y., Murayama, C., Kurihara, N., Tada, A., Ge, Y., Lu, H., Yan, R., LeDue, J. M., Matsumoto, H., Kiyonari, H., Kirino, Y., Matsuzaki, F., Suzuki, T., Murphy, T. H., Wang, Y. T., Yamamoto, T., & Craig, A. M. (2016b). Altered Cortical Dynamics and Cognitive Function upon Haploinsufficiency of the Autism-Linked Excitatory Synaptic Suppressor MDGA2. *Neuron*, *91*(5), 1052–1068. https://doi.org/10.1016/j.neuron.2016.08.016

Connor, S. A., Ammendrup-Johnsen, I., Kishimoto, Y., Karimi Tari, P., Cvetkovska, V., Harada, T., Ojima, D., Yamamoto, T., Wang, Y. T., & Craig, A. M. (2017a). Loss of Synapse Repressor MDGA1 Enhances Perisomatic Inhibition, Confers Resistance to Network Excitation, and Impairs Cognitive Function. *Cell Reports*, *21*(13), 3637–3645. https://doi.org/10.1016/j.celrep.2017.11.109

Connor, S. A., Ammendrup-Johnsen, I., Kishimoto, Y., Karimi Tari, P., Cvetkovska, V., Harada, T., Ojima, D., Yamamoto, T., Wang, Y. T., & Craig, A. M. (2017b). Loss of Synapse Repressor MDGA1 Enhances Perisomatic Inhibition, Confers Resistance to Network Excitation, and Impairs Cognitive Function. *Cell Reports*, *21*(13), 3637–3645. https://doi.org/10.1016/j.celrep.2017.11.109

Connor, S. A., Elegheert, J., Xie, Y., & Craig, A. M. (2019). Pumping the brakes: Suppression of synapse development by MDGA-neuroligin interactions. *Current Opinion in Neurobiology*, *57*, 71–80. https://doi.org/10.1016/j.conb.2019.01.002

Crider, A., & Pillai, A. (2017). Estrogen Signaling as a Therapeutic Target in Neurodevelopmental Disorders. *The Journal of Pharmacology and Experimental Therapeutics*, *360*(1), 48–58. https://doi.org/10.1124/jpet.116.237412

Cruces-Solis, H., Babaev, O., Ali, H., Piletti Chatain, C., Mykytiuk, V., Balekoglu, N., Wenger, S., & Krueger-Burg, D. (2021). Altered theta and beta oscillatory synchrony in a genetic mouse model of pathological anxiety. *The FASEB Journal*, *35*(6), e21585. https://doi.org/10.1096/fj.202002028RR

Cutsuridis, V., & Hasselmo, M. (2012). GABAergic contributions to gating, timing, and phase precession of hippocampal neuronal activity during theta oscillations. *Hippocampus*, *22*(7), 1597–1621. https://doi.org/10.1002/hipo.21002

Darnell, R. B. (2020). The Genetic Control of Stoichiometry Underlying Autism. *Annual Review of Neuroscience*, *43*, 509–533. https://doi.org/10.1146/annurev-neuro-100119-024851

Davachi, L., & DuBrow, S. (2015). How the hippocampus preserves order: The role of prediction and context. *Trends in Cognitive Sciences*, *19*(2), 92–99. https://doi.org/10.1016/j.tics.2014.12.004

Dedovic, K., Duchesne, A., Andrews, J., Engert, V., & Pruessner, J. C. (2009). The brain and the stress axis: The neural correlates of cortisol regulation in response to stress. *NeuroImage*, *47*(3), 864–871. https://doi.org/10.1016/j.neuroimage.2009.05.074

DeFelipe, J., & Fariñas, I. (1992). The pyramidal neuron of the cerebral cortex: Morphological and chemical characteristics of the synaptic inputs. *Progress in Neurobiology*, *39*(6), 563–607. https://doi.org/10.1016/0301-0082(92)90015-7

Díaz-López, A., Rivas, C., Iniesta, P., Morán, A., García-Aranda, C., Megías, D., Sánchez-Pernaute, A., Torres, A., Díaz-Rubio, E., Benito, M., & De Juan, C. (2005).

Characterization of MDGA1, a novel human glycosylphosphatidylinositol-anchored protein localized in lipid rafts. *Experimental Cell Research*, *307*(1), 91–99. https://doi.org/10.1016/j.yexcr.2005.02.016

Dionne, O., Sabatié, S., & Laurent, B. (2024). Deciphering the physiopathology of neurodevelopmental disorders using brain organoids. *Brain: A Journal of Neurology*, awae281. https://doi.org/10.1093/brain/awae281

D'Mello, A. M., & Stoodley, C. J. (2015). Cerebro-cerebellar circuits in autism spectrum disorder. *Frontiers in Neuroscience*, *9*, 408. https://doi.org/10.3389/fnins.2015.00408

Du, X., Li, J., Li, M., Yang, X., Qi, Z., Xu, B., Liu, W., Xu, Z., & Deng, Y. (2020). Research progress on the role of type I vesicular glutamate transporter (VGLUT1) in nervous system diseases. *Cell & Bioscience*, *10*(1), 26. https://doi.org/10.1186/s13578-020-00393-4

Elder, J. H., Kreider, C. M., Brasher, S. N., & Ansell, M. (2017). Clinical impact of early diagnosis of autism on the prognosis and parent-child relationships. *Psychology Research and Behavior Management*, *10*, 283–292. https://doi.org/10.2147/PRBM.S117499

Elegheert, J., Cvetkovska, V., Clayton, A. J., Heroven, C., Vennekens, K. M., Smukowski, S. N., Regan, M. C., Jia, W., Smith, A. C., Furukawa, H., Savas, J. N., De Wit, J., Begbie, J., Craig, A. M., & Aricescu, A. R. (2017). Structural Mechanism for Modulation of Synaptic Neuroligin-Neurexin Signaling by MDGA Proteins. *Neuron*, *95*(4), 896-913.e10. https://doi.org/10.1016/j.neuron.2017.07.040

Estes, M. L., & McAllister, A. K. (2016). Maternal immune activation: Implications for neuropsychiatric disorders. *Science (New York, N.Y.)*, *353*(6301), 772–777. https://doi.org/10.1126/science.aag3194

Fabrichny, I. P., Leone, P., Sulzenbacher, G., Comoletti, D., Miller, M. T., Taylor, P., Bourne, Y., & Marchot, P. (2007). Structural Analysis of the Synaptic Protein Neuroligin and Its β-Neurexin Complex: Determinants for Folding and Cell Adhesion. *Neuron*, *56*(6), 979–991. https://doi.org/10.1016/j.neuron.2007.11.013

Fan, S., Gangwar, S. P., Machius, M., & Rudenko, G. (2021). Interplay between hevin, SPARC, and MDGAs: Modulators of neurexin-neuroligin transsynaptic bridges. *Structure*, *29*(7), 664-678.e6. https://doi.org/10.1016/j.str.2021.01.003

Fanselow, M. S., & Dong, H.-W. (2010). Are the dorsal and ventral hippocampus functionally distinct structures? *Neuron*, *65*(1), 7–19. https://doi.org/10.1016/j.neuron.2009.11.031

Fass, S. B., Mulvey, B., Chase, R., Yang, W., Selmanovic, D., Chaturvedi, S. M., Tycksen, E., Weiss, L. A., & Dougherty, J. D. (2024). Relationship between sex biases in gene expression and sex biases in autism and Alzheimer's disease. *Biology of Sex Differences*, *15*(1), 47. https://doi.org/10.1186/s13293-024-00622-2

Fertan, E., Wong, A. A., Montbrun, T. S. G., Purdon, M. K., Roddick, K. M., Yamamoto, T., & Brown, R. E. (2023). Early postnatal development of the MDGA2+/- mouse model of synaptic dysfunction. *Behavioural Brain Research*, *452*, 114590. https://doi.org/10.1016/j.bbr.2023.114590

Francés, L., Quintero, J., Fernández, A., Ruiz, A., Caules, J., Fillon, G., Hervás, A., & Soler, C. V. (2022). Current state of knowledge on the prevalence of neurodevelopmental disorders in childhood according to the DSM-5: A systematic review in accordance with the PRISMA criteria. *Child and Adolescent Psychiatry and Mental Health*, *16*(1), 27. https://doi.org/10.1186/s13034-022-00462-1

Fujimura, Y., Iwashita, M., Matsuzaki, F., & Yamamoto, T. (2006). MDGA1, an IgSF molecule containing a MAM domain, heterophilically associates with axon- and muscle-associated binding partners through distinct structural domains. *Brain Research*, *1101*(1), 12–19. https://doi.org/10.1016/j.brainres.2006.05.030

Futai, K., Doty, C. D., Baek, B., Ryu, J., & Sheng, M. (2013). Specific Trans-Synaptic Interaction with Inhibitory Interneuronal Neurexin Underlies Differential Ability of Neuroligins to Induce Functional Inhibitory Synapses. *Journal of Neuroscience*, *33*(8), 3612–3623. https://doi.org/10.1523/JNEUROSCI.1811-12.2013

Gangwar, S. P., Zhong, X., Seshadrinathan, S., Chen, H., Machius, M., & Rudenko, G. (2017). Molecular Mechanism of MDGA1: Regulation of Neuroligin 2:Neurexin Trans-synaptic Bridges. *Neuron*, *94*(6), 1132-1141.e4. https://doi.org/10.1016/j.neuron.2017.06.009

Geschwind, D. H., & Levitt, P. (2007). Autism spectrum disorders: Developmental disconnection syndromes. *Current Opinion in Neurobiology*, *17*(1), 103–111. https://doi.org/10.1016/j.conb.2007.01.009

Geschwind, D. H., & State, M. W. (2015). Gene hunting in autism spectrum disorder: On the path to precision medicine. *The Lancet Neurology*, *14*(11), 1109–1120. https://doi.org/10.1016/S1474-4422(15)00044-7

Ghasemi, M., Navidhamidi, M., Rezaei, F., Azizikia, A., & Mehranfard, N. (2022). Anxiety and hippocampal neuronal activity: Relationship and potential mechanisms. *Cognitive, Affective & Behavioral Neuroscience*, *22*(3), 431–449. https://doi.org/10.3758/s13415-021-00973-y

Ghatak, S., Talantova, M., McKercher, S. R., & Lipton, S. A. (2021). Novel Therapeutic Approach for Excitatory/Inhibitory Imbalance in Neurodevelopmental and

Neurodegenerative Diseases. *Annual Review of Pharmacology and Toxicology*, *61*, 701–721. https://doi.org/10.1146/annurev-pharmtox-032320-015420

Gibson, J. R., Huber, K. M., & Südhof, T. C. (2009). Neuroligin-2 Deletion Selectively Decreases Inhibitory Synaptic Transmission Originating from Fast-Spiking but Not from Somatostatin-Positive Interneurons. *Journal of Neuroscience*, *29*(44), 13883–13897. https://doi.org/10.1523/JNEUROSCI.2457-09.2009

Giovedí, S., Corradi, A., Fassio, A., & Benfenati, F. (2014). Involvement of synaptic genes in the pathogenesis of autism spectrum disorders: The case of synapsins. *Frontiers in Pediatrics*, *2*, 94. https://doi.org/10.3389/fped.2014.00094

Good, K. V., Vincent, J. B., & Ausió, J. (2021). MeCP2: The Genetic Driver of Rett Syndrome Epigenetics. *Frontiers in Genetics*, *12*, 620859. https://doi.org/10.3389/fgene.2021.620859

Gordleeva, S., Dembitskaya, Y., Kazantsev, V., & Postnikov, E. B. (2023). Estimation of cumulative amplitude distributions of miniature postsynaptic currents allows characterising their multimodality, quantal size and variability. *Scientific Reports*, *13*(1), 15660. https://doi.org/10.1038/s41598-023-42882-9

Graf, E. R., Kang, Y., Hauner, A. M., & Craig, A. M. (2006). Structure Function and Splice Site Analysis of the Synaptogenic Activity of the Neurexin-1β LNS Domain. *The Journal of Neuroscience*, *26*(16), 4256–4265. https://doi.org/10.1523/JNEUROSCI.1253-05.2006

Graf, E. R., Zhang, X., Jin, S.-X., Linhoff, M. W., & Craig, A. M. (2004). Neurexins Induce Differentiation of GABA and Glutamate Postsynaptic Specializations via Neuroligins. *Cell*, *119*(7), 1013–1026. https://doi.org/10.1016/j.cell.2004.11.035

Graham, B. M., & Milad, M. R. (2011). The study of fear extinction: Implications for anxiety disorders. *The American Journal of Psychiatry*, *168*(12), 1255–1265. https://doi.org/10.1176/appi.ajp.2011.11040557

Groen, W., Teluij, M., Buitelaar, J., & Tendolkar, I. (2010). Amygdala and hippocampus enlargement during adolescence in autism. *Journal of the American Academy of Child and Adolescent Psychiatry*, *49*(6), 552–560. https://doi.org/10.1016/j.jaac.2009.12.023

Guneykaya, D., Ugursu, B., Logiacco, F., Popp, O., Feiks, M. A., Meyer, N., Wendt, S., Semtner, M., Cherif, F., Gauthier, C., Madore, C., Yin, Z., Çınar, Ö., Arslan, T., Gerevich, Z., Mertins, P., Butovsky, O., Kettenmann, H., & Wolf, S. A. (2023). Sex-specific microglia state in the Neuroligin-4 knock-out mouse model of autism spectrum disorder. *Brain, Behavior, and Immunity*, *111*, 61–75. https://doi.org/10.1016/j.bbi.2023.03.023

Halff, E. F., Szulc, B. R., Lesept, F., & Kittler, J. T. (2019). SNX27-Mediated Recycling of Neuroligin-2 Regulates Inhibitory Signaling. *Cell Reports*, *29*(9), 2599-2607.e6. https://doi.org/10.1016/j.celrep.2019.10.096

Hanamsagar, R., Alter, M. D., Block, C. S., Sullivan, H., Bolton, J. L., & Bilbo, S. D. (2017). Generation of a microglial developmental index in mice and in humans reveals a sex difference in maturation and immune reactivity. *Glia*, *65*(9), 1504–1520. https://doi.org/10.1002/glia.23176

Harris, S. R. (2017). Early motor delays as diagnostic clues in autism spectrum disorder. *European Journal of Pediatrics*, *176*(9), 1259–1262. https://doi.org/10.1007/s00431-017-2951-7

Hengen, K. B., Lambo, M. E., Van Hooser, S. D., Katz, D. B., & Turrigiano, G. G. (2013). Firing Rate Homeostasis in Visual Cortex of Freely Behaving Rodents. *Neuron*, *80*(2), 335–342. https://doi.org/10.1016/j.neuron.2013.08.038

Henke, P. G. (1990). Hippocampal pathway to the amygdala and stress ulcer development. *Brain Research Bulletin*, *25*(5), 691–695. https://doi.org/10.1016/0361-9230(90)90044-z

Herman, J. P., Ostrander, M. M., Mueller, N. K., & Figueiredo, H. (2005). Limbic system mechanisms of stress regulation: Hypothalamo-pituitary-adrenocortical axis. *Progress in Neuro-Psychopharmacology & Biological Psychiatry*, *29*(8), 1201–1213. https://doi.org/10.1016/j.pnpbp.2005.08.006

Hernandez, L. M., Rudie, J. D., Green, S. A., Bookheimer, S., & Dapretto, M. (2015). Neural signatures of autism spectrum disorders: Insights into brain network dynamics. *Neuropsychopharmacology: Official Publication of the American College of Neuropsychopharmacology*, *40*(1), 171–189. https://doi.org/10.1038/npp.2014.172

Heshmati, M., Aleyasin, H., Menard, C., Christoffel, D. J., Flanigan, M. E., Pfau, M. L., Hodes, G. E., Lepack, A. E., Bicks, L. K., Takahashi, A., Chandra, R., Turecki, G., Lobo, M. K., Maze, I., Golden, S. A., & Russo, S. J. (2018). Cell-type-specific role for nucleus accumbens neuroligin-2 in depression and stress susceptibility. *Proceedings of the National Academy of Sciences of the United States of America*, *115*(5), 1111–1116. https://doi.org/10.1073/pnas.1719014115

Hines, R. M., Wu, L., Hines, D. J., Steenland, H., Mansour, S., Dahlhaus, R., Singaraja, R. R., Cao, X., Sammler, E., Hormuzdi, S. G., Zhuo, M., & El-Husseini, A. (2008). Synaptic Imbalance, Stereotypies, and Impaired Social Interactions in Mice with Altered

Neuroligin 2 Expression. *Journal of Neuroscience*, *28*(24), 6055–6067. https://doi.org/10.1523/JNEUROSCI.0032-08.2008

Hoon, M., Soykan, T., Falkenburger, B., Hammer, M., Patrizi, A., Schmidt, K.-F., Sassoè-Pognetto, M., Löwel, S., Moser, T., Taschenberger, H., Brose, N., & Varoqueaux, F. (2011). Neuroligin-4 is localized to glycinergic postsynapses and regulates inhibition in the retina. *Proceedings of the National Academy of Sciences*, *108*(7), 3053–3058. https://doi.org/10.1073/pnas.1006946108

Horn, M. E., & Nicoll, R. A. (2018). Somatostatin and parvalbumin inhibitory synapses onto hippocampal pyramidal neurons are regulated by distinct mechanisms. *Proceedings of the National Academy of Sciences of the United States of America*, *115*(3), 589–594. https://doi.org/10.1073/pnas.1719523115

Huang, C., Voglewede, M. M., Ozsen, E. N., Wang, H., & Zhang, H. (2023). SHANK3 Mutations Associated with Autism and Schizophrenia Lead to Shared and Distinct Changes in Dendritic Spine Dynamics in the Developing Mouse Brain. *Neuroscience*, *528*, 1–11. https://doi.org/10.1016/j.neuroscience.2023.07.024

Hui, K. K., & Tanaka, M. (2019). Autophagy links MTOR and GABA signaling in the brain. *Autophagy*, *15*(10), 1848–1849. https://doi.org/10.1080/15548627.2019.1637643

Iascone, D. M., Li, Y., Sümbül, U., Doron, M., Chen, H., Andreu, V., Goudy, F., Segev, I., Peng, H., & Polleux, F. (2018). *Whole-neuron synaptic mapping reveals local balance between excitatory and inhibitory synapse organization* [Preprint]. Neuroscience. https://doi.org/10.1101/395384

Ichtchenko, K., Nguyen, T., & Südhof, T. C. (1996a). Structures, Alternative Splicing, and Neurexin Binding of Multiple Neuroligins. *Journal of Biological Chemistry*, *271*(5), 2676–2682. https://doi.org/10.1074/jbc.271.5.2676

Ichtchenko, K., Nguyen, T., & Südhof, T. C. (1996b). Structures, alternative splicing, and neurexin binding of multiple neuroligins. *The Journal of Biological Chemistry*, *271*(5), 2676–2682. https://doi.org/10.1074/jbc.271.5.2676

Ip, J. P. K., Mellios, N., & Sur, M. (2018). Rett syndrome: Insights into genetic, molecular and circuit mechanisms. *Nature Reviews Neuroscience*, *19*(6), 368–382. https://doi.org/10.1038/s41583-018-0006-3

Jamain, S., Quach, H., Betancur, C., Råstam, M., Colineaux, C., Gillberg, I. C., Soderstrom, H., Giros, B., Leboyer, M., Gillberg, C., Bourgeron, T., & Paris Autism Research International Sibpair Study. (2003). Mutations of the X-linked genes encoding neuroligins NLGN3 and NLGN4 are associated with autism. *Nature Genetics*, *34*(1), 27–29. https://doi.org/10.1038/ng1136

Jedlicka, P., Hoon, M., Papadopoulos, T., Vlachos, A., Winkels, R., Poulopoulos, A., Betz, H., Deller, T., Brose, N., Varoqueaux, F., & Schwarzacher, S. W. (2011). Increased Dentate Gyrus Excitability in Neuroligin-2-Deficient Mice in Vivo. *Cerebral Cortex*, *21*(2), 357–367. https://doi.org/10.1093/cercor/bhq100

Jiang, D.-Y., Wu, Z., Forsyth, C. T., Hu, Y., Yee, S.-P., & Chen, G. (2018). GABAergic deficits and schizophrenia-like behaviors in a mouse model carrying patient-derived neuroligin-2 R215H mutation. *Molecular Brain*, *11*(1), 31. https://doi.org/10.1186/s13041-018-0375-6

Jiang, L., Tian, L., Yuan, J., Xu, X., Qu, F., Zhang, R., & Wang, J. (2022). Associations Between Sex Hormone Levels and Autistic Traits in Infertile Patients With Polycystic Ovary

Syndrome and Their Offspring. *Frontiers in Endocrinology*, *12*. https://doi.org/10.3389/fendo.2021.789395

Kähler, A. K., Djurovic, S., Kulle, B., Jönsson, E. G., Agartz, I., Hall, H., Opjordsmoen, S., Jakobsen, K. D., Hansen, T., Melle, I., Werge, T., Steen, V. M., & Andreassen, O. A. (2008). Association analysis of schizophrenia on 18 genes involved in neuronal migration: MDGA1 as a new susceptibility gene. *American Journal of Medical Genetics Part B: Neuropsychiatric Genetics*, *147B*(7), 1089–1100. https://doi.org/10.1002/ajmg.b.30726

Kajita, Y., & Mushiake, H. (2021). Heterogeneous GAD65 Expression in Subtypes of GABAergic Neurons Across Layers of the Cerebral Cortex and Hippocampus. *Frontiers in Behavioral Neuroscience*, *15*, 750869. https://doi.org/10.3389/fnbeh.2021.750869

Kang, Y., Zhang, X., Dobie, F., Wu, H., & Craig, A. M. (2008). Induction of GABAergic Postsynaptic Differentiation by α-Neurexins. *Journal of Biological Chemistry*, *283*(4), 2323–2334. https://doi.org/10.1074/jbc.M703957200

Kasem, E., Kurihara, T., & Tabuchi, K. (2018). Neurexins and neuropsychiatric disorders. *Neuroscience Research*, *127*, 53–60. https://doi.org/10.1016/j.neures.2017.10.012

Kazdoba, T. M., Leach, P. T., Yang, M., Silverman, J. L., Solomon, M., & Crawley, J. N. (2016). Translational Mouse Models of Autism: Advancing Toward Pharmacological Therapeutics. *Current Topics in Behavioral Neurosciences*, *28*, 1–52. https://doi.org/10.1007/7854_2015_5003

Kennedy, D. P., & Adolphs, R. (2014). Violations of personal space by individuals with autism spectrum disorder. *PloS One*, *9*(8), e103369. https://doi.org/10.1371/journal.pone.0103369

Kheirbek, M. A., Drew, L. J., Burghardt, N. S., Costantini, D. O., Tannenholz, L., Ahmari, S. E., Zeng, H., Fenton, A. A., & Hen, R. (2013). Differential control of learning and anxiety along the dorsoventral axis of the dentate gyrus. *Neuron*, *77*(5), 955–968. https://doi.org/10.1016/j.neuron.2012.12.038

Kienzler-Norwood, F., Costard, L., Sadangi, C., Müller, P., Neubert, V., Bauer, S., Rosenow, F., & Norwood, B. A. (2017). A novel animal model of acquired human temporal lobe epilepsy based on the simultaneous administration of kainic acid and lorazepam. *Epilepsia*, *58*(2), 222–230. https://doi.org/10.1111/epi.13579

Kim, H.-G., Kishikawa, S., Higgins, A. W., Seong, I.-S., Donovan, D. J., Shen, Y., Lally, E., Weiss, L. A., Najm, J., Kutsche, K., Descartes, M., Holt, L., Braddock, S., Troxell, R., Kaplan, L., Volkmar, F., Klin, A., Tsatsanis, K., Harris, D. J., … Gusella, J. F. (2008). Disruption of Neurexin 1 Associated with Autism Spectrum Disorder. *The American Journal of Human Genetics*, *82*(1), 199–207. https://doi.org/10.1016/j.ajhg.2007.09.011

Kim, J. A., Kim, D., Won, S. Y., Han, K. A., Park, D., Cho, E., Yun, N., An, H. J., Um, J. W., Kim, E., Lee, J.-O., Ko, J., & Kim, H. M. (2017). Structural Insights into Modulation of Neurexin-Neuroligin Trans -synaptic Adhesion by MDGA1/Neuroligin-2 Complex. *Neuron*, *94*(6), 1121-1131.e6. https://doi.org/10.1016/j.neuron.2017.05.034

Kim, J. J., & Fanselow, M. S. (1992). Modality-specific retrograde amnesia of fear. *Science (New York, N.Y.)*, *256*(5057), 675–677. https://doi.org/10.1126/science.1585183

Kim, J., Kim, S., Kim, H., Hwang, I.-W., Bae, S., Karki, S., Kim, D., Ogelman, R., Bang, G., Kim, J. Y., Kajander, T., Um, J. W., Oh, W. C., & Ko, J. (2022). MDGA1 negatively regulates amyloid precursor protein-mediated synapse inhibition in the hippocampus.

Proceedings of the National Academy of Sciences of the United States of America, *119*(4), e2115326119. https://doi.org/10.1073/pnas.2115326119

Kim, Y.-H. (2021). How can pediatricians treat neurodevelopmental disorders. *Clinical and Experimental Pediatrics*, *64*(1), 1–2. https://doi.org/10.3345/cep.2020.00507

Kjelstrup, K. G., Tuvnes, F. A., Steffenach, H.-A., Murison, R., Moser, E. I., & Moser, M.-B. (2002). Reduced fear expression after lesions of the ventral hippocampus. *Proceedings of the National Academy of Sciences of the United States of America*, *99*(16), 10825–10830. https://doi.org/10.1073/pnas.152112399

Klausberger, T., & Somogyi, P. (2008). Neuronal diversity and temporal dynamics: The unity of hippocampal circuit operations. *Science (New York, N.Y.)*, *321*(5885), 53–57. https://doi.org/10.1126/science.1149381

Klintwall, L., Holm, A., Eriksson, M., Carlsson, L. H., Olsson, M. B., Hedvall, A., Gillberg, C., & Fernell, E. (2011). Sensory abnormalities in autism. A brief report. *Research in Developmental Disabilities*, *32*(2), 795–800. https://doi.org/10.1016/j.ridd.2010.10.021

Koehnke, J., Jin, X., Budreck, E. C., Posy, S., Scheiffele, P., Honig, B., & Shapiro, L. (2008). Crystal structure of the extracellular cholinesterase-like domain from neuroligin-2. *Proceedings of the National Academy of Sciences*, *105*(6), 1873–1878. https://doi.org/10.1073/pnas.0711701105

Kohl, C., Riccio, O., Grosse, J., Zanoletti, O., Fournier, C., Schmidt, M. V., & Sandi, C. (2013). Hippocampal Neuroligin-2 Overexpression Leads to Reduced Aggression and Inhibited Novelty Reactivity in Rats. *PLOS ONE*, *8*(2), e56871. https://doi.org/10.1371/journal.pone.0056871

Kohl, C., Wang, X.-D., Grosse, J., Fournier, C., Harbich, D., Westerholz, S., Li, J.-T., Bacq, A., Sippel, C., Hausch, F., Sandi, C., & Schmidt, M. V. (2015). Hippocampal neuroligin-2 links early-life stress with impaired social recognition and increased aggression in adult mice. *Psychoneuroendocrinology*, *55*, 128–143. https://doi.org/10.1016/j.psyneuen.2015.02.016

Koide, T., Banno, M., Aleksic, B., Yamashita, S., Kikuchi, T., Kohmura, K., Adachi, Y., Kawano, N., Kushima, I., Nakamura, Y., Okada, T., Ikeda, M., Ohi, K., Yasuda, Y., Hashimoto, R., Inada, T., Ujike, H., Iidaka, T., Suzuki, M., … Ozaki, N. (2012). Common variants in MAGI2 gene are associated with increased risk for cognitive impairment in schizophrenic patients. *PloS One*, *7*(5), e36836. https://doi.org/10.1371/journal.pone.0036836

Krueger-Burg, D., Papadopoulos, T., & Brose, N. (2017). Organizers of inhibitory synapses come of age. *Current Opinion in Neurobiology*, *45*, 66–77. https://doi.org/10.1016/j.conb.2017.04.003

Kubota, Y. (2014). Untangling GABAergic wiring in the cortical microcircuit. *Current Opinion in Neurobiology*, *26*, 7–14. https://doi.org/10.1016/j.conb.2013.10.003

Leachman, C., Nichols, E. S., Al-Saoud, S., & Duerden, E. G. (2024). Anxiety in children and adolescents with autism spectrum disorder: Behavioural phenotypes and environmental factors. *BMC Psychology*, *12*(1), 534. https://doi.org/10.1186/s40359-024-02044-6

Lee, H., Chofflet, N., Liu, J., Fan, S., Lu, Z., Resua Rojas, M., Penndorf, P., Bailey, A. O., Russell, W. K., Machius, M., Ren, G., Takahashi, H., & Rudenko, G. (2023). Designer molecules of the synaptic organizer MDGA1 reveal 3D conformational control of

biological function. *The Journal of Biological Chemistry*, *299*(4), 104586. https://doi.org/10.1016/j.jbc.2023.104586

Lee, K., Kim, Y., Lee, S.-J., Qiang, Y., Lee, D., Lee, H. W., Kim, H., Je, H. S., Südhof, T. C., & Ko, J. (2013). MDGAs interact selectively with neuroligin-2 but not other neuroligins to regulate inhibitory synapse development. *Proceedings of the National Academy of Sciences*, *110*(1), 336–341. https://doi.org/10.1073/pnas.1219987110

Leow, K. Q., Tonta, M. A., Lu, J., Coleman, H. A., & Parkington, H. C. (2024). Towards understanding sex differences in autism spectrum disorders. *Brain Research*, *1833*, 148877. https://doi.org/10.1016/j.brainres.2024.148877

Li, J., Liu, J., Feng, G., Li, T., Zhao, Q., Li, Y., Hu, Z., Zheng, L., Zeng, Z., He, L., Wang, T., & Shi, Y. (2011). The MDGA1 gene confers risk to schizophrenia and bipolar disorder. *Schizophrenia Research*, *125*(2–3), 194–200. https://doi.org/10.1016/j.schres.2010.11.002

Liang, J., Xu, W., Hsu, Y.-T., Yee, A. X., Chen, L., & Südhof, T. C. (2015). Conditional neuroligin-2 knockout in adult medial prefrontal cortex links chronic changes in synaptic inhibition to cognitive impairments. *Molecular Psychiatry*, *20*(7), Article 7. https://doi.org/10.1038/mp.2015.31

Litwack, E. D., Babey, R., Buser, R., Gesemann, M., & O'Leary, D. D. M. (2004). Identification and characterization of two novel brain-derived immunoglobulin superfamily members with a unique structural organization. *Molecular and Cellular Neuroscience*, *25*(2), 263–274. https://doi.org/10.1016/j.mcn.2003.10.016

Loh, K. H., Stawski, P. S., Draycott, A. S., Udeshi, N. D., Lehrman, E. K., Wilton, D. K., Svinkina, T., Deerinck, T. J., Ellisman, M. H., Stevens, B., Carr, S. A., & Ting, A. Y.

(2016). Proteomic Analysis of Unbounded Cellular Compartments: Synaptic Clefts. *Cell*, *166*(5), 1295-1307.e21. https://doi.org/10.1016/j.cell.2016.07.041

Longley, C. M., Xu, X., Messier, J. E., Cai, Z.-L., Park, J. W., Chen, H., Reznik, D. L., Jadi, M. P., & Xue, M. (2022). *Cell-type specific deletions of Neuroligin 2 reveal a vital role of synaptic excitation-inhibition balance* [Preprint]. Neuroscience. https://doi.org/10.1101/2022.09.23.509267

Lord, C., Brugha, T. S., Charman, T., Cusack, J., Dumas, G., Frazier, T., Jones, E. J. H., Jones, R. M., Pickles, A., State, M. W., Taylor, J. L., & Veenstra-VanderWeele, J. (2020). Autism spectrum disorder. *Nature Reviews. Disease Primers*, *6*(1), 5. https://doi.org/10.1038/s41572-019-0138-4

Loureiro, M., Kramar, C., Renard, J., Rosen, L. G., & Laviolette, S. R. (2016). Cannabinoid Transmission in the Hippocampus Activates Nucleus Accumbens Neurons and Modulates Reward and Aversion-Related Emotional Salience. *Biological Psychiatry*, *80*(3), 216–225. https://doi.org/10.1016/j.biopsych.2015.10.016

Love, M. I., Huber, W., & Anders, S. (2014). Moderated estimation of fold change and dispersion for RNA-seq data with DESeq2. *Genome Biology*, *15*(12), 550. https://doi.org/10.1186/s13059-014-0550-8

Masuda, F., Nakajima, S., Miyazaki, T., Tarumi, R., Ogyu, K., Wada, M., Tsugawa, S., Croarkin, P. E., Mimura, M., & Noda, Y. (2019). Clinical effectiveness of repetitive transcranial magnetic stimulation treatment in children and adolescents with neurodevelopmental disorders: A systematic review. *Autism: The International Journal of Research and Practice*, *23*(7), 1614–1629. https://doi.org/10.1177/1362361318822502

Mattheisen, M., Grove, J., Als, T. D., Martin, J., Voloudakis, G., Meier, S., Demontis, D., Bendl, J., Walters, R., Carey, C. E., Rosengren, A., Strom, N. I., Hauberg, M. E., Zeng, B., Hoffman, G., Zhang, W., Bybjerg-Grauholm, J., Bækvad-Hansen, M., Agerbo, E., … Børglum, A. D. (2022). Identification of shared and differentiating genetic architecture for autism spectrum disorder, attention-deficit hyperactivity disorder and case subgroups. *Nature Genetics*, *54*(10), 1470–1478. https://doi.org/10.1038/s41588-022-01171-3

May, T., Adesina, I., McGillivray, J., & Rinehart, N. J. (2019). Sex differences in neurodevelopmental disorders. *Current Opinion in Neurology*, *32*(4), 622–626. https://doi.org/10.1097/WCO.0000000000000714

McIntire, S. L., Reimer, R. J., Schuske, K., Edwards, R. H., & Jorgensen, E. M. (1997). Identification and characterization of the vesicular GABA transporter. *Nature*, *389*(6653), 870–876. https://doi.org/10.1038/39908

McLean, C. P., Asnaani, A., Litz, B. T., & Hofmann, S. G. (2011). Gender differences in anxiety disorders: Prevalence, course of illness, comorbidity and burden of illness. *Journal of Psychiatric Research*, *45*(8), 1027–1035. https://doi.org/10.1016/j.jpsychires.2011.03.006

Megías, M., Emri, Z., Freund, T. F., & Gulyás, A. I. (2001). Total number and distribution of inhibitory and excitatory synapses on hippocampal CA1 pyramidal cells. *Neuroscience*, *102*(3), 527–540. https://doi.org/10.1016/s0306-4522(00)00496-6

Meyza, K. Z., & Blanchard, D. C. (2017). The BTBR mouse model of idiopathic autism – current view on mechanisms. *Neuroscience and Biobehavioral Reviews*, *76*(Pt A), 99–110. https://doi.org/10.1016/j.neubiorev.2016.12.037

Missler, M., & Südhof, T. C. (1998). Neurexins: Three genes and 1001 products. *Trends in Genetics*, *14*(1), 20–26. https://doi.org/10.1016/S0168-9525(97)01324-3

Mizuno, S., Hirota, J., Ishii, C., Iwasaki, H., Sano, Y., & Furuichi, T. (2020). Comprehensive Profiling of Gene Expression in the Cerebral Cortex and Striatum of BTBRTF/ArtRbrc Mice Compared to C57BL/6J Mice. *Frontiers in Cellular Neuroscience*, *14*. https://doi.org/10.3389/fncel.2020.595607

Morellini, F., Malyshev, A., Volgushev, M., Chistiakova, M., Papashvili, G., Fellini, L., Kleene, R., Schachner, M., & Dityatev, A. (2017). Impaired Fear Extinction Due to a Deficit in Ca2+ Influx Through L-Type Voltage-Gated Ca2+ Channels in Mice Deficient for Tenascin-C. *Frontiers in Integrative Neuroscience*, *11*, 16. https://doi.org/10.3389/fnint.2017.00016

Morgan, L. K., Macevoy, S. P., Aguirre, G. K., & Epstein, R. A. (2011). Distances between real-world locations are represented in the human hippocampus. *The Journal of Neuroscience: The Official Journal of the Society for Neuroscience*, *31*(4), 1238–1245. https://doi.org/10.1523/JNEUROSCI.4667-10.2011

Moser, M. B., & Moser, E. I. (1998). Functional differentiation in the hippocampus. *Hippocampus*, *8*(6), 608–619. https://doi.org/10.1002/(SICI)1098-1063(1998)8:6<608::AID-HIPO3>3.0.CO;2-7

Moser, M. B., Moser, E. I., Forrest, E., Andersen, P., & Morris, R. G. (1995). Spatial learning with a minislab in the dorsal hippocampus. *Proceedings of the National Academy of Sciences of the United States of America*, *92*(21), 9697–9701. https://doi.org/10.1073/pnas.92.21.9697

Muhle, R. A., Reed, H. E., Stratigos, K. A., & Veenstra-VanderWeele, J. (2018). The Emerging Clinical Neuroscience of Autism Spectrum Disorder: A Review. *JAMA Psychiatry*, *75*(5), 514–523. https://doi.org/10.1001/jamapsychiatry.2017.4685

Murray, A. J., Sauer, J.-F., Riedel, G., McClure, C., Ansel, L., Cheyne, L., Bartos, M., Wisden, W., & Wulff, P. (2011). Parvalbumin-positive CA1 interneurons are required for spatial working but not for reference memory. *Nature Neuroscience*, *14*(3), 297–299. https://doi.org/10.1038/nn.2751

Nelson, S. B., & Valakh, V. (2015). Excitatory/Inhibitory Balance and Circuit Homeostasis in Autism Spectrum Disorders. *Neuron*, *87*(4), 684–698. https://doi.org/10.1016/j.neuron.2015.07.033

Nguyen, Q.-A., Horn, M. E., & Nicoll, R. A. (2016). Distinct roles for extracellular and intracellular domains in neuroligin function at inhibitory synapses. *eLife*, *5*, e19236. https://doi.org/10.7554/eLife.19236

Nicolini, C., & Fahnestock, M. (2018). The valproic acid-induced rodent model of autism. *Experimental Neurology*, *299*(Pt A), 217–227. https://doi.org/10.1016/j.expneurol.2017.04.017

Nowacka, A., Borczyk, M., Salamian, A., Wójtowicz, T., Włodarczyk, J., & Radwanska, K. (2020). PSD-95 Serine 73 phosphorylation is not required for induction of NMDA-LTD. *Scientific Reports*, *10*(1), 2054. https://doi.org/10.1038/s41598-020-58989-2

Numakawa, T., Yokomaku, D., Richards, M., Hori, H., Adachi, N., & Kunugi, H. (2010). Functional interactions between steroid hormones and neurotrophin BDNF. *World Journal of Biological Chemistry*, *1*(5), 133–143. https://doi.org/10.4331/wjbc.v1.i5.133

Ojima, D., Tominaga, Y., Kubota, T., Tada, A., Takahashi, H., Kishimoto, Y., Tominaga, T., & Yamamoto, T. (2024). Impaired Hippocampal Long-Term Potentiation and Memory Deficits upon Haploinsufficiency of MDGA1 Can Be Rescued by Acute Administration

of D-Cycloserine. *International Journal of Molecular Sciences*, *25*(17), 9674. https://doi.org/10.3390/ijms25179674

O'Keefe, J., & Dostrovsky, J. (1971). The hippocampus as a spatial map. Preliminary evidence from unit activity in the freely-moving rat. *Brain Research*, *34*(1), 171–175. https://doi.org/10.1016/0006-8993(71)90358-1

Omer, D. B., Maimon, S. R., Las, L., & Ulanovsky, N. (2018). Social place-cells in the bat hippocampus. *Science (New York, N.Y.)*, *359*(6372), 218–224. https://doi.org/10.1126/science.aao3474

Panzanelli, P., Früh, S., & Fritschy, J.-M. (2017). Differential role of GABAA receptors and neuroligin 2 for perisomatic GABAergic synapse formation in the hippocampus. *Brain Structure and Function*, *222*(9), 4149–4161. https://doi.org/10.1007/s00429-017-1462-7

Parente, D. J., Garriga, C., Baskin, B., Douglas, G., Cho, M. T., Araujo, G. C., & Shinawi, M. (2017). Neuroligin 2 nonsense variant associated with anxiety, autism, intellectual disability, hyperphagia, and obesity. *American Journal of Medical Genetics. Part A*, *173*(1), 213–216. https://doi.org/10.1002/ajmg.a.37977

Park, D., Bae, S., Yoon, T. H., & Ko, J. (2018). Molecular Mechanisms of Synaptic Specificity: Spotlight on Hippocampal and Cerebellar Synapse Organizers. *Molecules and Cells*, *41*(5), 373–380. https://doi.org/10.14348/molcells.2018.0081

Patrizi, A., Scelfo, B., Viltono, L., Briatore, F., Fukaya, M., Watanabe, M., Strata, P., Varoqueaux, F., Brose, N., Fritschy, J.-M., & Sassoè-Pognetto, M. (2008). Synapse formation and clustering of neuroligin-2 in the absence of GABAA receptors. *Proceedings of the National Academy of Sciences*, *105*(35), 13151–13156. https://doi.org/10.1073/pnas.0802390105

Pelkey, K. A., Chittajallu, R., Craig, M. T., Tricoire, L., Wester, J. C., & McBain, C. J. (2017). Hippocampal GABAergic Inhibitory Interneurons. *Physiological Reviews*, *97*(4), 1619–1747. https://doi.org/10.1152/physrev.00007.2017

Perez-Garcia, C. G., & O'Leary, D. D. M. (2016). Formation of the Cortical Subventricular Zone Requires MDGA1-Mediated Aggregation of Basal Progenitors. *Cell Reports*, *14*(3), 560–571. https://doi.org/10.1016/j.celrep.2015.12.066

Pettem, K. L., Yokomaku, D., Takahashi, H., Ge, Y., & Craig, A. M. (2013a). Interaction between autism-linked MDGAs and neuroligins suppresses inhibitory synapse development. *The Journal of Cell Biology*, *200*(3), 321–336. https://doi.org/10.1083/jcb.201206028

Pettem, K. L., Yokomaku, D., Takahashi, H., Ge, Y., & Craig, A. M. (2013b). Interaction between autism-linked MDGAs and neuroligins suppresses inhibitory synapse development. *Journal of Cell Biology*, *200*(3), 321–336. https://doi.org/10.1083/jcb.201206028

Pettem, K. L., Yokomaku, D., Takahashi, H., Ge, Y., & Craig, A. M. (2013c). Interaction between autism-linked MDGAs and neuroligins suppresses inhibitory synapse development. *Journal of Cell Biology*, *200*(3), 321–336. https://doi.org/10.1083/jcb.201206028

Poulopoulos, A., Aramuni, G., Meyer, G., Soykan, T., Hoon, M., Papadopoulos, T., Zhang, M., Paarmann, I., Fuchs, C., Harvey, K., Jedlicka, P., Schwarzacher, S. W., Betz, H., Harvey, R. J., Brose, N., Zhang, W., & Varoqueaux, F. (2009). Neuroligin 2 Drives Postsynaptic Assembly at Perisomatic Inhibitory Synapses through Gephyrin and Collybistin. *Neuron*, *63*(5), 628–642. https://doi.org/10.1016/j.neuron.2009.08.023

Ringnér, M. (2008). What is principal component analysis? *Nature Biotechnology*, *26*(3), 303–304. https://doi.org/10.1038/nbt0308-303

Rosene, D. L., & Van Hoesen, G. W. (1977). Hippocampal efferents reach widespread areas of cerebral cortex and amygdala in the rhesus monkey. *Science (New York, N.Y.)*, *198*(4314), 315–317. https://doi.org/10.1126/science.410102

Rusina, E., Bernard, C., & Williamson, A. (2021). The Kainic Acid Models of Temporal Lobe Epilepsy. *eNeuro*, *8*(2), ENEURO.0337-20.2021. https://doi.org/10.1523/ENEURO.0337-20.2021

Salari, N., Rasoulpoor, S., Rasoulpoor, S., Shohaimi, S., Jafarpour, S., Abdoli, N., Khaledi-Paveh, B., & Mohammadi, M. (2022). The global prevalence of autism spectrum disorder: A comprehensive systematic review and meta-analysis. *Italian Journal of Pediatrics*, *48*(1), 112. https://doi.org/10.1186/s13052-022-01310-w

Sandin, S., Lichtenstein, P., Kuja-Halkola, R., Hultman, C., Larsson, H., & Reichenberg, A. (2017). The Heritability of Autism Spectrum Disorder. *JAMA*, *318*(12), 1182–1184. https://doi.org/10.1001/jama.2017.12141

Schizophrenia Working Group of the Psychiatric Genomics Consortium. (2014). Biological insights from 108 schizophrenia-associated genetic loci. *Nature*, *511*(7510), 421–427. https://doi.org/10.1038/nature13595

Schreiner, D., Nguyen, T.-M., Russo, G., Heber, S., Patrignani, A., Ahrné, E., & Scheiffele, P. (2014). Targeted Combinatorial Alternative Splicing Generates Brain Region-Specific Repertoires of Neurexins. *Neuron*, *84*(2), 386–398. https://doi.org/10.1016/j.neuron.2014.09.011

Schultz, C., & Engelhardt, M. (2014). Anatomy of the hippocampal formation. *Frontiers of Neurology and Neuroscience*, *34*, 6–17. https://doi.org/10.1159/000360925

Schumann, C. M., Hamstra, J., Goodlin-Jones, B. L., Lotspeich, L. J., Kwon, H., Buonocore, M. H., Lammers, C. R., Reiss, A. L., & Amaral, D. G. (2004). The amygdala is enlarged in children but not adolescents with autism; the hippocampus is enlarged at all ages. *The Journal of Neuroscience: The Official Journal of the Society for Neuroscience*, *24*(28), 6392–6401. https://doi.org/10.1523/JNEUROSCI.1297-04.2004

Scott, E., Zhang, Q., Wang, R., Vadlamudi, R., & Brann, D. (2012). Estrogen neuroprotection and the critical period hypothesis. *Frontiers in Neuroendocrinology*, *33*(1), 85–104. https://doi.org/10.1016/j.yfrne.2011.10.001

Scoville, W. B., & Milner, B. (1957). Loss of recent memory after bilateral hippocampal lesions. *Journal of Neurology, Neurosurgery, and Psychiatry*, *20*(1), 11–21. https://doi.org/10.1136/jnnp.20.1.11

Sebat, J., Lakshmi, B., Malhotra, D., Troge, J., Lese-Martin, C., Walsh, T., Yamrom, B., Yoon, S., Krasnitz, A., Kendall, J., Leotta, A., Pai, D., Zhang, R., Lee, Y.-H., Hicks, J., Spence, S. J., Lee, A. T., Puura, K., Lehtimäki, T., … Wigler, M. (2007). Strong Association of De Novo Copy Number Mutations with Autism. *Science*, *316*(5823), 445–449. https://doi.org/10.1126/science.1138659

Severino, L., Kim, J., Nam, M.-H., & McHugh, T. J. (2024). From synapses to circuits: What mouse models have taught us about how autism spectrum disorder impacts hippocampal function. *Neuroscience and Biobehavioral Reviews*, *158*, 105559. https://doi.org/10.1016/j.neubiorev.2024.105559

Sohal, V. S., & Rubenstein, J. L. R. (2019). Excitation-inhibition balance as a framework for investigating mechanisms in neuropsychiatric disorders. *Molecular Psychiatry*, *24*(9), 1248–1257. https://doi.org/10.1038/s41380-019-0426-0

Somogyi, P., & Klausberger, T. (2005). Defined types of cortical interneurone structure space and spike timing in the hippocampus. *The Journal of Physiology*, *562*(Pt 1), 9–26. https://doi.org/10.1113/jphysiol.2004.078915

Song, J.-Y., Ichtchenko, K., Südhof, T. C., & Brose, N. (1999). Neuroligin 1 is a postsynaptic cell-adhesion molecule of excitatory synapses. *Proceedings of the National Academy of Sciences*, *96*(3), 1100–1105. https://doi.org/10.1073/pnas.96.3.1100

Steffen, D. M., Ferri, S. L., Marcucci, C. G., Blocklinger, K. L., Molumby, M. J., Abel, T., & Weiner, J. A. (2021). The γ-Protocadherins Interact Physically and Functionally with Neuroligin-2 to Negatively Regulate Inhibitory Synapse Density and Are Required for Normal Social Interaction. *Molecular Neurobiology*, *58*(6), 2574–2589. https://doi.org/10.1007/s12035-020-02263-z

Südhof, T. C. (2008a). Neuroligins and neurexins link synaptic function to cognitive disease. *Nature*, *455*(7215), 903–911. https://doi.org/10.1038/nature07456

Südhof, T. C. (2008b). Neuroligins and neurexins link synaptic function to cognitive disease. *Nature*, *455*(7215), 903–911. https://doi.org/10.1038/nature07456

Südhof, T. C. (2017). Synaptic Neurexin Complexes: A Molecular Code for the Logic of Neural Circuits. *Cell*, *171*(4), 745–769. https://doi.org/10.1016/j.cell.2017.10.024

Südhof, T. C. (2018). Towards an Understanding of Synapse Formation. *Neuron*, *100*(2), 276–293. https://doi.org/10.1016/j.neuron.2018.09.040

Sun, C., Cheng, M.-C., Qin, R., Liao, D.-L., Chen, T.-T., Koong, F.-J., Chen, G., & Chen, C.-H. (2011). Identification and functional characterization of rare mutations of the neuroligin-2 gene (NLGN2) associated with schizophrenia. *Human Molecular Genetics*, *20*(15), 3042–3051. https://doi.org/10.1093/hmg/ddr208

Suzuki, K., Hayashi, Y., Nakahara, S., Kumazaki, H., Prox, J., Horiuchi, K., Zeng, M., Tanimura, S., Nishiyama, Y., Osawa, S., Sehara-Fujisawa, A., Saftig, P., Yokoshima, S., Fukuyama, T., Matsuki, N., Koyama, R., Tomita, T., & Iwatsubo, T. (2012). Activity-Dependent Proteolytic Cleavage of Neuroligin-1. *Neuron*, *76*(2), 410–422. https://doi.org/10.1016/j.neuron.2012.10.003

Swanson, L. W. (1981). A direct projection from Ammon's horn to prefrontal cortex in the rat. *Brain Research*, *217*(1), 150–154. https://doi.org/10.1016/0006-8993(81)90192-x

Szabó, A., Schlett, K., & Szücs, A. (2021). Conventional measures of intrinsic excitability are poor estimators of neuronal activity under realistic synaptic inputs. *PLoS Computational Biology*, *17*(9), e1009378. https://doi.org/10.1371/journal.pcbi.1009378

Tannenholz, L., Jimenez, J. C., & Kheirbek, M. A. (2014). Local and regional heterogeneity underlying hippocampal modulation of cognition and mood. *Frontiers in Behavioral Neuroscience*, *8*, 147. https://doi.org/10.3389/fnbeh.2014.00147

Thomas, S. D., Jha, N. K., Ojha, S., & Sadek, B. (2023). mTOR Signaling Disruption and Its Association with the Development of Autism Spectrum Disorder. *Molecules (Basel, Switzerland)*, *28*(4), 1889. https://doi.org/10.3390/molecules28041889

Thouta, S., Waldbrook, M. G., Lin, S., Mahadevan, A., Mezeyova, J., Soriano, M., Versi, P., Goodchild, S. J., & Parrish, R. R. (2022). Pharmacological determination of the fractional block of Nav channels required to impair neuronal excitability and ex vivo seizures. *Frontiers in Cellular Neuroscience*, *16*, 964691. https://doi.org/10.3389/fncel.2022.964691

Toledo, A., Letellier, M., Bimbi, G., Tessier, B., Daburon, S., Favereaux, A., Chamma, I., Vennekens, K., Vanderlinden, J., Sainlos, M., de Wit, J., Choquet, D., & Thoumine, O.

(2022). MDGAs are fast-diffusing molecules that delay excitatory synapse development by altering neuroligin behavior. *eLife*, *11*, e75233. https://doi.org/10.7554/eLife.75233

Tolin, D. F., & Foa, E. B. (2006). Sex differences in trauma and posttraumatic stress disorder: A quantitative review of 25 years of research. *Psychological Bulletin*, *132*(6), 959–992. https://doi.org/10.1037/0033-2909.132.6.959

Troyano-Rodriguez, E., Wirsig-Wiechmann, C. R., & Ahmad, M. (2019). Neuroligin-2 Determines Inhibitory Synaptic Transmission in the Lateral Septum to Optimize Stress-Induced Neuronal Activation and Avoidance Behavior. *Biological Psychiatry*, *85*(12), 1046–1055. https://doi.org/10.1016/j.biopsych.2019.01.022

Tyagarajan, S. K., & Fritschy, J.-M. (2014). Gephyrin: A master regulator of neuronal function? *Nature Reviews Neuroscience*, *15*(3), 141–156. https://doi.org/10.1038/nrn3670

Tzakis, N., & Holahan, M. R. (2019). Social Memory and the Role of the Hippocampal CA2 Region. *Frontiers in Behavioral Neuroscience*, *13*, 233. https://doi.org/10.3389/fnbeh.2019.00233

Uchigashima, M., Ohtsuka, T., Kobayashi, K., & Watanabe, M. (2016). Dopamine synapse is a neuroligin-2–mediated contact between dopaminergic presynaptic and GABAergic postsynaptic structures. *Proceedings of the National Academy of Sciences*, *113*(15), 4206–4211. https://doi.org/10.1073/pnas.1514074113

Ullrich, B., Ushkaryov, Y. A., & Südhof, T. C. (1995). Cartography of neurexins: More than 1000 isoforms generated by alternative splicing and expressed in distinct subsets of neurons. *Neuron*, *14*(3), 497–507. https://doi.org/10.1016/0896-6273(95)90306-2

Ushkaryov, Y. A., Petrenko, A. G., Geppert, M., & Südhof, T. C. (1992). Neurexins: Synaptic Cell Surface Proteins Related to the α-Latrotoxin Receptor and Laminin. *Science*, *257*(5066), 50–56. https://doi.org/10.1126/science.1621094

Uzunova, G., Pallanti, S., & Hollander, E. (2016). Excitatory/inhibitory imbalance in autism spectrum disorders: Implications for interventions and therapeutics. *The World Journal of Biological Psychiatry: The Official Journal of the World Federation of Societies of Biological Psychiatry*, *17*(3), 174–186. https://doi.org/10.3109/15622975.2015.1085597

van der Kooij, M. A., Fantin, M., Kraev, I., Korshunova, I., Grosse, J., Zanoletti, O., Guirado, R., Garcia-Mompó, C., Nacher, J., Stewart, M. G., Berezin, V., & Sandi, C. (2014). Impaired Hippocampal Neuroligin-2 Function by Chronic Stress or Synthetic Peptide Treatment is Linked to Social Deficits and Increased Aggression. *Neuropsychopharmacology*, *39*(5), Article 5. https://doi.org/10.1038/npp.2013.315

Van Zandt, M., Weiss, E., Almyasheva, A., Lipior, S., Maisel, S., & Naegele, J. R. (2019). Adeno-associated viral overexpression of neuroligin 2 in the mouse hippocampus enhances GABAergic synapses and impairs hippocampal-dependent behaviors. *Behavioural Brain Research*, *362*, 7–20. https://doi.org/10.1016/j.bbr.2018.12.052

Varghese, M., Keshav, N., Jacot-Descombes, S., Warda, T., Wicinski, B., Dickstein, D. L., Harony-Nicolas, H., De Rubeis, S., Drapeau, E., Buxbaum, J. D., & Hof, P. R. (2017). Autism spectrum disorder: Neuropathology and animal models. *Acta Neuropathologica*, *134*(4), 537–566. https://doi.org/10.1007/s00401-017-1736-4

Varoqueaux, F., Jamain, S., & Brose, N. (2004). Neuroligin 2 is exclusively localized to inhibitory synapses. *European Journal of Cell Biology*, *83*(9), 449–456. https://doi.org/10.1078/0171-9335-00410

Vogt, D., Cho, K. K. A., Shelton, S. M., Paul, A., Huang, Z. J., Sohal, V. S., & Rubenstein, J. L. R. (2018). Mouse *Cntnap2* and Human *CNTNAP2* ASD Alleles Cell Autonomously Regulate PV+ Cortical Interneurons. *Cerebral Cortex*, *28*(11), 3868–3879. https://doi.org/10.1093/cercor/bhx248

Wang, R., Dong, J.-X., Wang, L., Dong, X.-Y., Anenberg, E., Jiang, P.-F., Zeng, L.-H., & Xie, Y.-C. (2019). A negative regulator of synaptic development: MDGA and its links to neurodevelopmental disorders. *World Journal of Pediatrics: WJP*, *15*(5), 415–421. https://doi.org/10.1007/s12519-019-00253-3

Wang, X., Lin, D., Jiang, J., Liu, Y., Dong, X., Fan, J., Gong, L., Shen, W., Zeng, L., Xu, T., Jiang, K., Connor, S. A., & Xie, Y. (2024). MDGA2 Constrains Glutamatergic Inputs Selectively onto CA1 Pyramidal Neurons to Optimize Neural Circuits for Plasticity, Memory, and Social Behavior. *Neuroscience Bulletin*. https://doi.org/10.1007/s12264-023-01171-1

Wang, Y., Kakizaki, T., Sakagami, H., Saito, K., Ebihara, S., Kato, M., Hirabayashi, M., Saito, Y., Furuya, N., & Yanagawa, Y. (2009). Fluorescent labeling of both GABAergic and glycinergic neurons in vesicular GABA transporter (VGAT)-venus transgenic mouse. *Neuroscience*, *164*(3), 1031–1043. https://doi.org/10.1016/j.neuroscience.2009.09.010

Werling, D. M., Brand, H., An, J.-Y., Stone, M. R., Zhu, L., Glessner, J. T., Collins, R. L., Dong, S., Layer, R. M., Markenscoff-Papadimitriou, E., Farrell, A., Schwartz, G. B., Wang, H. Z., Currall, B. B., Zhao, X., Dea, J., Duhn, C., Erdman, C. A., Gilson, M. C., … Sanders, S. J. (2018). An analytical framework for whole-genome sequence association studies and its implications for autism spectrum disorder. *Nature Genetics*, *50*(5), 727–736. https://doi.org/10.1038/s41588-018-0107-y

Werling, D. M., & Geschwind, D. H. (2013). Sex differences in autism spectrum disorders. *Current Opinion in Neurology*, *26*(2), 146–153. https://doi.org/10.1097/WCO.0b013e32835ee548

Wierenga, C. J., & Wadman, W. J. (1999). Miniature inhibitory postsynaptic currents in CA1 pyramidal neurons after kindling epileptogenesis. *Journal of Neurophysiology*, *82*(3), 1352–1362. https://doi.org/10.1152/jn.1999.82.3.1352

Winden, K. D., Ebrahimi-Fakhari, D., & Sahin, M. (2018). Abnormal mTOR Activation in Autism. *Annual Review of Neuroscience*, *41*, 1–23. https://doi.org/10.1146/annurev-neuro-080317-061747

Wingo, A. P., Liu, Y., Gerasimov, E. S., Vattathil, S. M., Liu, J., Cutler, D. J., Epstein, M. P., Blokland, G. A. M., Thambisetty, M., Troncoso, J. C., Duong, D. M., Bennett, D. A., Levey, A. I., Seyfried, N. T., & Wingo, T. S. (2023). Sex differences in brain protein expression and disease. *Nature Medicine*, *29*(9), 2224–2232. https://doi.org/10.1038/s41591-023-02509-y

Wöhr, M., Silverman, J. L., Scattoni, M. L., Turner, S. M., Harris, M. J., Saxena, R., & Crawley, J. N. (2013). Developmental delays and reduced pup ultrasonic vocalizations but normal sociability in mice lacking the postsynaptic cell adhesion protein neuroligin2. *Behavioural Brain Research*, *251*, 50–64. https://doi.org/10.1016/j.bbr.2012.07.024

Wüstner, L.-S., Beuter, S., Kriebel, M., & Volkmer, H. (2024). Dissection of signaling pathways regulating TrkB-dependent gephyrin clustering. *Frontiers in Molecular Neuroscience*, *17*, 1480820. https://doi.org/10.3389/fnmol.2024.1480820

Yao, J., Irwin, R., Chen, S., Hamilton, R., Cadenas, E., & Brinton, R. D. (2012). Ovarian hormone loss induces bioenergetic deficits and mitochondrial β-amyloid. *Neurobiology of Aging*, *33*(8), 1507–1521. https://doi.org/10.1016/j.neurobiolaging.2011.03.001

Yu, G., Wang, L.-G., Han, Y., & He, Q.-Y. (2012). clusterProfiler: An R Package for Comparing Biological Themes Among Gene Clusters. *OMICS: A Journal of Integrative Biology*, *16*(5), 284–287. https://doi.org/10.1089/omi.2011.0118

Zhang, P., Lu, H., Peixoto, R. T., Pines, M. K., Ge, Y., Oku, S., Siddiqui, T. J., Xie, Y., Wu, W., Archer-Hartmann, S., Yoshida, K., Tanaka, K. F., Aricescu, A. R., Azadi, P., Gordon, M. D., Sabatini, B. L., Wong, R. O. L., & Craig, A. M. (2018). Heparan Sulfate Organizes Neuronal Synapses through Neurexin Partnerships. *Cell*, *174*(6), 1450-1464.e23. https://doi.org/10.1016/j.cell.2018.07.002

Zhou, Y., Kaiser, T., Monteiro, P., Zhang, X., Van der Goes, M. S., Wang, D., Barak, B., Zeng, M., Li, C., Lu, C., Wells, M., Amaya, A., Nguyen, S., Lewis, M., Sanjana, N., Zhou, Y., Zhang, M., Zhang, F., Fu, Z., & Feng, G. (2016). Mice with Shank3 Mutations Associated with ASD and Schizophrenia Display Both Shared and Distinct Defects. *Neuron*, *89*(1), 147–162. https://doi.org/10.1016/j.neuron.2015.11.023

Appendix

Meta-analysis of risk factors for autism spectrum disorder (ASD)

Abstract

Objective To explore the risk factors of ASD by means of systematic evaluation. **Methods** The literatures published from January 1st 2020 to March 1st 2025 were searched in the Cochrane Library, PubMed, Web of Science and Embase. 'autism spectrum disorder', 'autistic spectrum disorders', 'risk factors' and their free words were selected as keywords. The Newcastle-Ottawa Scale was used to assess the quality of the studies. The Meta-analysis was performed in the literatures scored above 7. **Results** A total of 20 articles were included in the Meta-analysis with the cumulative number of cases and controls reaching 35,902 and 382,570 respectively. Meta-analysis showed that the risk factors for ASD were gender (male) (OR = 2.59, 95 % CI: 2.00-3.35) and family history of ASD (OR 6.78, 95% CI: 3.94-11.68). **Conclusion** Male gender and family history of ASD are robust risk factors for ASD, with the latter exhibiting a particularly strong effect.

Keywords Autism spectrum disorder, Risk factors, Case-control, Meta-analysis

Methods

1. Search strategy

We searched the PubMed, Web of Science, Embase and Cochrane Systematic Review electronic databases and used the following search strategies to identify relevant studies: the search keywords are 'Autism spectrum disorder' OR 'Autistic Spectrum Disorder' OR 'Autistic Spectrum Disorders' OR 'Disorder, Autistic Spectrum' OR 'Autism Spectrum Disorders' AND 'Dangerous factors' OR 'Related factors' OR 'Influence factors' AND 'Case control study'. The time of the retrieved

literature was from January 1, 2020 to March 1, 2025. The process of literature screening is shown in Figure 34.

2. Selection criteria

2.1 Inclusion criteria

①The design type was case-control study ②The sources of the cases were patients with ASD diagnosed in various medical institutions, and the control group was based on a large community population living in the same area as the cases ③Published literatures from 1 January 2020 to 1 March 2025 ④Data in the study results provided or can be converted to odds ratio (OR) values, 95%CI and standard error (SE).

2.2 Exclusion criteria

①Duplicate publication ②Non-English literatures ③There were no control groups, incomplete basic data and too many lost follow-up studies ④Review literatures ⑤Risk factor definitions differ significantly from general standards or most research standards.

3. Literature screening, data extraction and quality evaluation

By reading the title, irrelevant literature and duplicate clinical studies were excluded, and literature meeting the inclusion criteria was detected by reading the full text. Evaluation was conducted using the Newcastle-Ottawa Scale (NOS) with a total score of 9 points, and only literature with a score of 7 points or more was included (Table 3).

4. Data analysis

Meta-analysis is performed by Review Manager 5.3 software. The heterogeneity between the results is analysed by the Q test, with the test level of $\alpha = 0.1$, and I^2 is used to measure the

heterogeneity. If there is no statistical and clinical heterogeneity between the results of each study ($p > 0.1$, $I^2 < 50\%$), a fixed-effect model is used for meta-analysis; if there is moderate or higher heterogeneity between the results ($p < 0.1$, $I^2 > 50\%$), subgroup analysis or sensitivity analysis can be conducted to find the source of heterogeneity, and a random-effect model is used for meta-analysis. A funnel plot is used to analyse whether there is publication bias in the included studies.

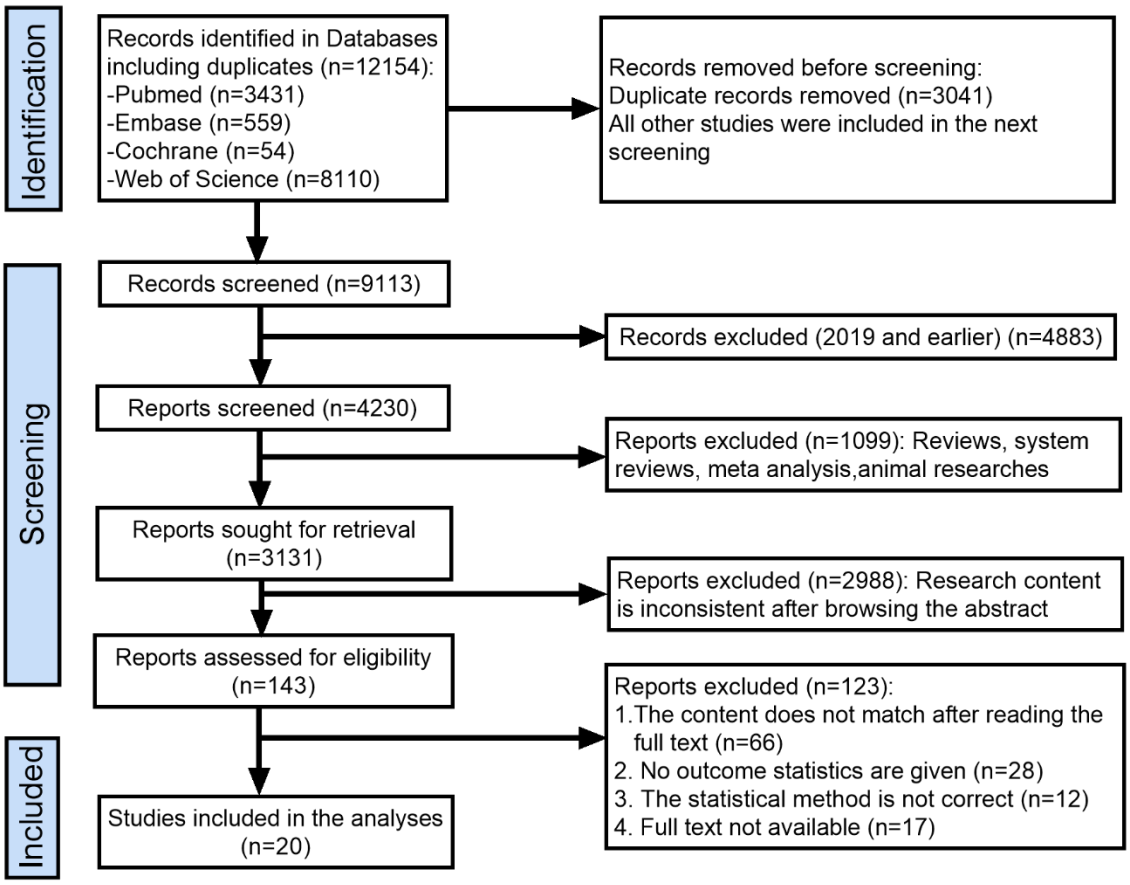

Figure 34. The flowchart of the literature retrieval and screening.

Table 3. Quality assessment of NOS

Author	Year	Selection	Comparability	Outcome	NOS score
Yuanyuan	2023	★★★	★★	★★★	8 stars
Thekra	2021	★★★★	★★	★★★	9 stars
Watfa	2021	★★★★	★★	★★★	9 stars
Jian-Hui	2022	★★★	★★	★★★	8 stars
Anita	2020	★★★	★★	★★★	8 stars
Xiaoping	2022	★★★★	★★	★★	8 stars
Yan	2024	★★★★	★★	★★★	9 stars
Wei-chao	2020	★★★★	★★	★★★	9 stars
Yi-Ling	2022	★★★	★★	★★★	8 stars
Torkel	2022	★★★	★★	★★★	8 stars
Jian-Hui	2021	★★★	★★	★★★	8 stars
Jian-Hui	2022	★★★	★★	★★★	8 stars
Ohad	2021	★★★★	★★	★★	8 stars
Bo	2021	★★★	★★	★★★	8 stars
Shahid	2024	★★★	★★	★★★	8 stars
Jehad	2021	★★★★	★★	★★	8 stars
Andre	2021	★★★★	★★	★★★	9 stars
Andre	2023	★★★★	★★	★★★	9 stars
Ahmed	2022	★★★★	★★	★★★	9 stars
Leonardo	2022	★★★	★★	★★	7 stars

Results

1. Literature search results

A total of 12154 articles were retrieved, and 3041 duplicate items were excluded. After reading the titles and abstracts, 143 remaining articles were evaluated for full-text reading, and finally, 20 articles met the inclusion criteria (Figure 34).

2. Characteristics of included studies

All 20 included studies were case–control studies, and published between 2020 and 2025. There were 35, 902 cases of cumulative disease in the group and 382, 570 cases in the control group. The specific characteristics of the included studies are shown in Table 4.

Table 4. Summary of research features

Author	Year	Research type	Case	Control	Control source	Risk factors involved
Yuanyuan	2023	Case control	192	74060	Healthy population	1, 2, 3, 4, 5, 6, 7
Thekra	2021	Case control	160	145	Healthy population	8, 9, 10, 11
Watfa	2021	Case control	278	722	Healthy population	12
Jian Hui	2022	Case control	1871	60501	Healthy population	13
Anita	2020	Case control	86	670	Healthy population	14, 15,16
Xiaoping	2022	Case control	67	134	Healthy population	17
Yan	2024	Case control	146	1460	Healthy population	18, 19
Wei-chao	2020	Case control	83	83	Healthy population	20
Yi-Ling	2022	Case control	24279	97715	Healthy population	8,21, 22, 23, 24, 25, 26, 27, 28, 29, 30, 31, 32, 33, 34, 35, 36, 37, 38, 39, 40, 41, 42, 43, 44
Torkel	2022	Case control	586	15115	Healthy population	27
Jian-Hui	2021	Case control	1960	63357	Healthy population	13, 45, 46, 47
Jian-Hui	2022	Case control	1958	63285	Healthy population	48, 45
Ohad	2021	Case control	174	176	Healthy population	49
Bo	2021	Case control	88	639	Healthy population	50, 51
Shahid	2024	Case control	310	310	Healthy population	5, 22, 1
Jehad	2021	Case control	163	326	Healthy population	31, 45
Andre	2021	Case control	1558	1558	Healthy population	52, 53, 54
Andre	2023	Case control	1558	1558	Healthy population	55
Ahmed	2022	Case control	268	504	Healthy population	26, 31, 56, 57, 8, 58, 45, 59, 30, 28, 60,61, 62
Leonardo	2022	Case control	117	252	Healthy population	1, 63, 64

Note: 1 Gender (male); 2 Anoxia or Asphyxia at Birth; 3 Artificial feeding; 4 Complications during pregnancy; 5 High paternal education; 6 Introverted father; 7 Daily TV viewing (≥ 3 hours); 8 Family history of ASD; 9 Exposure to anesthesia during pregnancy; 10 Absence of folic acid consumption in the first trimester; 11 Exposure to X-rays in the first trimester; 12 Maternal education of bachelor's degree or higher; 13 Maternal cooking oil fumes (COFs) exposure; 14 mothers with low HDL-C and above median valine concentrations; 15 Mothers with low HDL-C and above median BCAA concentrations; 16 Males whose mothers had low HDL-C; 17 mitochondrial DNA copy number (mtDNAcn) levels; 18 NDVI (Normalized Difference Vegetation Index) 500m exposure before birth; 19 NDVI500m exposure first 3 years after birth; 20 Serum neurofilament light chain (sNfL); 21 Maternal age at delivery (40 +); 22 Paternal age at

delivery (40 +); 23 Maternal unemployment; 24 Paternal unemployment; 25 Maternal urbanization (high); 26 Paternal urbanization (high); 27 Low birthweight (<2500 gm); 28 Preterm birth (GA <37 weeks); 29 Cesarean delivery; 30 Hypertension complicating pregnancy; 31 Diabetes mellitus complicating pregnancy; 32 Maternal schizophrenia; 33 Maternal Bipolar spectrum disorders; 34 Maternal Depressive disorders; 35 Maternal Obsessive–compulsive disorder; 36 Maternal Adjustment disorders; 37 Maternal ADHD; 38 Maternal ASD; 39 Paternal schizophrenia; 40 Paternal Depressive disorders; 41 Paternal Adjustment disorders; 42 Paternal Substance use disorders; 43 Paternal ADHD; 44 Paternal ASD; 45 Maternal prenatal exposure to tobacco smoke (ETS); 46 Maternal prenatal exposure to mosquito coils; 47 Maternal prenatal exposure to home renovations; 48 Children's exposure to environmental tobacco smoke (ETS) in early life; 49 abnormal fetal head growth (smaller biparietal diameter (BPD)); 50 Postpartum maternal Low-density lipoprotein (LDL); 51 Postpartum maternal LDL in overweight and obese mothers; 52 Increasing maternal vitamin D; 53 Deficient (< 30 nmol/L) vitamin D; 54 insufficient (30–49.9 nmol/L) vitamin D; 55 High maternal vitamin B12 levels (⩾81th percentile) during pregnancy; 56 Previous abortion; 57 Assisted fertility; 58 Multiple pregnancy; 59 Threatened abortion; 60 Intake of vitamins; 61 Neonatal convulsions; 62 Admission to neonatal intensive care unit; 63 Nuclear de novo mutations (DNMs); 64 mtDNA variants with 15%–5% heteroplasmy.

3. Quality evaluation of the included literatures

A total of 20 articles were included in this meta-analysis, all of which were of high quality (Table 3).

4. Meta-analysis results

4.1 Meta-analysis of risk factors for ASD

4.1.1 The risk of gender (male) in the offspring of ASD

Three studies provided data on the risk of gender (male) in the offspring of ASD, involving a total of 619 cases in the ASD group and 74622 cases in the non-ASD group. There was no statistical

significance in heterogeneity (I^2 = 0%, p = 0.57). The results showed that the risk of gender (male) in the offspring of ASD was relatively high (OR = 2.59, 95% CI [2.00, 3.35], p <0.00001) (Figure 35).

4.1.2 The risk of family history of ASD in the offspring of ASD

Three studies provided data on the risk of family history of ASD in the offspring of ASD, involving a total of 24707 cases in the ASD group and 98364 cases in the non-ASD group. There was no statistical significance in heterogeneity (I^2 = 3%, p = 0.36). The results showed that the risk of family history of ASD in the offspring of ASD was relatively high (OR = 6.78, 95% CI [3.94, 11.68], p <0.00001) (Figure 36).

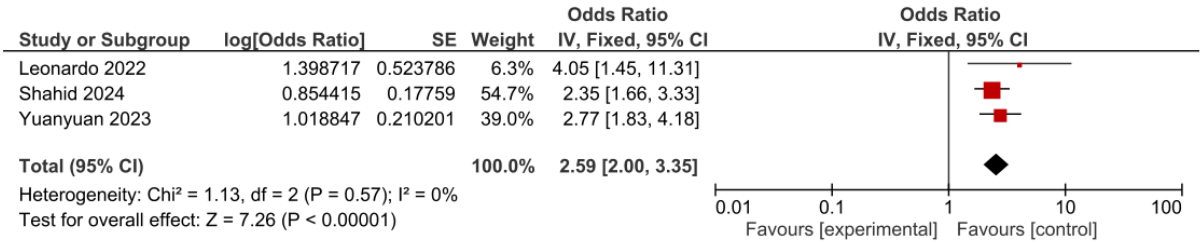

Figure 35. Meta-analysis forest map of gender (male) analysis.

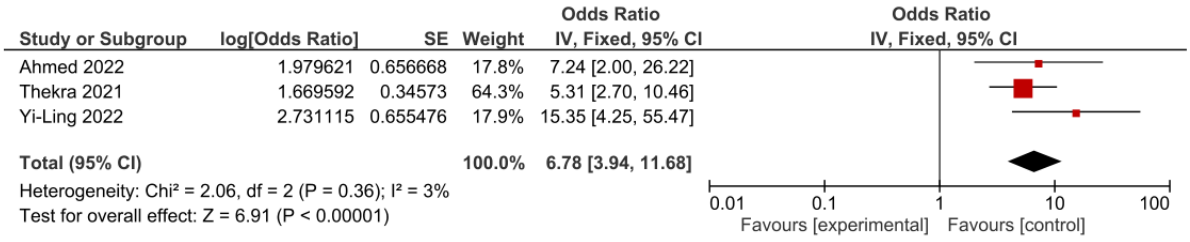

Figure 36. Meta-analysis forest map of autism spectrum disorder (ASD) family history analysis.

4.2 Bias test

Funnel plot analysis was conducted for the gender (male) and family history of ASD studies to assess the potential bias of the studies and found that the funnel plots of the gender (male) group and family history of ASD group were basically within 95% CI and symmetrical (Figure 37), indicating that there was no obvious publication bias in our included studies.

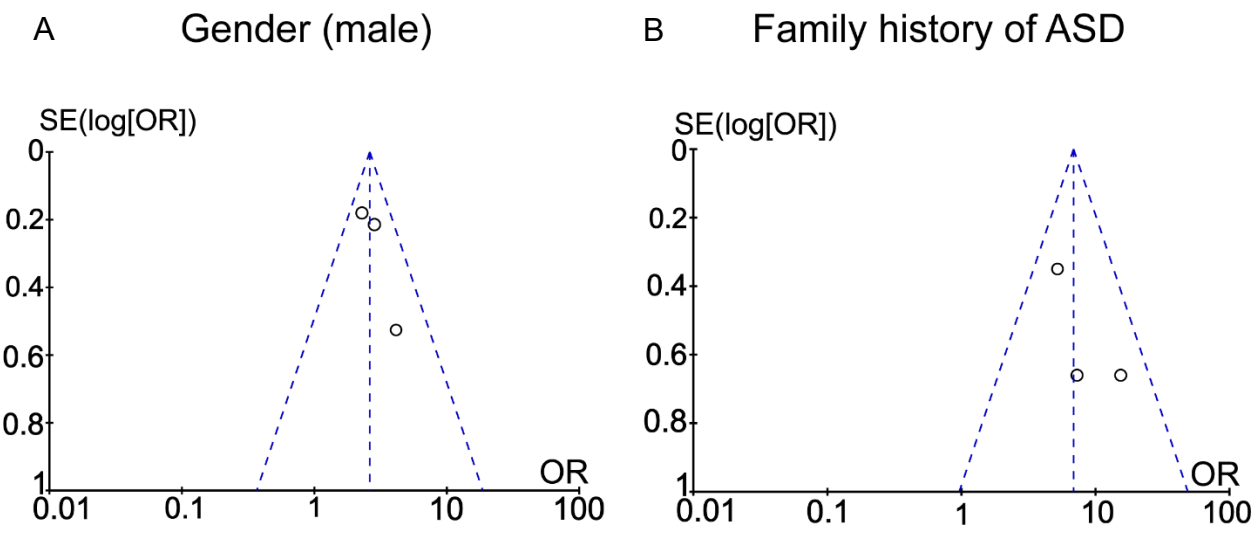

Figure 37. Funnel plots for gender (male) (A) and family history analysis of autism spectrum disorder (ASD) (B).

Discussion

1. Result analysis

In this study, we conducted a meta-analysis on 20 newly published articles that included ASD offspring (35,902 cases) and non-ASD offspring (382,570 cases). This meta-analysis identified male gender (OR = 2.59, 95% CI [2.00, 3.35]) and family history of autism (OR = 6.78, 95% CI [3.94, 11.68]) as significant risk factors for ASD in offspring. These findings align with existing research and further supports the role of both genetic and sex-linked biological factors in

the pathogenesis of ASD (Sandin et al., 2017; Werling & Geschwind, 2013). In particular, male individuals had a significantly higher risk of ASD (OR = 2.59), which is consistent with well-documented sex disparities in autism prevalence (Baron-Cohen et al., 2011; Werling & Geschwind, 2013). Possible explanations include: 1. **Genetic and hormonal influences**. The male predominance may reflect sex-linked genetic vulnerabilities, such as X-chromosome-related mechanisms or androgen exposure during neurodevelopment. The genetic risk of ASD is not due to mutations in just one gene but often involves the accumulation of many minor variations in hundreds or thousands of genes (Mattheisen et al., 2022). Interestingly, both NL2 and NL4 are present at inhibitory synapses and mutations in NL4 in mice results in ASD (Guneykaya et al., 2023). NL4 gene localizes on the X chromosome and even with a neurotypical maternal carrier, corresponding mutation proteins are restricted to male offspring (Jamain et al., 2003). Males have only one X chromosome, while females have two, but one of them is randomly inactivated (X Chromosome Inactivation (XCI)). Some X chromosome genes can escape XCI, and the expression of two X chromosomes in females may provide a protective buffer, while males are more susceptible to mutations due to a single copy. If there are key genes related to ASD on the X chromosome (such as NL3/NL4X, MECP2, FMR1), males are more likely to have functional abnormalities due to mutations due to the lack of compensation from the second X chromosome (Jamain et al., 2003; Werling et al., 2018). Also, Y chromosome genes (such as Sex-determining Region Y (SRY)) may enhance the disease-causing effects of X-linked genes, or amplify ASD risks through sex hormones (such as testosterone) (Baron-Cohen et al., 2015; Chura et al., 2010). Importantly, sex hormones also contribute to ASD. Researches have noted that female ASD patients have a tendency to show increased testosterone levels compared with their neurotypical developing counterparts, indicating a connection between higher fetal testosterone levels and the

etiology of ASD (Auyeung et al., 2009). Also, during the developmental stages, ASD-associated genes involved in synaptic formation, maintenance and cell adhesion are influenced by hormones, further confirm that male predominance in ASD (Baron-Cohen et al., 2020). In particular, the lipid nature of steroids allows them to directly modulate genes by passing through cell membranes, interacting with their according receptors, and navigating into the nucleus. This process controls specific gene activation and expression differently across cell types and sexes. Hormones like testosterone can regulate such selective gene activation mainly governed by various cellular signaling molecules, contributing to different physiological and behavioural outcomes between males and females (Leow et al., 2024). Also, ASD tend to be more common in the offspring of mothers who have high levels of testosterone during pregnancy (L. Jiang et al., 2022). Notably, the neuroprotective effects of estrogen in females (Almey et al., 2015; Crider & Pillai, 2017) may contribute to this disparity. Estradiol is the bioactive form of estrogen. Estradiol can diffuse through the cell membrane and translocate and bind to estrogen receptors to genes in the nucleus, enabling estrogens to promote or inhibit the transcription of antiapoptotic or proapoptotic genes, respectively (Scott et al., 2012). To protect the brain, estradiol can also enhance cerebral blood flow, facilitate glucose metabolism and increase electron transport chain activity to supply energy to neurons (Yao et al., 2012). In addition, estrogen protects the brain against inflammation and stress through promoting the synthesis of neurotrophins such as brain-derived neurotrophic factor (BDNF), which is a key molecule related with neuronal survival, differentiation and synaptic plasticity (Numakawa et al., 2010). 2. **Diagnostic bias**. The female individuals with ASD may exhibit with subtler or different phenotypic profiles, resulting in underdiagnosis and thus an inflated male-to-female ratio in clinical samples. Although these findings support the male predominance in ASD, future research is needed to explore whether existing diagnostic criteria

and assessment tools adequately capture autism presentations in females to reduce potential diagnostic bias.

In addition, the substantially high risk associated with a family history of ASD (OR = 6.78) highlights the heritability of ASD, which aligns with the heritable nature estimated in twin and family studies (60–90%) (Bai et al., 2019; Jamain et al., 2003). Possible explanations include: 1. **Synaptic dysfunction.** ASD-related genes (e.g. SHANK3, NL3/4, NRXN1) encode synaptic adhesion molecules and scaffold proteins, and their mutations can lead to E/I imbalances, affecting neural signaling (Bourgeron, 2015). When the genetic mutations occur in coding regions which are crucial to protein synthesis, it can change encoded protein structures and disrupt neuronal circuitry (Geschwind & State, 2015). This may lead to phenotypic differences related to ASD symptoms. For example, single nucleotide polymorphism (SNP) that result in alteration of synaptic proteins may affect neuronal connectivity and communication, which supports some cognitive and behavioural performance of ASD (Geschwind & Levitt, 2007). Some genome-wide association studies (GWAS) have emphasized genes related to synaptic function and neuronal connectivity are pivotal to determining the manifestation of ASD (H.-G. Kim et al., 2008; Sebat et al., 2007). The key players among vast amounts of synaptic protein organizers include neurexin, neuroligin, SHANK and PSD95 (Leow et al., 2024). Disruption of NRXN-NL interaction contributes to E/I imbalance, which is evident in ASD (Nelson & Valakh, 2015). In addition, the activity of excitatory glutamatergic pyramidal neurons and inhibitory GABAergic interneurons contribute to the E/I balance (Uzunova et al., 2016). Activated excitatory synapses results in sodium influxing through the postsynaptic AMPARs, leading to depolarization and Ca^{2+} influx through NMDARs where magnesium is removed. The Ca^{2+}-dependent kinases begin to regulate gene transcription and synapse strengthening, causing LTP, increase in the amplitude of excitatory post-synaptic

potentials (EPSPs). Heritable anomalies in ASD disrupt these procedures and alter cognition and behaviors (Leow et al., 2024). GABA signaling can shift the cell direction from depolarization to hyperpolarization, which is crucial to the normal E/I ratio (Uzunova et al., 2016). The NL2 project complements the limited knowledge about the mechanism of how GABA signaling contribute to ASD. 2. **Abnormal immune and inflammatory responses.** Mutations in maternal immune activation (MIA) or inherited immune genes (e.g. C4, IL6) cause abnormal activation of microglia, affecting synaptic pruning and increasing the risk of ASD (Estes & McAllister, 2016). Notably, proteomic analysis and RNA sequencing studies identified 5.5% of the assessed genes exhibited sex-based different expression at both mRNA and protein levels across 13 brain regions (Fass et al., 2024; Wingo et al., 2023). In particular, female brains showed enhanced gene expression associated with immune response (including microglia and astrocytes), blood vessel regulation and zinc homeostasis, while male brains exhibited increased gene expression implicated in neurotransmitter transporters, ion channels, synaptic signalling and plasticity (Fass et al., 2024). These findings confirm that the immune activity in the female ASD brains (Hanamsagar et al., 2017) are increased and suggesting that predominantly in the male brains, ASD might disrupt important synaptic activities (Leow et al., 2024). 3. **Autophagy and hyperactivation of the mTOR signaling pathway.** Hyperactivation of mTOR intracellular signaling plays an essential role in the development of ASD (Winden et al., 2018). And during the development, autophagy is pivotal to the process for synaptic formation and pruning (Birdsall & Waites, 2019). Also**,** mTOR signaling is vital for the several cellular functions including synaptic plasticity, axonal guidance and autophagy (Thomas et al., 2023). The suppression of autophagy due to hyperactivation of mTOR results in neuronal hyperexcitability (Thomas et al., 2023). Specifically, $GABA_AR$s were trafficked from ER-Golgi to the cell surface of neurons to receive inhibitory inputs from

interneurons. However, in autophagy-deficient or mTOR hyperactivated neurons, the trafficking of $GABA_A$Rs were reduced by protein aggregates and therefore the affected neurons become hyperactive because of a loss of inhibitory signals leading to the E/I imbalance (Hui & Tanaka, 2019). Rapamycin (mTOR inhibitor) can improve ASD symptoms (Kazdoba et al., 2016). When ASD is present in the family, the risk of developing ASD in the offspring increases nearly 7-fold, which provides an important basis for genetic counseling. Further research needs to explore how familial genetic risk interacts with environmental factors such as prenatal exposures to influence the development of ASD.

The meta-analysis was limited to the last 5 years is because over the past five years, autism research has made significant progress in diagnostic criteria (such as the popularization of DSM-5), genetic techniques such as whole genome sequencing, and environmental factor assessment methods. Including the latest research can reduce the bias caused by differences such as inconsistent diagnostic tools in earlier studies. Secondly, Earlier studies may have included outdated treatment methods such as certain antiepileptic drugs or outdated diagnostic criteria such as confusing autism with intellectual disability, which could interfere with the results. Including studies from a longer period (e.g., 10 years or more) would have altered the results. In recent years, the increased understanding of female autism phenotypes such as "camouflaging" masking symptoms may have led to earlier studies underestimating the proportion of female patients. Incorporating long-term data may weaken the conclusion of "male dominance". Moreover, including more studies may increase the sample size, but it may also introduce heterogeneity such as changes in diagnostic criteria, which needs to be addressed through subgroup analysis, but it will reduce the comparability of the results.

Future studies could combine genetic screening (e.g., NL2, MDGA gene sequencing) with gender/family history data to improve early identification of ASD, especially in offspring from high-risk families. Biochemical markers of synaptic proteins, such as NL2 levels in cerebrospinal fluid or exosomes, may assist in the objective diagnosis of ASD. Drugs such as GABA receptor modulators that target synaptic adhesion molecular pathways such as the MDGA-NL2-GABAergic synapse may be effective against ASD, especially in patients carrying related genetic variants. Male patients with ASD may be more sensitive to interventions targeting GABA or glutamate systems due to more pronounced synaptic inhibition/excitation imbalance. Furthermore, for those with a positive family history, genetic testing including a synaptic gene panel is recommended to identify the risk of recurrence and guide reproductive decisions. Interventions during pregnancy such as optimizing nutrition and reducing environmental toxins may reduce the risk of ASD by protecting synaptic development, especially in families with high genetic load. Furthermore, the interaction of sex with synaptic molecules such as NL2/MDGA need to be validated in animal models to clarify the cellular basis of male susceptibility. Develop biomarkers or imaging tools based on synaptic proteins (such as positron emission tomography (PET) tracers) for stratified ASD diagnosis and treatment. Explore the efficacy of personalized treatments, such as GABA-promoting drugs, for genetically confirmed patients (e.g., NL2 mutations).

2. Strengths and limitations

This study incorporates the latest case-control studies (from 2020 to 2025) and the study population in this study involves multiple countries and ethnic groups around the world. In addition, the results of bias test show that our research results are relatively stable, and there is no obvious publication bias in the included studies. But this study is not without limitations. Firstly, some articles reported the influence of other factors on ASD, but due to the time search limit of only 5

years, less data or other reasons, they could not be included in this meta-analysis, which had a certain impact on the quality of the analysis and the results of the study. Secondly, only 3 literatures related to gender (male) and family history of ASD respectively were included in the meta-analysis, which may lead to certain bias in the meta-analysis and affect the results of the meta-analysis.

Conclusion

Male gender and family history of ASD are robust risk factors for ASD, with the latter exhibiting a particularly strong effect. These results highlight the need for gender-sensitive diagnostic strategies and the genetic studies of ASD should be further investigated. Early screening of offspring with a familial ASD history may facilitate prompt intervention and improve prognosis. Future studies should employ standardized phenotypic analyses and explore mechanisms such as epigenetics or gene-sex interactions in depth.

Vita

Name: Jie Jiang

Education

York University (Canada) Ph.D. candidate in Biology (Neuroscience stream) 2021.9-present

Drexel University (US) M.S. in Pharmacology & Physiology 2017.8-2019.12

China Pharmaceutical University (China) B.S. in Pharmaceutics 2013.9-2017.6

Publications

1. Xuehui Wang[#], Donghui Lin[#], **Jie Jiang**[#], Yuhua Liu, Xinyan Dong,…,Steven A Connor, Yicheng Xie. (2024) MDGA2 Constrains Glutamatergic Inputs Selectively onto CA1 Pyramidal Neurons to Optimize Neural Circuits for Plasticity, Memory, and Social Behavior. Neuroscience Bulletin. (Co-first author)
2. Xuehui Wang[#], Hao Wei[#], Zhe Hu[#], **Jie Jiang[#]**, Xinyan Dong, Jinpiao Zhu, Haiyan Chen, Nils Brose, Noa Lipstein, Tonghui Xu, Steven A. Connor, Daqing Ma, Yicheng Xie. (2025) Chronic stress induces depression through MDGA1-Neuroligin2 mediated suppression of inhibitory synapses in the lateral habenula. Theranostics. (Co-first author)
3. The regulation of astrocytic cell adhesion molecules in synaptic transmission and plasticity. (review, in preparation)

Conference presentations

1. Selective prevention of MDGA-Neuroligin-2 interactions increases inhibitory synaptic transmission, fear memory, and anxiety. **Invited talk at PhD exit seminar**. February 28th, 2025.

2. **Jie Jiang**, Donghui Lin, Xuehui Wang, Yicheng Xie, Steven A Connor. Selective prevention of MDGA-Neuroligin-2 interactions increases inhibitory synaptic transmission, fear memory, and anxiety. **CAN Meeting**. Vancouver. May 19-22, 2024.
3. **Jie Jiang**, Francis M Munoz, Xinghua Gao, Huijuan Hu. The role of spinal astrocytic store-operated calcium channel including STIM2 and Orai1 in the inflammatory pain. **Drexel Discovery Day**. Oct.23, 2017.

Teaching experience

1. Lab demonstrator for Animals Teaching Assistant 2024.1-2024.3
2. Marker/grader for Animals and Biology Teaching Assistant 2023.9-2023.12

Awards

China scholarship council scholarship 2017-2019